UNIVERSITY OF TWENTE.

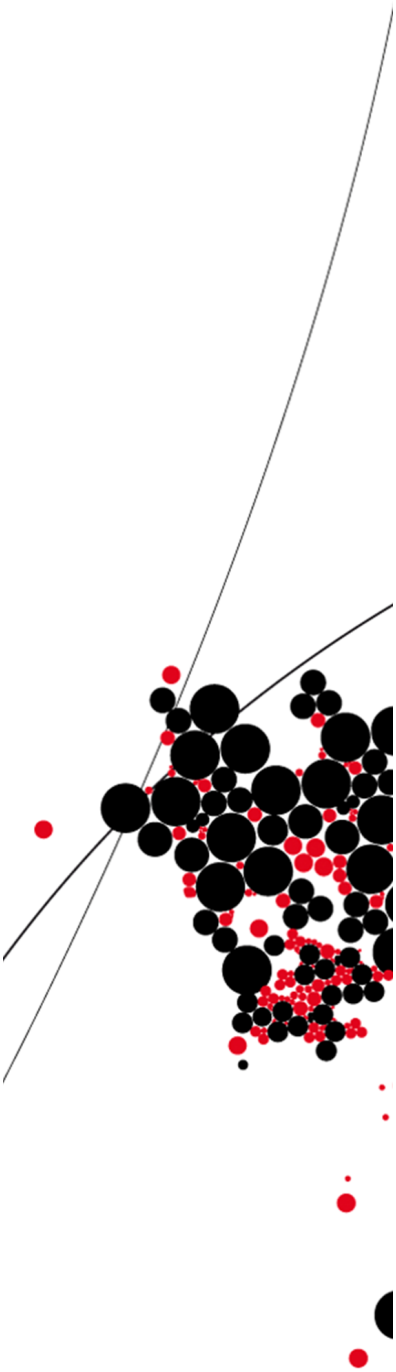

Usadel equation for a four terminal junction

T.H. Kokkeler

M.Sc. Thesis
June 2021

Supervisors:
dr. A.A.Golubov
prof. dr. ir. B.J.Geurts
prof. dr. ir. A. Brinkman

Quantum Transport Matter,
Faculty of Science and Technology
Multiscale Modeling and Simulation,
University of Twente
Faculty of Electrical Engineering,
Mathematics and Computer Science
University of Twente
P.O. Box 217
7500 AE Enschede
The Netherlands

Contents

1 Introduction

In this thesis, a model of the a four terminal SNS junction is investigated. The model predicts outcomes of experiments on spectral supercurrent, total supercurrent, differential conductance and local density of states in junctions with two conventional or unconventional superconductor terminals and two normal metal terminals. The two normal metal terminals are used to change the occupation of electron levels in the junction. The differences between the results for s-wave and p-wave superconducting electrodes is investigated. These differences can be used for experimental verification of the existence of p-wave superconductors, which are predicted to host Majorana fermions [1].
The model used is based on the non-equilibrium Green's function theory. This theory is applied to the four terminal junction in the quasiclassical dirty limit [2], [3]. The model uses Tanaka Nazarov boundary conditions [4] for the superconducting electrodes. The resulting equations in the so-called θ-parametrisation will be derived.
The setup allows for variation to include topological insulators. This is important, both from a theoretical viewpoint and from the viewpoint of applications [1]. For theoretical fundamentals it is important because it has never been proved that p-wave superconductivity exists, for applications it is of interest because in unconventional superconductivity Majorana fermions might exist, which are important for quantum computing.
In this thesis, first a motivation for the work will be given in chapters 2 and 3. The theory behind the model and its application to the junction under consideration will be discussed in chapters 4 to 8. Chapters 9 to 16 include results that can be extracted from the code. Some results are used for validation of the model compared to theory, other results are predictions of the model. The thesis is concluded with a conclusion and an outlook.

2 Energy consumption and computers

Ever since the computer was invented, the computational effort has continuously increased to meet the demand from society. To accommodate this demand, transistors were made more efficient and successively smaller [5]. The number of transistors on a chip has doubled every two years following Moore's law for decades [6], the energy per elementary operation has decreased likewise [5], [7]. In this way, the demand for improvement of performance could be accommodated by exponentially increasing the number of components. However, there is a limit to the size reduction and the energy per elementary operation that can be obtained. There are three different factors that set this limit:

- Technological challenges. Over the course of the previous decades scientists have been able to overcome technological challenges to make transistors smaller and smaller [5]. However, as demand is increasing, the challenges become harder and harder to solve, which means, that it becomes harder and harder to overcome the technological challenges at a rate sufficient to meet the demand [8].
- Quantum effects. If the size of the transistors becomes very small, quantum effects, such as tunnelling, play a role. If the tunnelling probability becomes high, this leads to errors in calculations using classical transistors [9]. This can be overcome by adjusting the way of computation, in order to make use of quantum effects, rather than to be hindered by them. This is the concept of quantum computing.
- Entropy. Lastly, there is a thermodynamic lower bound to computation energy [8], [10]. A computer usually does not execute only one computation in its entire lifetime. After each calculation, the information of a previous calculation must be erased to start a new calculation. Such erasure is not free, Landauer [10] has shown that the erasure of any bit of information is accompanied by a dissipation of at least $kT \ln 2$. This implies that there is a minimum to the energy dissipation per elementary operation.

The end of Moore's law has been predicted before [11], [12]. However, Moore's law has held up for some years after these predictions. Still, progress in the past few years indicates that Moore's law truly comes at its end [5]. The demand for computational resources, on the other hand, is still growing at an enormous rate. It was reported [13] that in the period between 2010 and 2018, the total number of computing instances at data centres has increased by 550%. This has led to an increase of 6% in the energy consumption of these datacentres [13]. These figures are more optimistic than figures for servers world wide. Considering all servers world wide, an increase of 25% in energy consumption has been observed [13]. This figure is in good correspondence with the figures for the US and Europe in a slightly longer period [14], [15]. This shows that electricity consumption per computation has decreased enormously in this period, but that it is still not enough to stabilise electricity consumption. New solutions are required in the form of new materials and/or different ways of computing. A promising solution is the quantum computer. The quantum computer will be introduced in the next section. It will be seen that the quantum computer, instead of being negatively influenced by quantum effects, uses them to become far more powerful.

3 Quantum computing

In this section quantum computing is introduced, some of the numerous advantages are listed, and requirements for the hardware of a quantum computer are listed. In particular, Josephson junctions (subsection 3.1) and Majorana fermions (subsection 3.2.1) will be considered. It will become clear why Majorana fermions are such an opportunity for quantum computers, and how they relate to the research of this thesis. To start, the difference between conventional computers and quantum computers will be discussed. This discussion is by no means sufficient to fully understand the advantage of quantum computers, that is not the goal of this thesis. Rather, the coming section serves to give an intuition as to why quantum computers are different from classical computers. This explanation is mainly based on the work in [16], a useful source for extra reading is [17]. Conventional computers perform computations using bits, which can be either 0 or 1. Thus, for n bits there are 2^n possible sequences. The quantum computer, instead of bits uses qubits. The state of n qubits is much more diverse - in fact, it can not only be any of the 2^n states possible for bits, but also any superposition of these states. For example, the possible state for two qubits are

$$|\psi\rangle = a\,|11\rangle + b\,|10\rangle + c\,|01\rangle + d\,|00\rangle \tag{3.1}$$

$$|a|^2 + |b|^2 + |c|^2 + |d|^2 = 1 \tag{3.2}$$

$$a, b, c, d \in \mathbf{C}. \tag{3.3}$$

Thus, a qubit can be in infinitely many, even uncountable infinitely many, states. For those familiar with the concept of entropy this might be a concern, as it seems the qubit would carry an infinite amount of information. However, this is not the case.
The reason for this is that for qubits, not all states can be distinguished with 100% accuracy, in contrast to bit states. As an illustration of this principle, consider for example a single qubit. To extract information from it, we must do a measurement. A measurement always projects the state onto a single basis state. What these basis states are, can be chosen by the person carrying out the experiment. However, it must always be an orthogonal basis of the space, such as $\{|0>, |1>\}$ or $\{\frac{1}{\sqrt{2}}(|0> + |1>), \frac{1}{\sqrt{2}}(|0> - |1>)\}$. Consider a measurement that projects on the basis $\{|0>, |1>\}$. If the qubit is in state $|0>$, then there is a 100% probability that the measurement will yield the outcome $|0>$, and if the qubit is in state $|1>$, the measurement is certain to yield $|1>$. However, if the qubit is initially in state $\frac{1}{\sqrt{2}}(|0> + |1>)$, then the measurement will yield $|0>$ with a probability of 50% and $|1>$ with a probability of 50%. This measurement thus does not distinguish 100% between $|0>$ and $\frac{1}{\sqrt{2}}(|0> + |1>)$.
Because the states $0>$ and $\frac{1}{\sqrt{2}}(|0> + |1>)$ are not orthogonal to each other, there is no orthogonal basis in which these two states will give a different outcome with a 100% probability. These states can thus never be distinguished with 100% accuracy. This means that a different view on information is needed in quantum mechanics. In quantum mechanics, the concept of Neumann entropy is used, rather than the concept of Shannon entropy, which is used in quantum computing. Neumann entropy is defined by

$$S = -\mathrm{Tr}\rho \log_2 \rho \tag{3.4}$$

$$= -\sum_{\lambda \in \mathrm{eig}(\rho)} \lambda \log_2 \lambda, \tag{3.5}$$

where ρ is the density matrix of the system and $\mathrm{eig}(\rho)$ denotes the set of eigenvalues of the matrix. In a simple example of two qubits, ρ would be a four by four matrix, and thus have four eigenvalues. This will thus be a sum over four eigenvalues, entirely analogous to the classical entropy, where the sum is over the probabilities of the four outcomes.
Thus, this is not where quantum computing makes the difference with classical computers. The advantage of quantum computers compared to normal computers is that the possibility of having a superposition gives much more flexibility for the algorithms that can be designed. To fully grasp this idea, it is best to study an example of a code that works on a quantum computer, but not

on a classical computer, such as the famous Shor's algorithm [18]. This however falls beyond the scope of this thesis. Rather, two examples will be given where quantum computers are essentially different from classical computers, and that are the basis of some important algorithms set up for the quantum computer:

- Suppose can set up the qubit in state $\frac{1}{\sqrt{2}}(|00> + |11>)$. A priori, a measurement of one of the two qubits will yield 0 with a probability of 50% and 1 with a probablity of 50%. However, if one of the qubits is measured, the state of the other is immediately fixed, that is, if the first qubit is measured to be 0, the second must also be 0. This is very useful in establishing a secure communication [16].
- The second example can best be illustrate by adding a third qubit. Consider a function $f : \mathbf{N} \to \mathbf{N}$. Now suppose there is an operation that sends $|000>$ to $|00f(0)>$, $|010>$ to $|01f(1)>$, $|100>$ to $|10f(2)>$ and $|110>$ to $|11f(3)>$. Now suppose that initially we know the qubit is initially in the state $\frac{1}{2}(|000> + |010> + |100> + |110>)$. This qubit is then mapped by the function to $\frac{1}{2}(|00f(0)> + |01f(1)> + |10f(2)> + |11f(3)>)$. From this state one can get the value of f at a single point. However, by applying a suitable measurement, one may also extract information about f at several points at the same time, even though the function f has been applied to only one qubit. This is the principle on which Shor's algorithm is based.

This has several advantages. A few explored in [16] are listed here:

- There are programs that are not in the class P on a classical computer. This means that the problem can not be solved by an algorithm that has a polynomial time complexity, at least. Some of these problems can be computed in polynomial time, or even log-polynomial time on a quantum computer. An example of this is Shor's algorithm, which factorises integers in polynomial time [18]. This means quantum computers break RSA, a widely used method for security in data transmission [19].
- Whereas quantum computers break modern security protocols as RSA, quantum computers allow for new ways of key distribution. These new key distribution protocols are secure, as it is not possible to copy the information without the receiver noticing it [20].
- Quantum computers can simulate more complex dynamics than classical computers. This enables quantum field theories to be tested. It is widely believed that a classical computer can not simulate a quantum computer, which would imply that a quantum computer can perform significantly more complex simulations than a classical one [21], [22].

With this, the reader has an idea as to why quantum computers are much more powerful than classical computers. Quantum computers are however, not yet widely used today. This is because quantum computers are hard to make, having a good and reliable qubit is hard. Potential systems that can serve as qubits need to satisfy the following conditions:

- The qubit can assume two different states. This is needed for computation.
- These states are at most weakly coupled to other states, otherwise the information is lost on small timescales. If the coupling is weak, the qubits will be reliable over a long time span.
- It must be possible to switch and measure the state of the qubit in order to encode information.
- The objective is too have as less dissipation as possible, a primary objective is too have at least less dissipation than a classical computer.

These conditions are very hard to meet. Over the years many systems have been proposed to serve as qubits, such as the helicity of photons, the electron spin, the nuclear spin, quantum dots, and also Josephson junctions with Majorana particles. Here, we pursue the latter option. In the next section the Josephson junction and Majorana particles will be introduced, and it will be indicated why this is a good platform for qubits.

3.1 Josephson junctions

Superconductors are described by a superconducting energy gap and the order parameter, which can be interpreted as the number of Cooper pairs. Cooper pairs are the carriers of the supercurrent, the current that can flow without an applied bias voltage [23]. These concepts will be discussed in more detail in the discussion of the microscopic theory of superconductivity in section 4. If a superconductor comes in contact with a material that is not superconducting, these Cooper pairs can penetrate in this material over a short distance. This has important consequences. If the non-superconducting material is thin compared to the penetration depth of the Cooper pairs, and is sandwiched between two superconductors, Cooper pairs may travel between these two superconductors, in that case we call these superconductors coherent. The structure just described is called a Josephson junction, named after the scientist who predicted and measured the effects Josephson junctions [24], [25]. More shortly, Josephson junctions are weak links between two superconductors. This weak link, in which superconductivity is suppressed, may be a normal metal, an insulator, or even a superconductor that is not in the superconducting state [23]. In a Josephson junction there can still be a supercurrent, that is, a current which generates no voltage, even though there is a non-superconducting material in the junction. The superconductors thus induce superconductivity in the non-superconducting material. This is called the proximity effect. In this thesis the proximity effect will be investigated for a special type of Josephson junction, a Josephson junction with two extra terminals, which are normal metal terminals. The advantage of these extra terminals is that they can be used to influence the transport properties of the junction. This will be discussed in section 15.
Josephson junctions are interesting for several reasons. A first reason is that new physics can be explored, be it in the superconductors itself or in the material that constitutes the weak link. For that goal, nowadays junctions with all sorts of weak links with special material properties, such as ferromagnetic material or a topological insulator are investigated [26], [27]. A second reason is that Josephson junctions can be used in technologies, for example in Squid devices [28], with which magnetic fields can be measured with high accuracy.

3.2 Majorana particles

Now that Josephson junctions have been introduced, attention will shift to Majorana particles. The concept of Majorana particles will be explained using relativistic quantum mechanics.
The first equation that is taught in quantum mechanics is the Schrödinger equation. The Schrödinger equation is a non-relativistic equation, that is, it is only valid in the regime where the velocity is much smaller than the light velocity c and potential energies are much smaller than the energy mc^2 associated with the mass m of the particle. In relativistic systems a different equation is needed. The relativistic counterpart of the Schrödinger equation is the Dirac equation [29]:

$$(i\gamma^\mu \partial_\mu - m)\psi = 0. \tag{3.6}$$

This equation contains some short hand notation that deserves some explanation. The Einstein summation convention was used, that is, $\gamma^\mu \delta_\mu$ is short for $-\gamma^0\delta_0 + \sum_{i=1}^{3} \gamma^i \delta_i$. The function ψ is the 'wavefunction', called spinor for the Dirac equation, ∂_0 is a time derivative and ∂_i, $i = 1, 2, 3$ are spatial derivatives. The matrices $\gamma^0 = \begin{bmatrix} \mathbf{1} & 0 \\ 0 & -\mathbf{1} \end{bmatrix}$ and for $i = 1, 2, 3$ $\gamma^i = \begin{bmatrix} 0 & \sigma^i \\ -\sigma^i & 0, \end{bmatrix}$ where σ^i are the Pauli matrices:

$$\sigma^1 = \begin{bmatrix} 0 & 1 \\ 1 & 0 \end{bmatrix}$$
$$\sigma^2 = \begin{bmatrix} 0 & -i \\ i & 0 \end{bmatrix}$$
$$\sigma^3 = \begin{bmatrix} 1 & 0 \\ 0 & -1 \end{bmatrix}$$

.

The Dirac equation is thus a equation for spinors with four entries. An important aspect of Dirac's equation is that it follows from this equation that every particle has an antiparticle, a particle with the same mass, but opposite charge and helicity [29].
Examples of antiparticles are the electron and the positron. An interesting question is whether there are particles that are there own antiparticles. The answer to this question is not yet unambiguously given. Theoretically this is allowed, as the Italian scientist Majorana has shown [30]. Named after him, fermions that are their own antiparticle are named Majorana particles or Majorana fermions. However, up to now no elementary particles have been proven to be Majorana particles, though there has been debate even in the most recent years on whether neutrino's might be Majorana fermions [31], [32].
In this thesis, the possibility of existence of elementary Majorana particles is not of interest. In condensed matter physics apart from particles, also quasiparticles exist. Quasiparticles are excitations of a material from the ground state, the lowest energy state, that behave similar to elementary particles [33]. Also quasiparticles can have antiparticles. The existence of these antiparticles can be argued very intuitively. At zero temperature, electrons fill the lowest energy states in a material. This means that there is a level below which all states are occupied, and above which all states are filled. This level is called the Fermi level. An excitation can be a particle that is added to the system and occupies one of the unoccupied states above the Fermi level. However, there is also an excitation if one of the particles present in the ground state, that is, a particle from below the Fermi level, is removed. The antiparticle of the quasiparticle is then a quasiparticle that has reversed charge, spin and energy with respect to the Fermi level. For example, in condensed matter physics, the antiparticle of an electron is a hole. Thus, analogously, the Majorana quasiparticle can be defined. From the definition of antiparticles of quasiparticles and Majorana particles, it follows that Majorana quasiparticles must be at the Fermi level, this will be called the zero energy condition. There is much debate on whether Majorana quasiparticles have already been observed [34], [35], [36], [37], [38].
With this, Majorana particles and quasiparticles have been introduced. As indicated, elementary Majorana particles are not of interest. This means that notation can be simplified greatly. In this thesis, condensed matter physics is studied. Therefore, the term Majorana particle will here refer to zero-mode Majorana quasiparticles, that is, zero charge particles that have the Fermi energy. In some literature, particles which do not have zero energy, but do satisfy all other properties to be a Majorana fermion are also called Majorana fermions. A short comment on the reason for this convention will be given in the section below in the discussion of Kitaev's model. This convention will however not be followed here, because it is of no importance for the rest of this thesis. In case an elementary Majorana particle or a quasiparticle with non-zero energy is considered this will be mentioned explicitly.

3.2.1 Realising Majorana fermions

Now that Majorana fermions have been introduced, it will be explained what are suitable platforms for a Majorana fermion.
Majorana fermions are difficult to realise experimentally. Majorana fermions need to be chargeless. This is difficult because in most materials the excitations do have a nonzero-charge. There are however, materials for which some of the excitations have a vanishing charge. A known platform for such chargeless excitations are superconductors [23]. There are, however, two reasons why Majorana fermions were not observed in the earliest found superconductors:

- In a conventional superconductor there is spin degeneracy, so antiparticles have opposite spin. To have Majorana particles, the system should be made effectively spinless, that is, only one spin degeneracy should be present near the Fermi level.
- The earliest found superconductors have a gap in their energy spectrum, that is, there are no states at the Fermi level.

The first of these problems can be overcome by applying a magnetic field. By applying a magnetic

field, particles with opposite spins get vastly different energies, which means that near the Fermi level, there is only one spin polarisation, and the system behaves effectively spinless. The second, however, is less trivial. There are ways to overcome this problem:

- Using a special type of superconductors. The superconductors found in the first half of the twentieth century are nowadays called conventional superconductors or s-wave superconductors. This last term refers to the isotropy of the state, similar to the notation used in quantum mechanics [39], and already earlier in chemistry. For a long time, it was assumed that this was the only type of superconductivity [23]. With the discovery of a superconductor which was later found not to have an isotropic superconducting potential in 1979 [40] and the discovery of high temperature superconductivity [41] however, the perspective changed, also other states are possible, such as p-wave [42], [43] and d-wave [44], [45] superconductors. Those unconventional superconductors have special properties, for example p-wave superconductors, for which there is no energy gap in certain directions [46]. P-wave superconductors will play an important role in this thesis.
- The second option is using the proximity effect that has been introduced above. It is predicted that in suitable materials this might result in p-wave superconductivity. Also the proximity effect will play an important role in this thesis. Not only to create platforms for Majorana fermions, but also for a method to distinguish the p-wave superconductors from s-wave superconductors.

By now, possible platforms for Majorana particles have been listed. To back the hypothesis that p-wave superconductors are a good platform, a theoretical model by Kitaev [46] will be revisited. With this model it was shown that in a theoretical p-wave superconductors Majorana fermions do indeed exist. This calculation will be briefly reviewed here, as it can also be used to highlight a property of Majorana fermions very convenient for quantum computing.
The derivation starts with the following Hamilitonian for a chain of L atoms

$$H = \sum_{j=1}^{L-1} -w(a_j^\dagger a_{j+1} + a_{j+1}^\dagger a_j) + \Delta a_j a_{j+1} + \Delta a_{j+1}^\dagger a_j^\dagger - \sum_{j=1}^{L} \mu(a_j^\dagger a_j - \frac{1}{2}). \tag{3.7}$$

Here, a_j is the annihilation operator on site j, $a_j^\dagger$ the creation operator on site j, Δ the superconducting gap, here assumed real, μ the chemical potential, and w the hopping parameter. The term s in this Hamiltonian can thus be interpreted as follows. The first term represents hopping from site $j+1$ to state j, the second term the reverse direction. The last term presents the energy of a particle at a certain site, $a_j^\dagger a_j$ is 1 if there is a particle in state j and 0 otherwise. The terms with Δ are the terms that are responsible for the superconductivity.
The Hamiltonian in equation (3.7) looks complicated, but can be made much more simple. It is convenient to do a transformation of operators in the Hamiltonian of Kitaev's model. The operators $c_{2j-1} = \frac{1}{2}(a_j + a_j^\dagger)$ and $c_{2j} = \frac{1}{2i}(a_j - a_j^\dagger)$ namely satisfy the relation $c_k = c_k^\dagger \quad \forall k$. They can thus be interpreted as (not necessarily zero energy) Majorana operators in the sense that the creation operator $c_k^\dagger$ equals the annihilation operator c_k. Because $a_j = c_{2j-1} + ic_{2j}$, the c-operators are also called half fermions in literature. The Hamiltonian can be written in terms of c_k as

$$H = \frac{i}{2} \sum_{j=1}^{L-1} -\mu c_{2j-1} c_{2j} + (\Delta + w) c_{2j} c_{2j+1} + (\Delta - w) c_{2j-2} c_{2j+1}. \tag{3.8}$$

The first term involves only c_{2j-1} and c_{2j}, which are linear combinations of a_j and $a_j^\dagger$. This is thus an interaction that only takes place on site j. This means that it is an energy term, in correspondence with the representation in a. The other two terms couple fermions on neighbouring sites, the second term involves c_{2j}, a linear combination of a_j and $a_j^\dagger$, and c_{2j+1}, a linear combination of a_{j+1} and $a_{j+1}^\dagger$, and thus couples sites j and $j+1$, the third couples sites j and $j-1$.
Now, for computational simplicity, consider the case $\mu = 0, w = \Delta$. Then the Hamiltonian reduces

to

$$H = i\Delta \sum_{j=1}^{L-1} c_{2j} c_{2j+1}. \tag{3.9}$$

The most important aspect of this new Hamiltonian is that c_1 and c_{2L} do not appear in the Hamiltonian, thus c_1 and c_{2L} are the desired zero-energy modes in this theoretical model. These are thus Majorana fermions that would exist at the edges of the chain. With this it has been shown that Majorana fermions can exist in a p-wave superconductors.
With this however, the derivation is not yet completely done. The derivation above holds for a very specific set of parameters. If μ or $w - \Delta$ is finite, the formalism changes slightly, but it remains true that near the ends of the wire there are modes of zero energy. A difference is that for finite μ or $w - \Delta$, the localisation is not exact, the fermions are not only found at locations 1 and N, the mode decays rather exponentially [46]. Striking here is that c_1 and c_{2L} are each located at a different end of the wire, so they are spatially separated. This is important, as this means that there is no local interaction possible between the two Majorana fermions, which would give them a nonzero energy. If the localisation is exact, as in the case of $\mu = w - \Delta = 0$, the length of the wire is of no influence. In all other conditions, the length of the wire should be much larger than the decay length of the Majorana modes.

3.3 Majorana fermions and quantum computing

Now that Majorana fermions have been introduced, it can be considered what makes them convenient for quantum computing. First, it will be shown that a system with a Majorana particle is a qubit, afterwards, it will be argued that this is a very robust qubit, following the requirements put forward in section 3.2.1.
Consider a physical system that can host a Majorana particle, described by $\gamma_1 + i\gamma_{2L}$ as in the previous section. Let $|0\rangle$ be a groundstate of the system. Then $|1\rangle = (\gamma_1 + i\gamma_{2L})\,|0\rangle$ is another state. Because Majorana fermions have no energy, states, $|1\rangle$ and $|0\rangle$ have the same energy. This means that also state $|1\rangle$ is a ground state of the system. The difference between the two states is that an electron is added, thus, in one of the two states there is an even number of electrons, whereas in the other there is an odd number of electrons. It can be concluded that this system behaves as a two-level system with two levels at the same energy, a qubit [47].
An advantage of a qubit constructed in this way is that a decoherence error can only occur via interactions that involve two Majorana particles. Because the Majorana particles are well separated, this is an unlikely event. Thus, quantum computing via Majorana fermions is robust against decoherence. Moreover, also the zero-energy mode is very robust. Because of the particle-hole symmetry of the superconductor, a state at energy $+E$ is always accompanied by a state at energy $-E$. Because the Majorana-state is only one state (it changes the parity), the only possibility is that for this state $E = -E$, that is, $E = 0$. This means that upon applying an extra interaction, the Majorana will still exist. This lies at the heart of the generalisation of Kitaev's model to nonzero μ and $\Delta - w$ discussed in the previous section. The only local ways the Majorana can be disturbed is if two different Majorana fermions can interact, in which case there is a, usually very small, energy splitting [47].
Now suppose there is an energy gap for excitations, which is the case in superconductors. Then at low temperatures there is only a very small coupling to other states. This means that there is also only a small decoherence due to these other states.
Thus, it has been shown that Majorana fermions satisfy many of the conditions for potential qubits listed in section 3.2.1. What has not been discussed so far is the third of these conditions, whether the state of the system can be switched and measured. Switching and measuring the state of a Majorana-based qubit is harder than in some other proposals for quantum computers [48], but it has been shown that it can be done. The switching even has an additional property that might be useful in computations. Namely, interchanging the Majorana fermions is non-commutative. In this context, this means that when encirling one Majorana fermion with another one, the initial state is

different from the final state. This means that a process is possible that is called braiding. In this thesis, braiding will not be discussed any further, interested readers are referred to [48].

By now, the importance of the development of quantum computers has been discussed, and it has been indicated that unconventional superconductivity and/or the proximity effect are a promising way to create qubits for the quantum computer. In this thesis, the proximity effect is considered in a Josephson junction in the so-called VT geometry, a geometry with extra terminals that will proof convenient in the later parts of this thesis. In the coming sections first the theory of superconductivity will be briefly reviewed and applied to the geometry under consideration.

4 Formalism

In this section the theoretical foundation for the equations used in the rest of this thesis will be laid. There will be two main topics of interest. The first is the phenomenon of superconductivity and the microscopic theory to explain it, to which a short introduction is given in sections 4.1 and 4.2. The second topic is the concept of non-equilibrium Green's functions, which is discussed in the subsequent subsections. The Green's function technique will be adopted to the models that will be motivated in section 5, of which the Usadel equations are central to this thesis.

4.1 BCS theory

Ever since in 1911 Kamerlingh Onnes discovered superconductivity in his laboratory in Leiden [49], the subject has got much attention. In the first half of the twentieth century mainly phenomenological theories where developed [50], [51]. A microscopic theory did not emerge until the late 1950s. This theory is the BCS-theory, which is nowadays still used to explain superconductivity. A short introduction to BCS theory will be given in this section. Here, the main are to introduce terminology often used in superconductivity and to make the reader familiar with the concepts used in the theory. For further background material, the reader is referred to [23], [33], [52], [53] and [54].

An important step to a microscopic theory was the work of Leon Cooper [55]. He showed that an effectively attractive interaction between electrons leads to bound states of two electrons, regardless of the strength of the attractive interaction [55]. The two electrons form a pair, now called a Cooper pair [23]. In 1957 Cooper, together with John Bardeen and Robert Schrieffer, developed a microscopic theory of superconductivity, called the BCS-theory [56], [57]. This theory rests on two main independent ingredients to come to a theory of superconductivity:

- The result obtained the year before by Cooper [55].
- The theory of Fröhlich [58] that was developed a few years earlier. In this theory two electrons are considered, one in state 1 with energy ϵ_1, the other in state 2 with energy ϵ_2. Fröhlich's theory shows that if the energy difference $|\epsilon_1 - \epsilon_2|$ of two states 1 and 2 is less than Planck's constant times the frequency of a possible lattice phonon, exchange of this phonon between the two electrons leads to an attractive interaction.

The BCS theory used Fröhlich's theory to account for the attractive interaction between electrons that is required in Cooper's theory. Combining the two results, the potential proposed in the BCS theory is

$$V_{kk'} = \begin{cases} -V & |\epsilon_k - \epsilon_{k'}| < \hbar\omega_D \\ 0 & |\epsilon_k - \epsilon_{k'}| > \hbar\omega_D, \end{cases} \tag{4.1}$$

where ϵ_k denotes the energy of an electron with wavenumber $\vec{k}$, ω_D is the Debye frequency, that is, maximum frequency of phonons carried by the underlying lattice, and thus the maximum frequency for which the phonon interaction renders the total potential effectively attractive according to Fröhlich's model [58]. The attraction has strength V. This parameter varies from material to material, and determines whether a material is a superconductor.

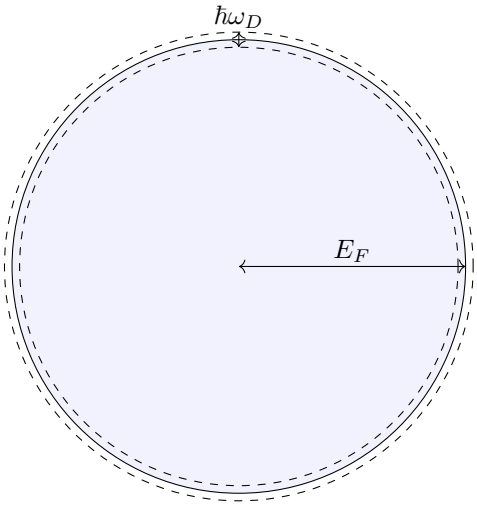

Figure 1: Illustration of superconductivity. The filled circle represents all states occupied in occupied, that is, with energy below E_F. The dotted circles indicate the electrons for which there is attraction, in a energy range $\hbar\omega_D \ll E_F$.

Next to the attractive interaction predicted by Fröhlich, there is also a repulsive electron-electron interaction, the Coulomb repulsion [59]. If V is small compared to the strength of these repulsive interactions, the attraction from Fröhlich's model is overcome by repulsive electron-electron interactions, and the material does not show superconductivity. If V is large compared to the strength of repulsive interactions, the material is a superconductor, and V controls the size of the superconducting gap. The strength of the Coulomb repulsion depends on the free electron density [54]. A larger electron density means a larger Coulomb repulsion. Thus, superconductors tend to have a low free electron density, and are generally bad conductors in the normal state [54].
Next to this, following [55], it was assumed that electrons form pairs in the ground state. The ground state and energy excitations of interacting electron pairs in a lattice can be calculated from the proposed potential (4.1) and occupancy rule. Here, a short description of such calculation will be given, following [23]. For simplicity of calculation, the repulsive interactions are ignored. First, a bit of terminology needs to be introduced. In the following sections, knowledge of quantum mechanics, on the level of the first few chapters of [39], is assumed. The terminology will also play a role in later stages. The term state can refer to two different concepts. There are the single particle states, that can either be occupied or not occupied. Then there is the system state, that describes which states are occupied and which states are unoccupied. The ground state is the lowest energy state, in which all single particle state below a given energy, called the Fermi energy, are occupied, whereas all single particle states above the Fermi energy are unoccupied. This is the system state assumed at zero temperature.
Now denote system states in which all single particle states have an occupation probability 0 or 1 as occupation states. In general, the state of the system consists of a superposition of those occupation states. Using Cooper's argument [55], state $\vec{k}$ can only be occupied if state $-\vec{k}$ is occupied. Following the notation of [23], denote the amplitude of states $(k, -k)$ by v_k. The occupation probability is then v_k^2, the probability that the states are not occupied is $u_k^2 = 1 - v_k^2$. If the energy of the single particle state is ϵ_k, than occupation of states $(k, -k)$ contributes $2\epsilon_k v_k^2$ to the energy of the system. The factor of 2 arises here because both single particle state k and single particle state $-k$ contribute. Their energy is the same as there is no angular dependence in the system, the energy of a state only depends on the magnitude of k. The interaction V couples states in which $(k, -k)$ is occupied and $(k', -k')$ is not occupied with states for which the reverse holds true. These terms thus give a contribution $(u_k v_{k'})V_{kk'}(v_k u_{k'})$. In conclusion, the energy of

the system can be written as

$$E_s = \sum_k 2\epsilon_k v_k^2 + \sum_{k,k'} V_{kk'} v_{k'} u_k v_k u_{k'}. \tag{4.2}$$

In the expression of the summand the first term is the energy of the electron that it would have if the attractive interaction were not present. The second term represents the energy due to the interaction.
This expression can subsequently be minimised [23] to find that in the ground state

$$v_k^2 = \frac{1}{2}\left(1 - \frac{\epsilon_k}{\sqrt{\epsilon_k^2 + \Delta^2}}\right), \tag{4.3}$$

where $\Delta = V \sum_k v_k u_k$ is the so-called superconducting potential of the superconductor [23]. The importance of this formula is that v_k is neither 0 nor 1. This is in contrast to normal metals, in which single states are either occupied, or not-occupied in the ground state.
Bardeen, Cooper and Schrieffer found that any excitation from this ground state has an energy of at least 2Δ. This implies the existence of a gap [57]. The factor 2 arises here because the excitation breaks up a pair of electrons, the energy per electron is thus Δ for the smallest energy excitation. This means that there is a nonzero energy barrier for scattering. Thus, this theory explains the absence of low energy scattering which would otherwise give rise to resistance in a normal metal. The excitations were given an interpretation as quasiparticles, that is, quantities that behave very similar to elementary particles, by Bogoliubov [60]. This means that the underlying theory of quasiparticles [33] can be used for superconductivity.

4.2 Unconventional superconductivity

In section 3.2.1 it was noted that there exists conventional and unconventional superconductivity. Here, 'conventional' superconductivity refers to superconductivity as described by BCS theory in which phonon exchange induces an effective attracting potential between pairs of interacting electrons.
As can be understood from equation (4.1), the BCS-theory assumes that the superconducting interactions are isotropic. In the 1960s this described all known superconductors, except small corrections due to non-isotropic crystal structures. However, in 1979 a superconductor was discovered which was later found not to have an isotropic superconducting potential [40]. A few years later, high temperature superconductors were discovered [41], of which many, such as the famous YBCO material, are not isotropic either [61]. Apart from superconductors with an isotropic potential, nowadays called conventional or s-wave superconductors, also other types were found or predicted to exist. These are labelled analogously to the different angular momentum states of an H atom: s,p,d,f ... A two-dimensional illustration is shown for s-wave and p-wave superconductors in figure 2. For d-wave superconductors a conclusive confirmation of existence was presented in [44]. Such confirmation is not available for possible p-wave superconductors. There are indications that Sr_2RuO_4 is a p-wave superconductor [62]. However, the evidence is not conclusive and there is debate on the nature of superconductivity in this material [43], [63], [42], [64]. Even though the attractive interaction in unconventional superconductors is not attributed to interactions via the exchange of phonons, as in Fröhlich's theory, the description of unconventional superconductors does not differ greatly from the description of conventional superconductors. In fact, only the potential $V_{k,k'}$ in equation (4.1) is proposed to be direction dependent. With this extension, the analysis can proceed largely as for conventional superconductors with technical developments in the theoretical analysis that involve the systematic use of Green's function formalism. This aspect will be addressed next.

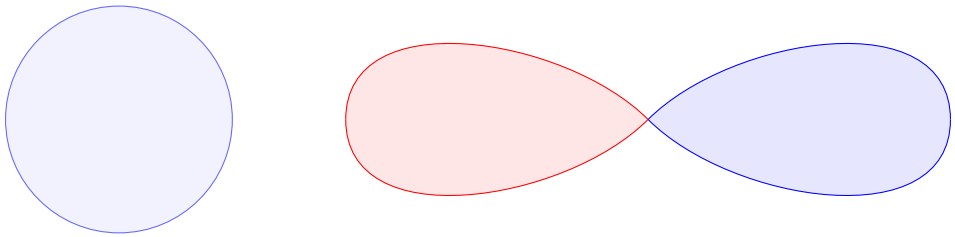

Figure 2: A two dimensional illustration of the pair potentials of s-wave (left) and p-wave (right) superconductors. For s-wave superconductors, the pair potential is isotropic, for p-wave superconductors, the pair potential has a strong angle dependence, $\Delta = \Delta_0 \cos\phi$, where ϕ is the angle made with a horizontal line. Colour coding has been used to indicate the sign of Δ. Note that a negative sign of Δ does not mean there is repulsion instead of attraction. Namely, $\Delta = V \sum_k v_k u_k$, that is, the sign of Δ also depends on the sign of $\sum_k v_k u_k$. It is this latter quantity that is negative if Δ is negative.

4.3 Green's functions

Now that the theory of superconductivity has been discussed, the second main topic of this section will be introduced, that is, the concept of Green's functions. First the concept of Green's functions in its own right will be discussed. In the next subsection the application to problems in superconductivity will be discussed, using so-called non-equilibrium Green's functions. The latter are needed for the description of transport problems. For further information on the use of the Green's function technique in physical problems, the interested reader is referred to [33].
Green's functions can be used to define a solution method for quite general partial differential equations. As such, these functions can be used for Hamiltonian systems. Given a Hamiltonian H, a Green's function $G(r, r')$, where $r = (t, x)$ contains both temporal and spatial coordinates, satisfies the equation

$$HG(r, r') = \delta(r - r'), \tag{4.4}$$

where $E \in \mathbb{R}$ is a scalar that is interpreted as the energy of the system. The Green's function can thus be interpreted as a generalisation of the impulse response of a system. If the Green's function of the system is known than equations of the form

$$Hu = F, \tag{4.5}$$

can be solved via

$$u = \int G(r, r')F(r')dr'. \tag{4.6}$$

This is not the only convenient aspect of Green's functions. From a Green's function also physical quantities, such as the density of states can be extracted. It is this latter use of Green's functions that will be important in the coming sections.
For a given Hamiltonian the Green's function is not uniquely defined, there is redundancy. In case of electronic systems the Green's functions of interest are the retarded Green's function G^R and the advanced Green's function G^A, which satisfy

$$HG^{R,A} = \delta(r - r'). \tag{4.7}$$

Next to this, also the electron correlation function $G^<$ and the hole correlation function $G^>$, which satisfy

$$HG^{>,<} = 0, \tag{4.8}$$

are often used to extract physical quantities. These four functions can be expressed as:

$$G^R(r,r') = \begin{cases} -i(\langle \Psi(r)\Psi^\dagger(r')\rangle + \langle \Psi^\dagger(r')\Psi(r)\rangle) & t > t' \\ 0 & t < t' \end{cases}. \tag{4.9}$$

$$G^A(r,r') = \begin{cases} i(\langle \Psi(r')\Psi^\dagger(r)\rangle + \langle \Psi^\dagger(r')\Psi(r)\rangle) & t > t' \\ 0 & t < t' \end{cases}. \tag{4.10}$$

$$G^<(r,r') = i\langle \Psi^\dagger(r')\Psi(r)\rangle. \tag{4.11}$$

$$G^>(r,r') = -i\langle \Psi(r)\Psi^\dagger(r')\rangle. \tag{4.12}$$

In this expression Ψ is the electron annihilation operator, while $\Psi^\dagger$ is the electron creation operator [2], the Hermitian conjugate of the annihilation operator. The notation $\langle ... \rangle$ is used to denote expectation values. This ensures that the Green's functions are functions, not operators.

4.4 Green's functions in superconductivity

In this section the application of Green's functions to superconductivity will be explained. This description is based on the theory presented in [2], [3]. The notation used in these articles is closely followed.

The idea to use Green's functions to solve problems in BCS theory is due to Gorkov [65]. In superconductivity the Green's function technique is slightly modified to describe the correlation of the Cooper pairs, the electrons paired via Cooper's interaction. In BCS-theory, there is a relation between the occupation of a state with momentum $\hbar\vec{k}$ and spin up $\left|\vec{k}\uparrow\right\rangle$ and the state with momentum $-\hbar\vec{k}$ and spin down $\left|-\vec{k}\downarrow\right\rangle$. In real materials, the eigenstates of the Hamiltonian are not necessarily momentum states. However, there is still a strong correlation between pairs of electrons. Therefore, in Green's functions in superconductivity, instead of using a single particle wavefunction Ψ, the vector-valued two particle function, called the Nambu spinor [23] $\Psi = \begin{bmatrix} \psi_{k\uparrow} \\ \psi^\dagger_{-k\downarrow} \end{bmatrix}$ is used. Here, $\psi_\uparrow$ is used to denote the annihilation operator of an electron with spin up, $\psi^\dagger_\downarrow$ a creation operator of an electron with spin up. Here, often the electron-hole correspondence is used. The creation operator of an electron, is the annihilation operator of a hole. Thus, one could say that Ψ contains two annihilation operators, one for an electron with spin up and momentum $\hbar k$, one for a hole with spin down and momentum $-\hbar k$. Note here that an electron with momentum $\hbar k$ and a hole with momentum $-\hbar k$ have opposite charge, and opposite velocity, they have thus the same current contribution.

Similar, to the case discussed in the previous section, Ψ is called an annihilation operator, and $\Psi^\dagger$ a creation operator. The space of these Nambu spinors is called Nambu space. Instead of a $\mathbb{C}$-valued, the equilibrium Green's function used for superconductivity is thus $\mathbb{C}^{2\times 2}$-valued [23], [33], [2]. The function is represented in position space rather than momentum space:

$$\mathbf{G}(x,x') = \langle T\Psi(x)\Psi^\dagger(x')\rangle = \begin{bmatrix} \langle T\psi_\uparrow(x)\psi^\dagger_\uparrow(x')\rangle & \langle T\psi_\uparrow(x)\psi_\downarrow(x')\rangle \\ -\langle T\psi^\dagger_\downarrow(x)\psi^\dagger_\uparrow(x')\rangle & -\langle T\psi^\dagger_\downarrow(x)\psi_\downarrow(x')\rangle \end{bmatrix}. \tag{4.13}$$

Analogous with the single-particle Green's function, this Green's function satisfies $HG = I\delta(r-r')$, where I is the identity matrix. The minus signs on the lower entries are in place because the first entry contains an electron creation / hole annihilation operator rather than an electron annihilation operator [3]. Here T denotes the time-ordering operator, that ensures that time is increasing from right to left. Thus, due to the time-ordering operator, operators at earlier times are applied first. The space of possible outcomes is called the Gorkov-Nambu space. The diagonal entries are the single-particle Green's functions , however, the off-diagonal entries are different. These are called the pair amplitudes. This is most easily viewed in momentum space, $\langle \psi_{k\uparrow}\psi_{-k\downarrow}\rangle$. In previous

sections, it was indicated that pairs of single particle states are occupied with a probability u_k that is neither 0 nor 1 at zero temperature. This is in contrast with a normal system state, in which all single particle states below the Fermi level are occupied with probability 1, and all those above the Fermi level are occupied with probability 0 at zero temperature. System states in which levels are either occupied with probability 1 or with probability 0 are labelled $\tilde{\Psi}_1, ..., \tilde{\Psi}_n$. These will be called occupation states. These occupation states are all orthogonal, that is, their inner product vanishes. The system state in a normal metal is $\tilde{\Psi^N} = \tilde{\Psi}_i$ for some $i \in 1, .., n$, the superconducting system state will be described by $\tilde{\Psi^{SC}} = \sum_{j=1}^{n} \alpha_j \Psi_j$, where α_j are nonzero constants. If now the annihilation operator $\psi_{k\uparrow}\psi_{-k\downarrow}$ is applied to these system states, all system states in which the pair is not present will be sent to the zero vector, all system states in which the pair is present will be sent to a system state in which the pair is not present. Thus, for each individual occupation state i, it holds that $\left\langle \tilde{\Psi}_i \middle| \psi_{k\uparrow}\psi_{-k\downarrow}\tilde{\Psi}_i \right\rangle = 0$. This immediately implies that $\left\langle \tilde{\Psi^N} \middle| \psi_{k\uparrow}\psi_{-k\downarrow}\tilde{\Psi^N} \right\rangle = 0$. However, for the superconductor we have a sum over occupation states, and $\psi_{k\uparrow}\psi_{-k\downarrow}\tilde{\Psi}_i$ will be included in the sum. Thus, for normal metals, $\left\langle \tilde{\Psi^N} \middle| \psi_{k\uparrow}\psi_{-k\downarrow}\tilde{\Psi^N} \right\rangle$ vanishes, whereas for superconductors the quantity will be nonzero.

4.4.1 Non-equilibrium Green's functions

The Green's function technique described in the previous paragraphs is suited well for the description of systems that are in equilibrium. From the Green's functions the density of states, that is, the density of available levels for electrons in energy space, and the spectral supercurrent, that is, the dissipationless current carried by the levels if they are occupied, can be calculated. In equilibrium, the occupation of the levels is given by the Fermi-Dirac distribution, and the description of the system is thus complete. However, in non-equilibrium systems, the occupation of levels is not given by the Fermi-Dirac distribution, and therefore, transport can not be described within the equilibrium Green's function technique. In Josephson junctions, also transport should be described. To obtain a kinetic equation, that is, an equation that describes transport, the non-equilibrium Green's function technique is used [3], [66]. In the equilibrium Green's function there is one definite time ordering. In the non-equilibrium Green's function also other time orderings are considered. In this way, also charge and current can be calculated [2], [3]. The non-equilibrium Green's function can be introduced as [3]

$$G = \begin{bmatrix} G^{\alpha\alpha} & G^{\alpha\beta} \\ G^{\beta\alpha} & G^{\beta\beta} \end{bmatrix}, \tag{4.14}$$

where

$$G^{\alpha\alpha} = -i\langle T\Psi(r)\Psi^\dagger(r')\rangle. \tag{4.15}$$
$$G^{\alpha\beta} = i\langle \Psi^\dagger(r')\Psi(r)\rangle = G^<. \tag{4.16}$$
$$G^{\beta\alpha} = -i\langle \Psi(r)\Psi^\dagger(r')\rangle = G^>. \tag{4.17}$$
$$G^{\beta\beta} = -i\langle \tilde{T}\Psi(r)\Psi^\dagger(r')\rangle. \tag{4.18}$$

Apart from the time ordering discussed previously, here also $\tilde{T}$, the opposite time ordering operator is used. The operator $\tilde{T}$ places the earliest time to the left instead of the right. The two off-diagonal elements have no time-ordering operators This Green's function satisfies

$$\begin{bmatrix} H & 0 \\ 0 & H \end{bmatrix} G = \begin{bmatrix} 1 & 0 \\ 0 & 1 \end{bmatrix}, \tag{4.19}$$

as follows from equations (4.7) and (4.8). The non-equilibrium Green's function listed above contains four components. However, there is a linear transformation possible such that one of the four blocks becomes zero [66], [3]. This linear transformation transforms the non-equilibrium

Green's function into

$$G = \begin{bmatrix} G^R & G^K \\ 0 & G^A \end{bmatrix} \tag{4.20}$$

where, as defined above [2],[3]:

$$G^R(r,r') = \begin{cases} -i(\langle \Psi(r)\Psi^\dagger(r')\rangle + \langle \Psi^\dagger(r')\Psi(r)\rangle) & t > t' \\ 0 & t < t' \end{cases}. \tag{4.21}$$

$$G^A(r,r') = \begin{cases} i(\langle \Psi(r')\Psi^\dagger(r)\rangle + \langle \Psi^\dagger(r')\Psi(r)\rangle) & t > t' \\ 0 & t < t' \end{cases}. \tag{4.22}$$

$$G^K(r.r') = i(\langle \Psi^\dagger(r')\Psi(r)\rangle - \langle \Psi(r)\Psi^\dagger(r')\rangle) \tag{4.23}$$

The diagonal elements of the matrix are the equilibrium Green's functions and contain information on the total density of states. However, a new function appears,

$$G^K = G^> + G^<, \tag{4.24}$$

which is called the Keldysh Green's function [2]. Note that the Keldysh Green's function is only a component of a Green's function, by itself it is notably not a Green's function, it rather satisfies $HG^K = 0$. This follows from equation (4.8).
The Keldysh Green's function is important in the description of the transport properties of the system. Specifically, from G^R and G^A only the total density of states can be extracted, to which the contributions of both electrons and holes is added. Moreover, in $G^K = G^> + G^< = i < \Psi^\dagger(r')\Psi(r) > -i < \Psi(r)\Psi^\dagger(r') >$, the contributions of electrons and holes are subtracted. Thus, G^K measures the total charge, while $G^K v_F$ is an indication of flow of charge, where v_F is the Fermi velocity.

4.4.2 Non-equilibrium Green's functions in superconductivity

Now that non-equilibrium Green's functions and superconductivity have been described, the two concepts can be combined for the description of Josephson junctions. The resulting non-equilibrium Green's function is $\mathbb{C}^{4\times4}$-valued,

$$G(r,r') = \begin{bmatrix} G^R(x,x) & G^K(x,x) \\ 0 & G^A(r,r') \end{bmatrix} \tag{4.25}$$

$$G^X \in \mathbb{C}^{2\times2} \qquad X = R, A, K, \tag{4.26}$$

where $r = (t,x)$ and $r' = (t',x')$ consist of both spatial and temporal coordinates [3]. A partial differential equation for the non-equilibrium Green's function in superconductivity is obtained, in the form of the Gorkov equation of motion [65] [2], [53], based on the Gorkov Hamiltonian. The Gorkov Hamiltonian is based on the principles laid out in this section, but contains a few more terms, which will be explained below. The Gorkov equations of motion read [2], [3]:

$$\left(\left(i\tau_3\frac{\partial}{\partial t} + \frac{1}{2m}(\frac{\partial}{\partial x})^2 - e\phi(r) + \mu\right)\delta(r-s) - \hat{\Delta}(r,s) - \Sigma(r,s)\right) \circledast G(s,r') = \delta(r-r') \tag{4.27}$$

$$G(r,s) \circledast \left(\left(i\tau_3\frac{\partial}{\partial t} + \frac{1}{2m}(\frac{\partial}{\partial x})^2 - e\phi(r) + \mu\right)\delta(s-r') - \hat{\Delta}(s,r') - \Sigma(s,r')\right) = \delta(r-r') \tag{4.28}$$

This equation deserves some explanation. First of all, there is the symbol $\circledast$. This symbol represents a convolution, that is, if k and l are two functions

$$k \circledast l(r,r') = \int k(r,s)l(s,r')ds. \tag{4.29}$$

If an operator is involved in the equation, it should be applied to the first argument if it is applied from the left, and on the second if it is applied from the right. Thus, in equation (4.27), the temporal derivative means $\frac{\partial G(r,r')}{\partial t}$, in equation (4.28) the temporal derivative is $\frac{\partial G(r,r')}{\partial t'}$.

The term $\hat{\Delta}(r,r') = \begin{bmatrix} 0 & \Delta \\ \Delta^* & 0 \end{bmatrix} \delta(r-r')$, where Δ is the superconducting potential as introduced in the previous section, describes the attraction that leads to superconductivity. Lastly, there is the term $\Sigma(r,r')$. This is the material specific self-energy due to scattering events. In the previous subsection the focus was on the attractive interaction by Cooper, but in a real material the Cooper interaction is not the only interaction that plays a role. All other interactions are grouped together in the self-energy. A discussion of this latter quantity will follow in section 5.1.1. Equations (4.27) and (4.28) can be subtracted from each other. This yields

$$[\left(\left(i\tau_3\frac{\partial}{\partial t} + \frac{1}{2m}(\frac{\partial}{\partial r})^2 - e\phi(r) + \mu\right)\delta(r-s) - \hat{\Delta}(r,s) - \Sigma(r,s)\right), G(s,r')]_- = 0, \tag{4.30}$$

where the notation $[\ ]_-$ is shorthand notation for the left hand side of equation (4.27) subtracted by the left hand side of equation (4.28). The spatial derivative term can be written explicitly as

$$[\frac{\partial}{\partial r}, G(r_1,r_2)] = \frac{\partial G}{\partial r_1} - \frac{\partial G}{\partial r_2}. \tag{4.31}$$

This new equation does not have the exact same set of solutions as equations (4.27) and (4.28). If G is a solution of equations (4.27), (4.28), (4.30), then also αG is a solution of (4.30) for all $\alpha \in \mathbf{C}$, but a solution of (4.27) and (4.28) only for one specific value of α. Thus, a normalisation condition is needed when using (4.30). The value of α to be used will be explained in the next section. There, a normalisation for a quantity related to the Green's function is introduced. Also this quantity needs a normalisation and it is convenient to derive the two normalisations together. This normalisation is based on the known solution in bulk superconductivity in equilibrium [2], [65], [67].

With the Green's function technique the density of states, the $(1,1)$-element of G^R, can be calculated. Moreover, the supercurrent, the current that can flow at zero voltage can be calculated [2], [3]:

$$j = -eN_0 \int dE \mathrm{Tr}\langle v_F \tau_3 G^K \rangle. \tag{4.32}$$

Here, the notation $\langle\rangle$ is meant to denote an angular average, v_F is the Fermi velocity and G^K is the Keldysh component. The third Pauli matrix is denoted by τ_3. It appears because of the minus-sign in the lower row in equation (4.13).
With this, the formalism has been introduced, and relevant quantities have been defined. However, it is not convenient to solve the Gorkov equation as it is stated in equation (4.30), it involves convolutions over both time and space. Rather, in the description of the problem under consideration here, transport in a four terminal junction, some approximations can be made. These will be introduced in the following section, leading to the more accessible Usadel formulation. The reason for this is that the Gorkov equations are hard to solve, and the simplified Usadel equations are a description that is good enough for the purpose of this thesis.

5 Approximations

In the previous sections superconductivity and Green's function theory have been introduced. As the Gorkov equation is very demanding computationally, and the level of detail provided by this equation not always required, we look into simplifying assumptions for transport in the diffusive, also called 'dirty', regime on which we focus in this work. There are two main approximations,

- The quasiclassical approximation, which reduces the Gorkov equations to the Eilenberger equations, developed independently by Eilenberger [68] and Larkin and Ovchinnikov [69].
- The dirty limit approximation, which reduces the Eilenberger equation to the Usadel equation, derived by Usadel [70], which is the main model for the work presented here.

The quasiclassical approximation is a well-known approximation form solid state physics [59], and gives an accurate enough [2], [3], though much less computational demanding, description of systems such as the system of interest here.
The dirty limit approximation is made because the junction that will be considered in this thesis is a dirty system, in which the Usadel equation is sufficient to describe the system.

5.1 From Gorkov to Eilenberger simplifications

The Gorkov equation (4.30) is a partial differential equation which in principle can be solved numerically [71], [72]. However, in view of the considerable computational costs and the often unnecessarily fine level of detail, a different method will be pursued in this thesis. The Gorkov equations are simplified first using the quasiclassical approximation. There are two reasons to use the quasiclassical approximation. The first is that solving the Gorkov equations directly was for a long time considered too hard even for a large computer [68]. Nowadays, the computational power of computers has improved and there are efforts to solve the Gorkov equations numerically [71], [72]. The second reason is more compelling. In general $\frac{\Delta}{E_F} \ll 1$ for superconductors [23], which means that the effect of superconductivity will be apparent only in a small region around the Fermi energy, and thus, all momenta will be close to the Fermi momentum. The quasiclassical approximation comes down to fixing the magnitude of the momentum to be the Fermi momentum. In many problems in solid state physics in which the Fermi energy is much larger than the energy of interactions, the quasiclassical approximation is successful in describing the relevant quantities. The full theory gives small corrections, which are here expected to be of order $\frac{\Delta}{E_F}$ [59]. Only very recently the first superconductor that has a critical temperature T_c at room temperature [73] has been found, whereas typical Fermi temperatures T_F are of the order $10^4 - 10^5$ K [59], indicating that $\frac{\Delta}{E_F} \sim \frac{T_c}{T_F} < 0.01 \ll 1$ typically. Thus, the conditions for the quasiclassical approximation are satisfied.
From a different viewpoint, for mesoscopic scales of the order of several tens of nm to mm, the very short wavelength physics is not important. If the superconducting coherence length $\xi = \frac{\hbar v_F}{\pi \Delta}$ is much larger than the Fermi wavelength $\lambda_F = k_F^{-1}$, the wavelength of electrons at the Fermi energy, oscillations with wavelength on the order of the Fermi-wavelength are completely averaged out in relevant physical quantities. The condition $\lambda_F \ll \xi$ is equivalent to the condition $\Delta \ll E_F$ [23].

An assumption for the quasiclassical approximation is that the parameters describing inputs for the system do not vary too rapidly, for else these transitions to states far from the Fermi energy would be possible. Mathematically, this condition is $\frac{\hbar \omega_h}{E_f} \ll 1$, where ω_h is a characteristic frequency in the Fourier decomposition of the input such that the power of inputs with higher frequencies are very small compared to the total input power.
The quasi-classical theory provides a basis to approximate the Gorkov equation by the Eilenberger formulation of superconductivity [68], [74]. In the coming section, the Eilenberger equations will be introduced and further simplified to the Usadel equations [70] in the dirty limit. The works of [2] and [3] will be closely followed.

5.1.1 Self energy

Before the quasiclassical approximation can be made, an expression for the last term on the left hand side in equation (4.27) should be found. This term is called the self-energy term. The self-energy is the contribution to the total energy due to all interactions with other particles that are not explicitly named in the Hamiltonian. In general, this term can be very complicated and non-local. In most cases an exact expression for the self-energy in a metal is not known. However, the most important contribution at low temperatures is the contribution of elastic scattering [3]. Following Fermi's golden rule the self energy Σ is given by

$$\Sigma(p) = N_i N_0 \int \frac{d\tilde{\xi}' d\Omega_{p'}}{(2\pi)^3} |V(\widehat{p}, \widehat{p'})|^2 G(p'), \tag{5.1}$$

where $\tilde{\xi}' = \epsilon_{p'} = \frac{p'^2}{2m} - \mu$, μ is the Fermi level, N_i is the number of impurities per unit volume, N_0 is the density of states, p is momentum, the notation $\hat{p}$ is used to denote the unit vector $\frac{\vec{p}}{|\vec{p}|}$, G is the Green's function transformed to momentum coordinate and V is the interaction potential, Fourier transformed to momentum space. In the so-called Born approximation [3], the self-energy is

$$\Sigma = \frac{\pi}{2\tau} \langle \int d\tilde{\xi} G \rangle_{p_F}. \tag{5.2}$$

Here τ is the material specific impurity scattering time, defined by

$$\frac{1}{\tau} = 2\pi N_0 N_i \int \frac{d\Omega_{p'}}{4\pi} |V(\widehat{p}, \widehat{p'}))|. \tag{5.3}$$

The notation $\langle ... \rangle_{p_F}$ is used to denote the average over the Fermi surface.

5.1.2 Quasiclassical approximation

Now that the self-energy has been defined, the quasiclassical approximations can be made. The quasiclassical approximation is rather technical, and will not be discussed in detail here, rather a short sketch will be given. Interested readers are referred to [2], [3], [68] and [67].
Before the quasiclassical approximation is performed, a suitable transformation will be introduced. The first step is to replace the variables r, r', t, t' by center of mass and difference coordinates R, ρ, t, τ. Note that in both presentations there is a time coordinate t in literature [2],[3], here this convention will be followed. Then a Fourier transform is taken with respect to the variables ρ, τ, introducing momentum p and energy E. In the Fourier representation, the Gorkov equations read

$$-\frac{p}{m} \partial_R G = [-iE\tau_3 + \hat{\Delta} + \frac{1}{2\tau} \langle G \rangle_{p_F}, G]. \tag{5.4}$$

The reader might be used to the idea that the magnitude of momentum and energy are closely related, for example via $E = \frac{p^2}{2m}$. However, in general, for Green's functions, one can vary E and p independently. In the case momentum and energy are closely related, this will appear as a δ-function.
To understand the reasoning behind the quasiclassical approximation, it should be considered what the Hamiltonian actually describes. The Hamiltonian describes only those electrons in the highest occupied levels, close to the Fermi level. The Hamiltonian contains the term Δ, which is only nonzero in the small region around the Fermi level $E_F - \hbar\omega_D < E < E_F + \hbar\omega_D$, where $\omega_D << E_F/\hbar$ is the Debye frequency of the phonons. Also for unconventional superconductors, this term is nonzero only in a small region around the Fermi level. Thus, the electrons described here occupy a correspondingly small region in momentum space, that is, $G_p(p, E, r, t) = \int G(r, r') e^{ip(r-r')} \approx g\delta(p - p_F)$ for some function g. This function does not depend on the magnitude of the momentum, but it does still depend on the direction of momentum, and on the other three variables, $g = g(r, t, E, v_F)$. The quasiclassical approximation now takes this relation to be an exact relation, most often written

as $G = g\delta(\frac{p^2}{2m} - \mu)$, where μ is used to denote the Fermi level. The function g is called the quasiclassical Green's function. It should not depend on $\xi = \frac{p^2}{2m} - \mu$ anymore, but still describe approximately the same system. This is the case if

$$g(p_F, R, E, t) = \frac{i}{\pi} \int d\xi G(p, R, E, t). \tag{5.5}$$

The existence of this integral is non-trivial, distinct approaches to this problem can be found in [68] and [75]. The microscopic Green's function can be inserted in equation (5.4). The δ-function then ensures that all momenta can be evaluated at the Fermi level.

As indicated before, the quasiclassical approximation is to consider all particles at the Fermi level, that is,

$$G \approx g\delta(\tilde{\xi}), \tag{5.6}$$

where $\tilde{\xi} = \frac{p^2}{2m} - \mu$, with μ being the Fermi level. The equation for the function g is called the Eilenberger equation. It can be found by integrating equation (5.4) over $\tilde{\xi}$ and then using that G is very peaked in momentum space, $G \approx g\delta(\tilde{\xi})$ to pull momentum out of the integrals. Note that the other terms can be pulled out of the integrals without any further approximation as they do not depend on $\tilde{\xi}$. The resulting Eilenberger equation reads

$$-v_F \partial_R g(r, v_F, E) = [-iE\tau_3 + \hat{\Delta} + \frac{1}{2\tau}\langle g(r, v_F, E)\rangle_{p_F}, g(r, v_F, E)], \tag{5.7}$$

where $v_F = \frac{p_F}{m}$. This equation is much simpler than the Gorkov equation. The Gorkov equation contained derivatives of four different quantities, here only one spatial derivative remains.

5.1.3 Adiabatic approximation

In general, the expressions in equation (5.7) are Fourier transforms of convolutions as indicated earlier. For the type of convolution used in the Gorkov equation the Fourier transform does not give simple products [3]. In quasi-stationary situations however, these extra terms are very small, and can be neglected from the equation [3]. Many of the problems considered in this thesis are quasi-stationary. That is, they are not stationary because there is a current flowing, but there is continuous time translation symmetry, that is, the system does not change under a time translation $t \to t+a$ for any $a \in \mathbb{R}$. However, for some experiments this does not hold, as is the case for Shapiro steps [76]. If the voltage varies sufficiently slowly, that is, $\frac{\omega}{\Delta} << 1$, the adiabatic approximation can be used and the static Eilenberger equation can be solved at each time instant. If the oscillations are much faster, other techniques are needed. These techniques will not be explored in this thesis since in the systems we consider either oscilations are not present or $\omega/\Delta \ll 1$.
In the coming section, the next, and last step in this series of approximations will be taken, that is, the dirty limit approximation. This will finally lead us to the Usadel equation.

5.2 Normalisation condition

As indicated in the discussion of the Gorkov equation the Green's function should be equipped with a normalisation condition. This normalisation condition is $g^2 = 1$, [69], that is, g is a function whose range lies within the space of matrices in $\mathbb{C}^{4\times4}$ that square to the identity. This can be derived in the adiabatic limit in the case one assumes the Born approximation for the self-energy. Note that for bulk superconductivity, these assumptions are not too restrictive. For bulk superconductivity, the derivation of the quasiclassical Green's function will be presented here, both to validate the normalisation condition and as a showcase of the application of the quasiclassical approximation and its subtleties. As indicated before, the convergence of integrals is such a subtlety. Here, it will be indicated how the integrals can be solved. In the solution method some choices will be needed. For a background of those choices, the reader is referred to [33], [68], [75]. The derivation

presented here is based on the work in [53] and the definition of the quasiclassical Green's function [2]. The derivation proceeds as follows:
First a Fourier transform is used on Gorkov equation (4.27) for both the temporal and spatial coordinates. This is possible because in bulk superconductivity the Green's function should only depend on the difference coordinates $r - r'$ [53]. In the adiabatic limit, this yields

$$(iE\tau_3 - (\frac{p^2}{2m} - \mu) - (e\phi + \Sigma) - \Delta)G = 1, \tag{5.8}$$

$$(iE\tau_3 - \xi - \Phi - \Delta)G = 1, \tag{5.9}$$

where $\xi = \frac{p^2}{2m} - \mu$ as in the previous subsection and $\Phi = e\phi + \Sigma$, where Σ is the self-energy as in the Born approximation. Thus

$$G(E,\xi) = (iE\tau_3 - (\xi + \Phi) - \Delta)^{-1} \tag{5.10}$$

$$= \frac{1}{(\xi+\Phi)^2 + E^2 - \Delta^2} \begin{bmatrix} (\xi+\Phi) - iE & -\Delta \\ -\Delta^* & (\xi+\Phi) + iE \end{bmatrix}. \tag{5.11}$$

From this it can be calculated that

$$\begin{aligned} g(E) &= \frac{i}{\pi}\int_{-\infty}^{\infty} G(E,\xi)d\xi \\ &= \frac{i}{\pi}\int_{-\infty}^{\infty} \left(\frac{1}{(\xi+\Phi)^2 + E^2 - \Delta^2} \begin{bmatrix} (\xi+\Phi) - iE & -\Delta \\ -\Delta^* & (\xi+\Phi) + iE \end{bmatrix} \right) d\xi. \end{aligned} \tag{5.12}$$

First consider the case $E > \Delta$. In that case the integrand has no poles on the real axis, and the integrals can be directly calculated. The term $\frac{(\xi+\Phi)}{(\xi+\Phi)^2+E^2-\Delta^2}$ goes as $\frac{1}{\xi+\Phi}$ for large ξ. The integral is thus not not converging. However, the principal value can be calculated. A motivation for using the principal value is that it results by taking a "high-energy" cutoff [75]. The term is odd, and thus the principal value will be 0. This leaves us with

$$\begin{aligned} g(E) &= \frac{i}{\pi} \begin{bmatrix} -iE & -\Delta \\ \Delta & iE \end{bmatrix} \int_{-\infty}^{\infty} \frac{1}{(\xi+\Phi)^2 + E^2 - \Delta^2} d\xi \\ &= \frac{i}{\pi} \begin{bmatrix} -iE & -\Delta \\ \Delta & iE \end{bmatrix} \frac{1}{\sqrt{E^2-\Delta^2}}\pi \\ &= \frac{1}{\sqrt{E^2-\Delta^2}} \begin{bmatrix} E & -i\Delta \\ -i\Delta^* & -E \end{bmatrix}. \end{aligned} \tag{5.13}$$

Note that the integral in this expression does indeed exist because it falls off as $\frac{1}{\xi^2}$ for large ξ.
Now consider the case $E < \Delta$. In that case the integrand has poles on the real axis and the integration is harder. indicated earlier. Complex integration theory as in [77] can be used. First define $z = \frac{\xi+\Psi}{\sqrt{\Delta^2-E^2}}$. Then the expression for g can be written:

$$-i\pi g(E) = \frac{1}{\sqrt{\Delta^2-E^2}} \int_{-\infty}^{\infty} \frac{1}{z^2-1} dz \begin{bmatrix} -iE & -\Delta \\ -\Delta^* & iE \end{bmatrix} \tag{5.14}$$

$$+ \int_{-\infty}^{\infty} \frac{z}{z^2-1} dz. \begin{bmatrix} 1 & 0 \\ 0 & 1. \end{bmatrix} \tag{5.15}$$

First consider the first of these integrals. As in [77], use the integration contour that consists of the interval $(-\rho, \rho)$ and the circular arc in the upper half plane, with indented contours at $z = -1$ and $z = 1$. It is convention in Green's function theory to have the indentation towards the upper half plane at $z = -1$ and in the lower half plane at $z = 1$ [33]. The reader is referred to [33] for elaboration on this choice. By virtue of lemma 6.1 in [77], the integral over the circular arc vanishes if $\rho \to \infty$. This means the integral equals $-i\pi\text{Res}(-1) + i\pi\text{Res}(1) = \pi i(\lim_{z\to-1} -\frac{1}{z-1} - \lim_{z\to1} -\frac{1}{z+1}) = i\pi$.

The second term is different. Lemma 6.1 in [77] can not be applied here. However, Jordan's lemma can be applied to $\int_{-\infty}^{\infty} \frac{z}{z^2-1} e^{imz} dz$ for all $m > z$. The same integration contour can be chosen. Jordan's lemma [77] indicates that the integration over the circular arc vanishes as $\rho \to \infty$. The residues can be calculated, and in this case, they cancel. Thus, $\int_{-\infty}^{\infty} \frac{z}{z^2-1} e^{imz} dz = 0$ for all $m > z$. This indicates that this term can be ignored. Thus, for $E < \Delta$ the expression for g reads

$$g(E) = \frac{1}{\sqrt{\Delta^2 - E^2}} \begin{bmatrix} -iE & -\Delta \\ -\Delta^* & iE \end{bmatrix}. \tag{5.16}$$

From expressions 5.13 and 5.16 it follows that $g(E)^2 = 1$ for all E. This result, combined with the result that g^2 is constant [69], [74], [67], shows that the normalisation $g^2 = 1$ can be used throughout the system under consideration.
This can be directly deduced from the Eilenberger equation [78]. Recall that the Eilenberger equation reads

$$-v_F \nabla g(r, v_F, E) = [-iE\tau_3 + \hat{\Delta} + \frac{1}{2\tau} \langle g(r, v_F, E) \rangle_{p_F}, g(r, v_F, E)]. \tag{5.17}$$

Now, $\nabla(g^2) = g(\nabla g) + (\nabla)gg$. Substituting this in equation 5.17, one obtains

$$-v_F \nabla(g^2) = -v_F g(\nabla g) - v_F(\nabla)gg \tag{5.18}$$

$$= -v_F g[-iE\tau_3 + \hat{\Delta} + \frac{1}{2\tau} \langle g \rangle_{p_F}, g] - v_F[-iE\tau_3 + \hat{\Delta} + \frac{1}{2\tau} \langle g \rangle_{p_F}, g]g \tag{5.19}$$

$$= -v_F g \left(-iE\tau_3 + \hat{\Delta} + \frac{1}{2\tau} \langle g \rangle_{p_F} \right) g + v_F g^2 \left(-iE\tau_3 + \hat{\Delta} + \frac{1}{2\tau} \langle g \rangle_{p_F} \right) \tag{5.20}$$

$$- v_F \left(-iE\tau_3 + \hat{\Delta} + \frac{1}{2\tau} \langle g \rangle_{p_F} \right) g^2 + v_F g \left(-iE\tau_3 + \hat{\Delta} + \frac{1}{2\tau} \langle g \rangle_{p_F} \right) g \tag{5.21}$$

$$= -v_F [\left(-iE\tau_3 + \hat{\Delta} + \frac{1}{2\tau} \langle g \rangle_{p_F} \right), g^2] \tag{5.22}$$

But the identity commutes with all matrices. Thus, if $g^2 = 1$, then $\nabla(g^2) = 0$. This shows that $g^2 = 1$ should be used troughout the system.

5.3 Dirty systems: From Eilenberger to Usadel

In this thesis, so-called dirty systems will be considered. In this section the Usadel equation, that is used to describe dirty superconducting systems [70], is introduced on the basis of the works presented in [2], [3]. A superconducting system is called dirty if the self-energy due to elastic scattering is large compared to the superconducting energy gap, that is,

$$\frac{|\Sigma|}{\Delta} \gg 1. \tag{5.23}$$

This condition is equivalent to the more intuitive condition

$$\frac{l}{\xi} \ll 1, \tag{5.24}$$

where l is the mean free path of the electron and ξ is the superconducting coherence length for clean systems defined as $\xi = \frac{\hbar v_F}{\Delta}$. That the two conditions are equivalent follows from BCS theory:

$$\Delta = \frac{\hbar v_F}{\pi \xi} \tag{5.25}$$

$$\Sigma = \frac{1}{\tau} < G >= \frac{v_F}{l} < G > \tag{5.26}$$

$$\frac{\Sigma}{\Delta} \sim \frac{\frac{\hbar v_F}{l}}{\frac{\hbar v_F}{\xi}} = \frac{\xi}{l} = \left(\frac{l}{\xi} \right)^{-1}. \tag{5.27}$$

This shows that the two conditions are equivalent. In the dirty limit it is often argued that the Green's function should be almost isotropic. In fact, frequent scattering effectively ensures angular averaging, since the direction of electrons changes vary rapidly with time. Quantitatively, this can be justified following the derivation of [4]. Therefore, an Ansatz for the quasiclassical Green's function will be used based on an expansion of the quasiclassical Green's function in spherical harmonics.
In the following, the procedure in [2] will be closely followed to derive the Usadel equation. Because the Green's function is almost isotropic, it can be approximated well using an expansion in the lower order spherical harmonics. In fact, keeping only the zeroth and first order terms in this expansion, $g \approx G_0 + G_1\hat{v}_F$ where $\hat{v}_F$ is a unit vector denoting direction of the momentum, and G_0 and G_1 are matrices in $\mathbb{C}^{4\times4}$. These are independent of the direction $\hat{v}_F$, and only depend on position r and energy E.
The normalisation condition implies that $1 = gg = (G_0 + G_1\hat{v}_F)^2 = G_0^2 + \{G_0, G_1\}\hat{v}_F + G_1^2$ [2], where $\{G_0, G_1\}$ is the anticommutator of G_0 and G_1. Because the Green's function is almost isotropic $|G_1| \ll |G_0|$ for all r, E, where $|\ |$ denotes the 2-norm on $\mathbb{C}^{4\times4}$. Because $|G_1| \ll |G_0|$, $G_1^2 \approx 0$. Thus,

$$G_0^2 \approx 1 \tag{5.28}$$
$$\{G_0, G_1\} = 0. \tag{5.29}$$

Substituting the expansion in equation (5.7), and noting that the angular averaging in the self-energy term gives precisely G_0, it is found that

$$-v_F\partial_r(G_0 + v_F G_1) = [-iE + \Delta + \frac{1}{2\tau}G_0, G_0 + v_F G_1] \tag{5.30}$$

The next step is to take an angular average. The terms odd in v_F drop out since they average to 0. The result is

$$-\frac{1}{3}v_F^2\partial_r, G_1 = [-iE + \Delta, G_0]. \tag{5.31}$$

Note that the self-energy term, though even in v_F, drops out because $[< g >_{v_F}, \frac{1}{\tau} < g >_{v_F}] = 0$. Similarly, when the average is taken after multiplication with v_F, only the terms odd in equation (5.30) remain. Now, in the dirty limit the self energy term is dominant, $|\frac{1}{2\tau} < g > | = |\frac{1}{2\tau}G_0| >> | - iE + \Delta|$, which can be used to simplify the right hand side of equation (5.30). The result using this simplification is

$$-\partial_r G_0 = \frac{1}{2\tau}[G_0, G_1]. \tag{5.32}$$

Using $\{G_0, G_1\} = 0$ and $G_0^2 = 1$ it follows that

$$\partial_r G_0 = -\frac{1}{2\tau}(G_0G_1 - G_1G_0) = -\frac{1}{2\tau}(G_0G_1 + G_0G_1) = -\frac{1}{\tau}G_0G_1 \tag{5.33}$$
$$G_1 = -\tau G_0\partial_r G_0. \tag{5.34}$$

Thus, G_1 can be expressed in terms of G_0 and its derivative. Substituting equation (5.33) into equation (5.31), and using equation (5.28), the Usadel equation is found:

$$\frac{1}{3}v_F^2\tau\partial_r(G_0\partial_r G_0) = [-iE\tau_3 + \Delta, G_0]. \tag{5.35}$$
$$G_0^2 = 1. \tag{5.36}$$

It is a second order nonlinear elliptic equation for matrices in $\mathbb{C}^{4\times4}$. In literature, it is conventional to drop the subscript on the isotropic part of the Green's function. In this thesis this convention will be followed. It should be kept in mind that when using the Usadel equation G denotes the

isotropic part of the quasiclassical Green's function, and not the full Green's function as used in the Gorkov equation. To solve the Usadel equation, boundary conditions need to be specified. Which boundary conditions are to be used depends on the boundaries of the system. These will be described in later sections. The quantity $\frac{1}{3}v_F^2\tau$ is called the diffusion coefficient and denoted by D. Using equation (5.33) also equation (4.32) for the supercurrent through the junction can be rewritten. Because of the appearance of v_F i equation (4.32), even terms are averaged to 0 in this expression. The dominant term is thus the first order term $G_1 = -\tau G_0 \nabla G_0$. Now recall that the non-equilibrium Green's function has the form $G = \begin{bmatrix} G^R & G^K \\ 0 & G^A \end{bmatrix}$. From this it follows that

$$(G\nabla G)^K = G^R \nabla G^K + G^K \nabla G^A. \tag{5.37}$$

Inserting this in equation (4.32) it follows that

$$j = \frac{\sigma_N}{2} \int dE \mathrm{Tr}(\tau_3 (G^R \nabla G^K + G^K \nabla G^A)), \tag{5.38}$$

where G^X, $X = R, A, K$ are now angular averaged Green's functions and $\sigma_N = -eN_0\tau$. The equations presented in this section are the equations that will be used in the rest of this thesis. However, they are not yet in the form in which they can be solved most easily. This preparation is what will follow next.

5.4 Parametrisation

The Usadel equation as presented in (5.35) is much simpler than the original Gorkov equation (4.30). However, it is still a differential equation for a matrix in Keldysh-Nambu space, as introduced in section 4.1. The equation can be simplified more. In this subsection the θ-parametrisation is introduced, following the notation from [2].
The structure of the matrices in Keldysh-Nambu is

$$G = \begin{bmatrix} G^R & G^K \\ 0 & G^A \end{bmatrix}. \tag{5.39}$$

The first observation is that the equations for the retarded (R) and advanced (A) components are self-supportive, that is, they can be solved without using the other equations. Even more, the advanced component can be calculated directly from the results for the retarded component and vice versa. Thus, only for one of these two components the differential equation needs to be solved. The equation for the Keldysh component is not self-supportive, the solutions to the retarded and advanced component are needed. However, it will be found that the resulting equation for the Keldysh component is actually easier to solve than the equation for the retarded component. Because of the zero-matrix in the left lower corner in equation (5.39), it is found that

$$\frac{1}{3}v_F^2\tau\partial_r(G^X\partial_r G^X) = [-iE\tau_3 + \Delta, G^X]. \tag{5.40}$$

$$(G^X)^2 = 1. \tag{5.41}$$

for $X = R, A$. Recall that only one of these equations needs to be calculated directly solved. Thus, instead of a differential equation for matrices in $\mathbf{C}^{4x4}$, differential equations for matrices in $\mathbf{C}^{2x2}$ can be used. An even simpler representation is possible. The functions G^R, G^A, are parametrised as [2]

$$G^X = \begin{bmatrix} \cosh(\theta^X) & \sinh(\theta^X)e^{i\chi^X} \\ -\sinh(\theta^X)e^{-i\chi^X} & -\cosh(\theta^X) \end{bmatrix}. \tag{5.42}$$

The advantage of this parametrisation, called the θ-parametrisation, is that equation (5.41) is automatically satisfied.

In the following, focus will be on the retarded component, and the superscripts on θ and χ will be dropped. The advanced Green's function can be calculated directly from the retarded Green's function via $G^A = -\tau_3(G^R)^\dagger\tau_3$. Substituting equation (5.42) into equation (5.40), differential equations for θ, χ are found:

$$D\frac{\partial\theta}{\partial r^2} = -2iE\sinh\theta + \frac{D}{2}\frac{\partial\chi}{\partial r^2}\sinh\theta. \tag{5.43}$$

$$\frac{\partial}{\partial r}\left(\sinh^2(\theta)\frac{\partial}{\partial r}\chi\right) = 0. \tag{5.44}$$

Following Suzuki, [79], the Usadel equation was recast in dimensionless form using $x \to \frac{x}{\xi}$ and $E \to \frac{E}{\Delta_0}$, where $\xi = \sqrt{\frac{D}{2\pi T_c}}$, with Δ_0 the superconducting potential introduced in section 4 and T_c the critical temperature in BCS theory, the maximum temperature at which the system is superconducting [23]. In these units the Usadel equation can be recast as

$$\begin{aligned}\frac{\partial\theta}{\partial r^2} &= -2iE\alpha\sinh\theta + \frac{1}{2}\left(\frac{\partial\chi}{\partial r}\right)^2\sinh\theta,\\ \frac{\partial}{\partial r}\left(\sinh^2(\theta)\frac{\partial}{\partial r}\chi\right) &= 0,\end{aligned} \tag{5.45}$$

where $\alpha = \frac{\Delta_0}{2\pi T_c} \approx 0.28$ according to BCS theory [57]. This is a natural constant in BCS theory, that is, it is independent of the material used. These are the equation that will be solved in the coming sections. In these sections a junction is considered. The normalisation is then done using Δ_0 and T_c in the superconducting electrodes.
The Keldysh component of the normalisation condition $G^2 = 1$ is

$$G^RG^K + G^KG^A = 0. \tag{5.46}$$

This equation is automatically satisfied using the parametrisation [3]:

$$G^K = G^Rh - hG^A \tag{5.47}$$

$$h = f_L + f_T\tau_3, \tag{5.48}$$

where f_L and f_T are called the distribution functions. The Keldysh equation is

$$\begin{aligned}&\nabla(D_L\nabla f_L) + \nabla(C_L\nabla f_T) + \mathrm{ImIs}\nabla f_T = 0,\\ &\nabla(D_T\nabla f_T) + \nabla(C_T\nabla f_L) + \mathrm{ImIs}\nabla f_L = 0.\end{aligned} \tag{5.49}$$

The functions $D_{L,T}, C_{L,T}$ and ImIs can be calculated directly from the solutions for the retarded equation. A derivation of the equations for the Keldysh component and expressions for the terms $D_{L,T}, C_{L,T}$ and ImIs can be found in appendix B.1. The expressions obtained are

$$D_L = \mathrm{Tr}(1 - G^RG^A) = 2 + 2|\cosh\theta|^2 - 2|\sinh\theta|^2\cosh\mathrm{Im}\chi, \tag{5.50}$$

$$D_T = \mathrm{Tr}(1 - \tau_3G^R\tau_3G^a) = 2 + 2|\cosh\theta|^2 + 2|\sinh\theta|^2\cosh\mathrm{Im}\chi, \tag{5.51}$$

$$C_L = \mathrm{Tr}(-G^R_{\tau_3}G^A) = -2|\sinh\theta|^2\sinh 2\mathrm{Im}\chi, \tag{5.52}$$

$$C_T = -C_L, \tag{5.53}$$

$$\mathrm{ImIs} = \mathrm{Tr}\left(\tau_3(G^R\nabla G^R - G^A\nabla G^A)\right) = -4\mathrm{Im}(\sinh^2\theta\frac{\partial\chi}{\partial x}). \tag{5.54}$$

Compared to literature [2],[3], the equations presented here contain two extra terms, the $C_{L,T}$-terms. These terms arise because in this thesis the parameter χ is allowed to be complex. In many problems, the imaginary part of the parameter χ can be discarded, and in that case $C_{L,T} = 0$.

However, as the results presented in this thesis show, in the junction considered here, Imχ does not vanish. Equations (5.49) are easier to solve than the equations for the retarded part, because they are linear in f_L and f_T. Thus, no iterative scheme is needed.
The equations for the retarded part are two coupled differential equations for scalar-valued functions. In some cases χ can be inferred to be constant from symmetry, in which case equation (5.43) is a single differential equation for θ. This equation can be solved if boundary conditions are supplied. However, in general both equations (5.43) and (5.44) are needed. After the equation is solved, it is possible to also calculate G_1 using equation (5.34), to confirm the consistency of the isotropy condition $|G_1| \ll |G_0|$.

With this, the equations for the interior of the domain have been specified. For a complete description of the system, also boundary conditions need to be specified. The boundary conditions used depend on the geometry of the system under consideration. Therefore, in section 6, the geometry will first be introduced.

6 VT Geometry

In the previous sections the Usadel equations and their theoretical foundations have been discussed. In this section, the theory will be applied to the geometry of a VT junction [80], [81], [82],[83], under consideration, and the boundary conditions necessary to solve the equations will be introduced. The resulting Usadel formulation is a bit harder to solve in this geometry than in the standard SNS geometry. However, this extra effort is justified as the thermal reservoirs will provide an extra mechanism to adjust the properties of the junction.
The Usadel equation can be implemented for several geometries. In this thesis, the geometries under consideration are quasi one-dimensional. The geometry that will be studied most in this thesis is the VT-junction. This junction is named after Volkov and Takayanagi, who have intensively studied this and similar geometries [80],[81],[82],[83]. A schematic of the VT-junction is shown in figure 3. The VT-junction is a four terminal junction, with two superconducting terminals and two normal metal terminals.

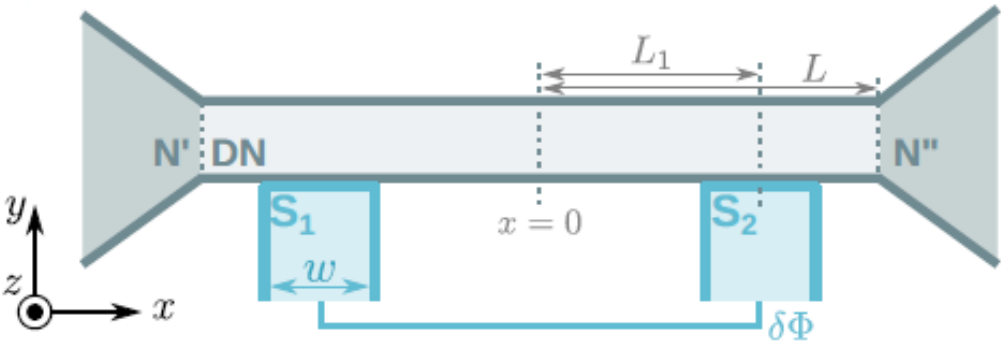

Figure 3: Schematic of the VT-junction. Figure adapted from [79] Two superconducting electrodes, S_1 and S_2, are connected to a dirty normal metal DN of length L, which is in turn forming an $N' - DN - N''$ junction with the two thermal contacts N' and N''. The presence of the superconducting electrodes can induce superconductivity in DN through the proximity effect.

The VT-junction can be seen as an $N'-DN-N''$ junction in which superconductivity is introduced using the proximity effect [23]. A quasi one-dimensional normal metal in which transport may be described in the 'dirty limit' dominated by diffusive mechanisms due to impurity scattering, is sandwiched between two normal metal reservoirs. The proximity effect is induced by two superconducting electrodes that are attached in the vertical direction. The approximation of these electrodes within a quasi one-dimensional setting is non-trivial as detailed next.
To incorporate the effect of the superconducting electrodes, the two-dimensional Usadel equation is considered. The two-dimensional equation reads

$$\frac{\partial}{\partial x}\left(G\frac{\partial G}{\partial x}\right)+\frac{\partial}{\partial y}\left(G\frac{\partial G}{\partial y}\right)+i\epsilon[G,\tau_3]=0. \tag{6.1}$$

for the Green's function G. This equation can be averaged over the y-direction, yielding

$$\frac{1}{L_y}\int_0^{L_y}\frac{\partial}{\partial x}\left(G\frac{\partial G}{\partial x}\right)dy+\frac{1}{L_y}\left(G\frac{\partial G}{\partial y}|_{y=L_y}-G\frac{\partial G}{\partial y}|_{y=0}\right)+\frac{i\epsilon}{L_y}\int_0^{L}[G,\tau_3]dy=0. \tag{6.2}$$

Now, the VT-junction is supposed to satisfy $\frac{L_y}{\xi}\ll 1$. Therefore, the y-dependence of the first and third term in equation (6.2) can be ignored and the equation reads:

$$\frac{\partial}{\partial x}\left(G\frac{\partial G}{\partial x}\right)+\frac{1}{L_y}\left(G\frac{\partial G}{\partial y}|_{y=L_y}-G\frac{\partial G}{\partial y}|_{y=0}\right)+i\epsilon[G,\tau_3]=0. \tag{6.3}$$

This leaves us with an equation similar to the one-dimensional Usadel equation. However, the second term, which consists of $G\frac{\partial G}{\partial y}$ evaluated at two positions represents an extra solution-dependent source term. At $y = L_y$ there is a boundary of the diffusive normal metal with vacuum or air. Because no current can flow into the air or into the vacuum, $G\frac{\partial G}{\partial y}|_{y=L_y} = 0$. For the boundary term at $y = 0$ the Tanaka Nazarov boundary conditions will be used [84],[85]:

$$G\frac{\partial G}{\partial y} = -S(G, y), \tag{6.4}$$

where S is the Tanaka Nazarov term. This term will be elaborated on in more detail in section 7, here it suffices to use equation (6.4). All in all, the Usadel equation for the VT -junction is

$$\frac{\partial}{\partial x}G\frac{\partial G}{\partial x} + i\epsilon[G, \tau_3] + S(G, y)\theta_S(x) = 0, \tag{6.5}$$

where $\theta_S(x)$ is the indicator function of the superconducting electrodes. To complete the system of equations, the boundary conditions at the reservoirs need to be specified. In the reservoirs, the Green's function should equal the bulk solution for a normal metal, $G = \mathbf{1}$. For the retarded equation this imposes the condition

$$\theta(-L/2) = \theta(L/2) = 0.$$

However, this condition leaves the parameter χ free. A boundary condition on χ can be motivated using that no supercurrent $\sinh\theta\frac{\partial\chi}{\partial x}$ should flow into the metal reservoir. In fact, there should only be a supercurrent induced between the two electrodes. A current flowing into the reservoir should always be a dissipative current. As close to the reservoir $\theta \neq 0$, it must hold $\frac{\partial\chi}{\partial x} = 0$ here to have no supercurrent flowing into the reservoir. But if this hold for all $x \in (\frac{-L}{2}, -\frac{-L_1}{2}) \cup (\frac{L_2}{2}, \frac{L}{2})$, then by taking the limit $x \to \pm L/2$, it is found that

$$\frac{\partial\chi}{\partial x}(-L/2) = \frac{\partial\chi}{\partial x}(L/2) = 0.$$

For the Keldysh equation, Dirichlet boundary conditions can be used. In the reservoirs, the Fermi-Dirac distribution [86], [87], is obeyed, so, according to [88]:

$$f_L(L/2) = f_L(-L/2) = \frac{1}{2}\big(\tanh\frac{\epsilon + V}{2T} + \tanh\frac{\epsilon - V}{2T}\big)$$

and

$$f_T(L/2) = -f_T(-L/2) = \frac{1}{2}\big(\tanh\frac{\epsilon + V}{2T} - \tanh\frac{\epsilon - V}{2T}\big),$$

where ϵ is the energy also appearing in the Usadel equation, $\pm\frac{V}{2}$ is the dimensionless voltage $V = \frac{e\tilde{V}}{\Delta}$ applied to respectively the left and right reservoir and T is the temperature dimensionless temperature $T = \frac{k_B\tilde{T}}{\Delta}$. Here e and k_B are the electron charge and the Boltzmann constant respectively. The notation $\tilde{}$ has been used here to denote the temperature and voltage in SI units. Here a difference between the VT-junction and a normal SNS-junction is apparent, the transport through the junction can be manipulated by applying a voltage on the reservoirs. The normal reservoirs thus provide an extra control that enables to investigate the junction. There is yet another possibility using the VT-junction. In principle, one could keep the two reservoirs at different temperatures, and in this way the thermo-electric effect can be investigated for the different types of superconducting electrodes. However, this does not fit in the current approach, as the quasiclassical Green's function cannot describe the thermo-electric effect [67].
With the specification of the geometry, the model of the VT junction is almost complete. What is left is a specification of the term S. As indicated, this will follow in the coming section.

7 Tanaka Nazarov boundary conditions

In this section the S-term in the Usadel equation applied to the VT-junction will be described using Tanaka Nazarov boundary conditions, developed in [4], [84], [85]. The derivation presented here closely follows these articles. This will result in equation (7.19), which was used in calculations.

Tanaka Nazarov boundary conditions are based on the solution of the Eilenberger equation in the region close to the interface, that is, for distances from the interface much smaller than the coherence length. The theory of Nazarov is used to calculate the current I through an interface. The boundary condition can then be expressed as

$$G\frac{\partial}{\partial x}G = -S = \frac{1}{\gamma_B}I, \tag{7.1}$$

where γ_B is a parameter characterising the contact resistance compared to the normal state resistance of the junction and I is the current through the interface, whose calculation will be shortly summarised here. The theory was first developed for s-wave superconductors by Nazarov [4]. This theory will be presented first, thereafter the generalisation to unconventional electrodes is discussed.
The Nazarov theory can be applied both to the interface between two isotropic superconductors with different superconducting gaps and to an SN interface in which the superconductor is isotropic. In the Nazarov theory, the current I is calculated. To calculate this current, the behaviour of the Green's function near the interface needs to be considered. Near the interface, the isotropy condition might break down. Therefore, this approach is based on the solution to the Eilenberger equation, with which non-isotropic systems can be described. An advantage that comes along with this is that the solution to the Eilenberger equation consists of left-travelling waves ($\sigma = -$) and right-travelling waves ($\sigma = +$). The current can thus be calculated by subtracting the contributions of these waves. Thus, in matrix representation, if the Green's function is of the form $\begin{bmatrix} G_+ & C_1 \\ C_2 & G_- \end{bmatrix}$, where $G_\sigma = \langle \Psi_\sigma^\dagger \Psi_\sigma \rangle$, and $C_i, i = 1, 2$ correspond to correlations between the left-travelling and right-travelling waves, then the current can be expressed as [4]

$$I = \sum_n \mathrm{Tr}\Sigma G \tag{7.2}$$

$$\Sigma = \sigma\delta_{\sigma,\sigma'} = \begin{bmatrix} 1 & 0 \\ 0 & -1 \end{bmatrix}, \tag{7.3}$$

where the summand is over the different directions that are possible. Note that this expression is in accordance with the expression for current in the Usadel equation by virtue of equation (5.34). In the following section, focus will be on a single mode, and the summand will be dropped.

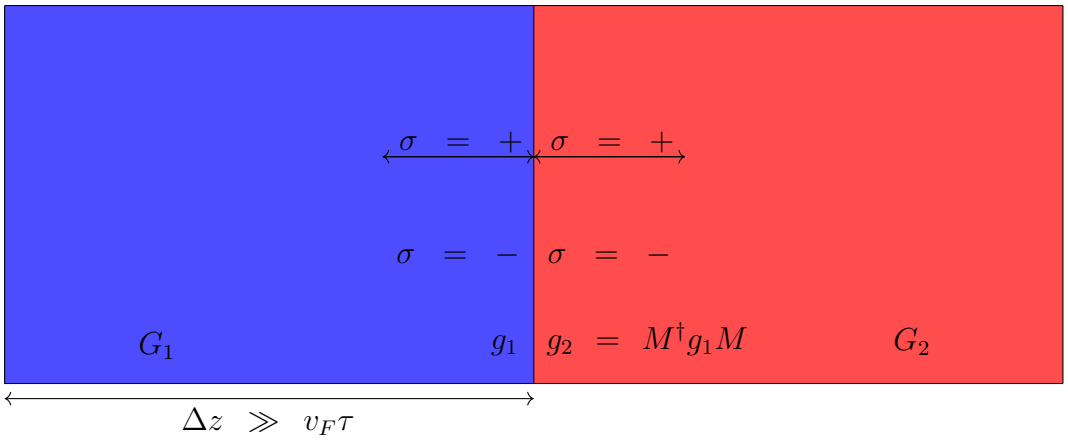

Figure 4: Interface region between materials 1 (blue) and 2 (red). The arrows indicate the right-travelling and left-travelling contributions, labelled by σ. The Green's function in the bulk of material 1 is named G_1, the Green's function at the interface in material 1 is named g_1. Similar naming conventions have been used for material 2. At the interfaces, g_1 and g_2 are related by a scattering matrix. The theory of Nazarov relates the Green's functions G_i at a distance far from the interface compared to scattering length to the interface Green's functions g_i.

The Nazarov approach relates the Green's functions at the interface to the Green's functions at distances far away from the interface compared to the scattering length $v_F\tau$. Here τ is the scattering time, a material parameter, that was noted before to be very small in the dirty limit. This relation is established by using the defining equation for Green's functions, $HG = \delta(r - r')$.

Consider an interface between two materials, here called materials 1 and 2 as depicted in figure 4. Far away from the interface between materials 1 and 2 the Green's functions assume values G_1 and G_2, near the interface, the Green's functions assume values g_1 and g_2. Their relation is established using the Eilenberger equation. The Hamiltonian in the dirty system is approximated by $H = \sigma v_n \frac{\partial}{\partial z} + \frac{\langle G \rangle}{\tau}$, as for the dirty limit, that is, small τ, this term dominates the full Hamiltonian [4]. The Green's functions at the interface g_i are then related to the Green's functions far away compared to the mean free path from the interface using this Hamiltonian. This can be used to calculate the Green's functions at the interface, from which the current through the interface can be calculated.
Focus will first be on material 1, the procedure in material 2 is entirely similar. The Green's function is decomposed as

$$G = \sum_{n,m,\sigma,\sigma'} G^{\sigma,\sigma'}_{n,m} e^{i\sigma p_n - i\sigma' p_m}, \tag{7.4}$$

where p_n, p_m are momentum amplitudes and $\sigma, \sigma' = \pm 1$ indicate direction. The parameters n, m label the mode of the system, they determine the angle made with the interface. This is the decomposition in right-travelling waves and left-travelling waves mentioned before.
As the Green's functions G_1 and G_2 in the region several mean free paths from the interface are isotropic, there is no σ, σ' dependence in G_1 and G_2. However, close to the interface the Green's function might depend on σ, σ'. Using the definition of Green's functions, the Green's function $G^{\sigma,\sigma'}_{n,m}(z, z')$ should satisfy

$$(\sigma v_n \frac{\partial}{\partial z} + \frac{\langle G \rangle}{\tau}) G^{\sigma,\sigma'}_{n,m} = i\sigma\delta(z - z')$$
$$G^{\sigma,\sigma'}_{n,m}(\sigma v_n \frac{\partial}{\partial z} - \frac{\langle G \rangle}{\tau}) = i\sigma\delta(z - z')$$

By defining

$$2iG^{\sigma,\sigma'}_{n,m} = \frac{1}{\sqrt{v_n v_m}} g^{\sigma,\sigma'}_{n,m} + \frac{1}{|v_n|}\sigma\delta_{\sigma,\sigma'}\text{sign}(z-z'), \tag{7.5}$$

continuous functions $g^{\sigma,\sigma'}_{n,m}$ are introduced, which satisfy

$$(\sigma v_n \frac{\partial}{\partial z} + \frac{\langle G\rangle}{\tau}) g^{\sigma,\sigma'}_{n,m} = 0,$$
$$g^{\sigma,\sigma'}_{n,m}(\sigma v_n \frac{\partial}{\partial z} - \frac{\langle G\rangle}{\tau}) = 0.$$

This equation can be solved by considering $\langle G\rangle$ to be constant, as the superconducting coherence length ξ is much longer than the scattering length $v_F\tau$. The solution to this equation can be substituted back in equation (7.5). This yields

$$G^{\sigma,\sigma'}_{n,m}(z,z) = P(z)(g_1 + \Sigma_z G_1)P(-z'), \tag{7.6}$$

where g_1 is the Green's function at the interface in material 1 and

$$P(z) = e^{\frac{z}{2v\tau}}(1-\Sigma G_1) + e^{-\frac{z}{2v\tau}}(1+\Sigma G_1). \tag{7.7}$$

A relation between g_i and G_i can now be found by requiring that $G^{\sigma,\sigma'}_{n,m}(z,z')$ remains finite as $z, z' \to -\infty$. For $P(z)$ the term growing with decreasing z is $e^{-\frac{z}{2v\tau}}(1+\Sigma G)$, for $P(-z')$ the term growing with decreasing z' is $e^{\frac{-z'}{2v\tau}}(1-\Sigma G)$. Using equation (7.6) the appropriate conditions are

$$(\Sigma + G_1)(\Sigma - g_1) = 0, \tag{7.8}$$
$$(\Sigma + g_1)(\Sigma - G_1) = 0, \tag{7.9}$$

where all terms have been multiplied with Σ.
For material 2, which is also a dirty system, the solution is similar to the solution presented in equation (7.6), with g_1 now replaced by g_2. For material 2, $G^{\sigma,\sigma'}_{n,m}(z,z')$ should remain finite as $z, z' \to \infty$. This yields the relations

$$(\Sigma - G_2)(\Sigma + g_2) = 0 \tag{7.10}$$
$$(\Sigma - g_2)(\Sigma + G_2) = 0. \tag{7.11}$$

By now, g_1 has been related to G_1, and g_2 to G_2. This describes the evolution within the materials. The missing link for a description of the interface is now the relation between g_1 and g_2. The potential barrier at the interface is represented using a scattering matrix M, which relates the Green's functions $g_{1,2}$ on either side of the interface by $g_2 = M^\dagger g_1 M$. The eigenvalues of this matrix M are related to the transmission coefficient T, for which the conventional expression is used:

$$T = \frac{\cos\phi^2}{\cos\phi^2 + z^2}, \tag{7.12}$$

where ϕ is the angle made by the wave with the interface. With this, G_1 has been related to g_1, g_1 to g_2 and g_2 to G_2. Because G_1 and G_2 are known, they will be inputs in the boundary conditions, these relations can be used to calculate the current through the interface.
It is important to note that M is of the form $\begin{bmatrix} M_{11} & M_{12} \\ M_{21} & M_{22} \end{bmatrix}$, where $M_{ij} = m_{ij}\mathbf{1}_{4\times4}$, that is, the interface can revert the direction of motion of the particle, but it does not affect the superconducting correlations and thus does not mix the retarded, advanced and Keldysh components [89]. Because G_1 and G_2 are of the form $G_i = \begin{bmatrix} \tilde{G}_i & 0 \\ 0 & \tilde{G}_i \end{bmatrix}$, these Green's functions commute with M. This will

play an important role in the derivation that follows. A second important relation on M is that $M^\dagger \Sigma M = \Sigma = M \Sigma M^\dagger$. This expression reflects current conservation.
If the first line of equation (7.8) is multiplied from the left by $M^\dagger$ and from the right by M one obtains

$$M^\dagger M + M^\dagger G_1 \Sigma M - M^\dagger \Sigma g_1 M - M^\dagger G_1 g_1 M = 0, \tag{7.13}$$
$$Q + G_1 \Sigma - (Q\Sigma + G_1) g_2 = 0, \tag{7.14}$$

where $Q = M^\dagger M$. In this step it was used both that G_1 and M commute in the second and the fourth term. That M obeys current conservation, that is, $M^\dagger \Sigma M = \Sigma$, and $M^\dagger \Sigma = Q \Sigma M^\dagger$, was used in the second and third terms. Lastly, it was used in the third and fourth term that by the definition above, $g_2 = M^\dagger g_1 M$.
The first line from equation (7.10) can be multiplied from the left by Q to give

$$Q - Q\Sigma g_2 - Q G_2 \Sigma - Q G_2 g_2 = 0. \tag{7.15}$$

Equations (7.13) and (7.15) can then be combined to give

$$g_2 = (QG_2 + G_1)^{-1}(2Q + (G_1 - QG_2)\Sigma). \tag{7.16}$$

Even though only two of the four equations are used to find this solution, it turns out that all four equations are satisfied [85].
The expression of the current through the interface becomes particularly simple in terms of g_1 and g_2. Now recall that the Green's function g_i consists of terms moving to the right ($\sigma = +$) and to the left ($\sigma = -$). Those terms with $\sigma = +$ contribute positively to the current, while those with $\sigma = -$ contribute negatively to the current [4]. Now recall that Σ is defined as $\Sigma = \sigma \delta_{\sigma,\sigma'}$ Therefore, the current can be expressed as

$$I = \mathrm{Tr} \Sigma g_1. \tag{7.17}$$

Because M should satisfy $\Sigma = M^\dagger \Sigma M$, it now immediately follows that

$$I = \mathrm{Tr} \Sigma g_1 = \mathrm{Tr} \Sigma g_2, \tag{7.18}$$

which shows that current is indeed conserved.
Expression (7.18) can be used in boundary condition (7.1). This results in

$$I = \mathrm{Tr} \Sigma g_2 = \mathrm{Tr}\left((QG_2 + G_1)^{-1}(2Q + (G_1 - QG_2)\Sigma)\right). \tag{7.19}$$

As noted, the theory of Nazarov is only valid for isotropic materials on both sides of the boundary. The theory by Nazarov was generalised to the junctions of unconventional superconductors with normal metals in [84] and [85]. The difference between the theory of non-isotropic materials with the theory of isotropic materials is that the Green's function G_i is not any more isotropic, rather we have $G_i = \begin{bmatrix} G_{i+} & 0 \\ 0 & G_{i-} \end{bmatrix}$. The difference between conventional and unconventional superconductors is thus that the solution of the equations give different results in the two cases. It was found however, that equation (7.10) should also hold in this case, although the derivation is slightly different, using a different Hamiltonian.
Expression 7.19 can be applied to the junction of a superconducting electrode for material 1 and a normal metal for material 2. In appendix B.4, the resulting equations for the Volkov Takayanagi junction are derived. The equations are applicable for both s-wave and p-wave superconductors.

They read

$$
\begin{aligned}
I =& [G, B] && (7.20)\\
B =& (D^R)^{-1} N^R && (7.21)\\
D^R =& \left(-T_{1n}\Psi G_1 \Psi R_p^{-1} + T_{1n} R_p^{-1} G_1 + 1 - T_{1n}^2 \Psi G_1 \Psi G_1\right)^{-1} && (7.22)\\
N^R =& \left(T_{1n} R_p^{-1} R_m - T_{1n} R_p^{-1} + T_{1n}\Psi G_1 \Psi\right) && (7.23)\\
B^A =& -\tau_3 (B^R)^\dagger \tau_3 && (7.24)\\
B^K =& (D^R)^{-1} N^K - (D^R)^{-1} D^K (D^A)^{-1} N^A, && (7.25)\\
D^K =& -T_{1n}\Psi R_1 \Psi (R_p^{-1} h_s - h_s A_p^{-1}) + T_{1n} R_p^{-1}(R_1 h - h A_1)\\
& - T_{1n}(H_+^{-1} H_- G_1 H_-^{-1} H_+)_K A_p^{-1} + T_{1n}(R_p^{-1} h - h A_p^{-1}) A_1\\
& - T_{1n}^2 \Psi R_1 \Psi (R_1 h - h A_1) - T_{1n}^2 (H_+^{-1} H_- G_1 H_-^{-1} H_+)_K A_1, && (7.26)\\
N^K =& T_{1n} R_p^{-1} R_m h_s - T_{1n} h_s A_p^{-1} A_m - T_{1n} R_p^{-1} h_s\\
& + T_{1n} h_s A_p^{-1} + T_{1n}^2 (H_+ H_- G_1 H_-^{-1} H_+)_K, && (7.27)\\
H_+ =& \frac{1}{2}(G_{2+} + G_{2-}) && (7.28)\\
H_- =& \frac{1}{2}(G_{2+} - G_{2-}), && (7.29)
\end{aligned}
$$

where G_1 denotes the Green's function in the normal metal, G_2 the possibly non-isotropic Green's function in the superconductor, $R_p = (H_+)^R$, $R_m = (H_-)^R$, $A_p = (H_+)^A$, $A_m = (H_-)^A$, T_{1n} has been used for the transparency, h and h_s denote the distribution functions in the normal metal and superconductor, and $\Psi = \begin{bmatrix} 0 & e^{i\psi} \\ e^{-i\psi} & 0 \end{bmatrix}$, where ψ is the superconducting phase in the superconductor. The expressions presented here are applicable to unconventional superconductivity by allowing H_-, and they are numerically stable as well if $H_- = 0$ or $H_- \approx 0$. A derivation of these expressions, and a discussion on the numerical stability for $H_- \approx 0$ can be found in appendix B.4.

If the superconducting phase χ in the normal metal is equal to the superconducting phase in the superconducting electrode, as is the case in equilibrium, the expression reduces to the expressions in [4], [90]:

$$I = 2T(4 + T(G_2 G_1 + G_1 G_2 - 2))^{-1}(G_2 G_1 - G_1 G_2). \tag{7.30}$$

In the case $T << 1$ this reduces to the well-known Kupriyanov Luckichev boundary conditions [91],

$$I = T(G_2 G_1 - G_1 G_2). \tag{7.31}$$

With this, the model of the junction is complete. The equations established in the previous sections

and the appendices can be summarised as follows

$$\frac{\partial^2\theta}{\partial x^2} + 2i\alpha\epsilon\sinh\theta - \frac{1}{2}(\frac{\partial\chi}{\partial x})^2\sinh 2\theta + S_\theta\Theta_S(x) = 0. \tag{7.32}$$

$$\frac{\partial}{\partial x}\left(\sinh^2\theta\frac{\partial\chi}{\partial x}\right) + S_\chi\Theta_S(x) = 0. \tag{7.33}$$

$$\frac{\partial}{\partial x}\left(D_L\frac{\partial f_L}{\partial x}\right) + \frac{\partial}{\partial x}\left(C_L\frac{\partial f_T}{\partial x}\right) + \mathrm{ImIs}\frac{\partial f_T}{\partial x} + \mathrm{Tr}(S^K) = 0. \tag{7.34}$$

$$\frac{\partial}{\partial x}\left(D_T\frac{\partial f_T}{\partial x}\right) + \frac{\partial}{\partial x}\left(C_T\frac{\partial f_L}{\partial x}\right) + \mathrm{ImIs}\frac{\partial f_L}{\partial x} + \mathrm{Tr}(\tau_3 S^K) = 0. \tag{7.35}$$

$$S = \frac{1}{\gamma_B}\mathrm{Tr}\left((QG_{DN}(x) + G_S)^{-1}(2Q + (G_{DN}(x) - QG_S)\Sigma)\right) \tag{7.36}$$

$$S_\theta = \frac{1}{2i}S^R(1,1) \tag{7.37}$$

$$S_\chi = \frac{1}{2}e^{-i\chi}S^R(1,2) + \frac{1}{2}e^{i\chi}S^R(2,1). \tag{7.38}$$

$$\theta(-\frac{L}{2}) = \theta(\frac{L}{2}) = 0. \tag{7.39}$$

$$\frac{\partial\chi}{\partial x} = \frac{\partial\chi}{\partial x} = 0. \tag{7.40}$$

$$f_L(\frac{-L}{2}) = f_L(\frac{L}{2}) = \frac{1}{2}\left(\tanh\frac{\epsilon+V}{2T} + \tanh\frac{\epsilon-V}{2T}\right). \tag{7.41}$$

$$-f_T(\frac{-L}{2}) = f_T(\frac{L}{2}) = \frac{1}{2}\left(\tanh\frac{\epsilon+V}{2T} - \tanh\frac{\epsilon-V}{2T}\right). \tag{7.42}$$

Here the notation G_{DN} is used for the Green's function in the dirty normal metal, which is to be solved, the notation G_S is the given Green's function in the superconducting electrodes, and the notation S^R, S^K is used to denote the retarded and advanced components of the Tanaka Nazarov term introduced in this section. All equations are presented in dimensionless form, thus, energies are understood in units of Δ voltages are measured in units of $\frac{\Delta}{e}$ and temperatures in units of $\frac{\Delta}{k_B}$. Equations (7.32) and (7.33) are the retarded equations that need to be solved with the boundary conditions at the normal reservoirs (7.39) and (7.40) and the source term due to the superconducting electrodes described by (7.36), (7.37) and (7.38). The solutions to these equations give the density of states and the spectral supercurrent.
The Keldysh equation is solved by solving equations (7.34) and (7.35), together with the normal reservoir boundary conditions (7.41) and (7.42), and the source term (7.36). With the solutions to these equations give the occupation of levels, and are thus needed for the calculation of transport.

The equations (7.32) to (7.42) were solved using MATLAB. Because some of the equations are nonlinear, this is not trivial. A discussion of the implementation of the problem in MATLAB is presented in section 8. The implementation in the code of equations (7.32) to (7.42) is discussed in appendix B.4.

8 Application of Usadel

In the previous section a model for the description of the four-terminal junction was developed. In this section its implementation in MATLAB will be discussed. Because the problem under consideration is a non-linear problem, an iterative method using linearisation was used to find solutions to the set of partial differential equations. The Usadel equations (7.32) to (7.42) were solved for $E/\Delta \in (0, 1.5)$. First the retarded equation was solved. This was done starting at $E \approx 1.5\Delta$, where solutions corresponding to a normal metal are a good initial Ansatz, and then for successively lower energies, using the solution of energy E as an initial Ansatz for energy $E - dE$. The bound $E = 1.5\Delta$ was chosen as it is well above $E = \Delta$, and higher energies are not expected to play a big role, based on previous results [90]. An overview of the method used is given in figure 5. In the coming sections, first the linearisation of the equations and an iterative method to solve the nonlinear equations will be introduced. Afterwards, the discretisation of the problem will be shortly discussed.

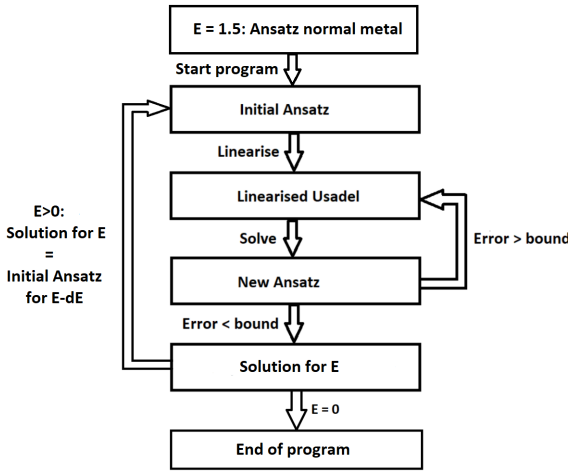

Figure 5: An overview of the iterative scheme of the computation method used to solve the Usadel equation.

8.1 Linearisation

In this section the implementation of the retarded Usadel equation in MATLAB will be discussed. The Usadel equation is a nonlinear equation, for which an iterative scheme was used. This scheme will be explained in this section. For clarity of presentation, the concept will be explained in the absence of a phase difference. The procedure for non-zero phase differences is entirely similar, although then two coupled equations are solved.
The parametrised Usadel equation for the VT-junction (5.43) including the boundary term from equation (6.5) reads

$$\frac{\partial^2\theta}{\partial x^2} + 2i\epsilon \sinh\theta + S(\epsilon,\theta)H_S(x) = 0. \tag{8.1}$$

This is a set of nonlinear partial differential equations indexed by energy ϵ. The solutions of different energy are independent. Therefore, in the following, the parameter ϵ will be fixed, the main procedure is independent of ϵ. The nonlinear partial differential equation is solved using an iterative method. Equation (5.43) can be linearised around an Ansatz to the solution θ_0, $\theta = \theta_0 + \delta\theta$. Substituting this in equation (5.43) results in

$$\frac{\partial^2(\theta_0 + \delta\theta)}{\partial x^2} + 2i\epsilon \sinh(\theta_0 + \delta\theta) + S(\epsilon, \theta_0 + \delta\theta)H_S(x) = 0. \tag{8.2}$$

If $\delta\theta$ is small, a Taylor approximation can be used on the second and the third term,

$$\frac{\partial^2\theta_0}{\partial x^2} + \frac{\partial^2\delta\theta}{\partial x^2} + 2i\epsilon\sinh\theta_0 + 2i\epsilon\cosh\theta_0\delta\theta + S(\epsilon,\theta_0)H_S(x) + \frac{\partial S}{\partial\theta}H_S(x)\delta\theta = 0. \tag{8.3}$$

After rewriting this equation to have only terms involving $\delta\theta$ on the left hand side, the following equation is obtained.

$$\frac{\partial^2\delta\theta}{\partial x^2} + \left(2i\epsilon\cosh\theta_0 + \frac{\partial S}{\partial\theta}H_S(x)\right)\delta\theta = -\frac{\partial^2\theta_0}{\partial x^2} - 2i\epsilon\sinh\theta_0 - S(\epsilon,\theta_0)H_S(x). \tag{8.4}$$

This is a linear equation that can be solved directly using discretisation of the second derivative term. After solving for $\delta\theta$ a new approximation of the solution $\theta_1 = \theta_0 + \delta\theta$ is found, and the procedure can be repeated, in the hope that the iteration will converge, that is $\max_x \delta\theta(x) \to 0$. Before going to the actual discretisation, a short note on the well-posedness of these equations will be given.

8.2 Weak solution

When discretising this equation directly, the Heaviside function in the last term is problematic. This can be solved by integrating the equation once with respect to position on the interval $e_n = (x_{n-\frac{1}{2}}, x_{n+\frac{1}{2}})$. The resulting equation after multiplying by $\frac{1}{a}$, where a is the length of an interval e_i:

$$\frac{1}{a}\left(\frac{\partial\delta\theta}{\partial x}|_{x_{n+\frac{1}{2}}} - \frac{\partial\delta\theta}{\partial x}|_{x_{n-\frac{1}{2}}}\right) + \frac{2i\epsilon}{a}\int_{e_n}\cosh\theta_0\delta\theta dx + \frac{1}{a}\int_{e_n}H_S\frac{\partial S(\epsilon,\theta_0)}{\partial\theta}\delta\theta dx = \tag{8.5}$$

$$-\frac{1}{a}\left(\frac{\partial\theta_0}{\partial x}|_{x_{n+\frac{1}{2}}} - \frac{\partial\theta_0}{\partial x}|_{x_{n-\frac{1}{2}}}\right) - \frac{2i\epsilon}{a}\int_{e_n}\sinh\theta_0 dx - \frac{1}{a}\int_{e_n}S(\epsilon,\theta_0)H_s dx. \tag{8.6}$$

Note that any solution to the Usadel equation (5.35) is also a solution to equation (8.5). However, solutions to the integral equation (8.5) need not have a second derivative everywhere, contrary to solutions to the partial differential equation. Therefore, solutions to equation (8.5) are called weak solutions. In the rest of this section, the term solution will always refer to weak solutions, as the discontinuity of the Heaviside function implies that in general no strong solution exists. This is not a physical problem, as the Heaviside function is an approximation of the real physical situation, the Heaviside function reflects that the thickness of the boundary region of the superconducting electrode with air or vacuum is much smaller than any relevant length scale.

8.3 Discretisation

In this section the discretisation of equation (8.5) will be discussed. Let $y_i, i = 1...N+1$ be a partition of the interval $(0, L)$, and let $e_i = (y_i, y_{i+1}), i = 1...N$. For small a all averages over the intervals e_i can be well approximated by the function value at the center $x_i, i = 1...N$. For the first term, a central discretisation is used. This results in equation (8.7), where the shorthand notation $\theta_n = \delta\theta(x_n)$ and $(\theta_0)_n = \theta_0(x_n)$ has been used:

$$\begin{aligned}&\frac{\theta_{n+1} + \theta_{n-1} - 2\theta_n}{a^2} + 2i\epsilon(\cosh(\theta_0)_n)\theta_n + \frac{\partial S(\epsilon,\theta_0)}{\partial\theta}\theta_n\frac{1}{a}\int_{e_n}H_S(x)dx = \\ &-\frac{(\theta_0)_{n+1} + (\theta_0)_{n-1} - 2(\theta_0)_n}{a^2} - 2i\epsilon\sinh(\theta_0)_n - S(\epsilon,(\theta_0)_n)\frac{1}{a}\int_{e_n}H_S dx.\end{aligned} \tag{8.7}$$

This is a linear equation in $\theta_{1...n}$ and can be solved using a matrix solver, for instance in MATLAB. This solution can then be used as a new Ansatz, as displayed in the scheme in figure 5. The question left over so far, is that of the initialisation. Because for $\epsilon >> \Delta$ the superconductor resembles a normal metal, it was found convenient to first solve the equation for energies well

above the gap. In this energy regime the solution has $|\theta| << 1$, so the zero function $\theta = 0$ can be used for initialisation. Then, when solving the equation for an energy $\epsilon - d\epsilon$, the solution as found for ϵ is used as Ansatz in the initialisation. If dϵ is small, the Ansatz is good, the linearisation method is found to converge.

8.3.1 Finite element method

The discrete Usadel equation can also be derived using the finite element method. It will be shown here that the finite element method yields equations that are almost equal to the equations obtained above. For the derivation, the method described in [92] will be used. Multiplication of equation (8.4) with a test function ϕ and integrating over x gives

$$\int_0^L \left(\frac{\partial^2 \delta\theta}{\partial x^2} + \left(2i\epsilon \cosh{(\theta_0)_n} + \frac{\partial S}{\partial \theta} H_S(x) \right) \delta\theta \right) \phi dx = - \int_0^L \left(\frac{\partial^2 \theta_0}{\partial x^2} - 2i\epsilon \sinh\theta_0 - S(\epsilon, \theta_0) H_S(x) \right) \phi dx \tag{8.8}$$

Now, using the homogeneous essential boundary conditions at $x = 0$ and $x = L$ the first integral can be adjusted. Integration by parts then implies that $\int_0^L \frac{\partial^2 \delta\theta}{\partial x^2} \phi dx = -\int_0^L \frac{\partial \delta\theta}{\partial x} \frac{\partial \phi}{\partial x} dx$. A similar integration by parts can be applied to the right hand side. Now let $\{\phi_i\}_{i=1...N_x}$ be the linear element functions in 1D. Then $\delta\theta \approx \sum_{i=1}^{N_x} \theta_i \phi_i$, where $\theta_i = \delta\theta(x_i)$ and $\theta_0 \approx \sum_{i=1}^{N_x} (\theta_0)_i \phi_i$, where $(\theta_0)_i = \theta_0(x_i)$. Substituting this in equation (8.8) and setting $\phi = \phi_j$ yields equations for $j = 1...N_x$

$$\begin{aligned} &- \sum_{i=1}^{N_x} \theta_i \int_0^L \frac{\partial \phi_i}{\partial x} \frac{\partial \phi_j}{\partial x} dx + \sum_i \theta_i \int_0^L \left(2i\epsilon \cosh \sum_{k=1}^{N_x} (\theta_0)_k \phi_k \right) \phi_i \phi_j dx + \int_0^L H_S(x) \frac{\partial S}{\partial \theta} \sum_{i=1}^{N_x} \theta_i \phi_i) \phi_j dx = \\ &- \sum_{i=1}^{N_x} (\theta_0)_i \int_0^L \frac{\partial \phi_i}{\partial x} \frac{\partial \phi_j}{\partial x} dx - \int_0^L \left(2i\epsilon (\sinh \sum_{i=1}^{N_x} (\theta_0)_i \phi_i) dx + \int_0^L H_S(x) S(\sum_{i=1}^{N_x} \theta_i \phi_i) \right) \phi_j dx \end{aligned} \tag{8.9}$$

For both the left hand side and the right hand side the first term can be calculated exactly. The term $\frac{\partial \phi_i}{\partial x}$ has support on (x_{i-1}, x_{i+1}), and equals $\frac{1}{a}$ on the first half on this interval, $-\frac{1}{a}$ on the second half of the interval. Thus

$$\int_0^L \frac{\partial \phi_i}{\partial x} \frac{\partial \phi_j}{\partial x} dx = \begin{cases} 0 & |i-j| > 1 \\ -\frac{1}{a} & |i-j| = 1 \\ \frac{2}{a} & i = j. \end{cases} \tag{8.10}$$

The first term thus becomes $\frac{\theta_{j+1} + \theta_{j-1} - 2\theta_j}{a^2}$. The second term on the left hand is nonlinear, therefore, an approximation is needed. The Newton-Cotes rule for a 1D element can be used on each interval. Only for $i = j$ there is a nonzero contribution, coming only from $x = x_i$, which implies that this term becomes $a\theta_j 2i\epsilon \cosh{(\theta_0)_j}$. The second term on the right can be treated in a similar way, this yields $a2i\epsilon \sinh{(\theta_0)_j}$. Again, the third term on both sides is different, because $H_S(x)$ is not continuous. On the support of the Heaviside function the function equals 1. Outside this interval, its contribution is 0. The Newton-Cotes rule can thus be used, but not only on the support of H_S. As the integral over the Heaviside function gives exactly the length of its support, it follows that

$$\int_0^L H_S(x) \frac{\partial S}{\partial \theta} \phi_j \sum_i \theta_i \phi_i dx = \frac{\theta_j}{2} \frac{\partial S}{\partial \theta} \int_{x_{j-1}}^{x_{j+1}} H_S dx \tag{8.11}$$

$$\int_0^L H_S(x) S(\sum_i \theta_i \phi_i) \phi_j dx = \frac{1}{2} S(\theta_j) \int_{x_{j-1}}^{x_{j+1}} H_S dx. \tag{8.12}$$

With these expressions the finite element equation can be written as

$$\begin{aligned}&\frac{\theta_{j+1}+\theta_{j-1}-2\theta_j}{a}+\left(2i\epsilon a(\cosh(\theta_0)_j)+\frac{1}{2}\frac{\partial S}{\partial\theta}\int_{x_{j-1}}^{x_{j+1}}H_S(x)\right)\theta_j\\=&-\frac{(\theta_0)_{j+1}+(\theta_0)_{j-1}-2(\theta_0)_j}{a}-2ia\epsilon\sinh(\theta_0)_j-\frac{1}{2}S(\theta_j)\int_{x_{j-1}}^{x_{j+1}}H_S dx.\end{aligned}\tag{8.13}$$

The equation found here is very similar to equation (8.7). The only difference is that the term $\int_{e_n} H_S dx = \int_{x_{j-\frac{1}{2}}}^{x_{j+\frac{1}{2}}} H_S dx$ has been replaced by $\frac{1}{2}\int_{x_{j-1}}^{x_{j+1}} H_S dx$.
With this, the model for the problem and the implementation have been discussed. In the following sections, the results of the code will be discussed. In the following sections, the discretisation from section 8.3 will be used.

9 Validation

This section will describe verification and validation results of the code developed in the previous sections. First, known results are reproduced here. This section will be the validation of the code. New results will be presented in subsequent sections. From section 10 onward, the model will be used to produce new results, some of which can be compared with analytical approximations to the problem.

9.1 Code for retarded part

The physical problem at zero phase difference is symmetric upon mirroring $x \to -x$, the numerical code should preserve this property. It was found that the code preserves this symmetry.

9.2 Minigap and Thouless energy

In this section it is explained and verified that there are two relevant energy scales in long VT junctions. Next to the superconducting gap Δ, there is the Thouless energy scale, as observed before [93], [94]. Moreover, the coherent low energy transport in long junctions mentioned in [95] will be discussed.

9.2.1 Analytical considerations

Recall that the Usadel equation in the region in between the electrodes reads in absence of a phase difference

$$\frac{\partial^2\theta}{\partial x^2} + 2i\alpha\epsilon \sinh\theta = 0. \tag{9.1}$$

Now, in case the proximity effect is small, that is, $|\theta| \ll 1$, this can be approximated by

$$\frac{\partial^2\theta}{\partial x^2} + 2i\alpha\epsilon\theta = 0. \tag{9.2}$$

The symmetric solution to this equation reads

$$\theta(x,\epsilon) = \theta_0(\epsilon)\frac{\cosh\sqrt{-2i\alpha\epsilon}x}{\cosh\sqrt{-2i\alpha\epsilon}\frac{L}{2}}, \tag{9.3}$$

where $\theta_0(\epsilon)$ is the value at the left and right endpoints of the interval under consideration, mainly determined by the superconducting electrodes. The value of θ_0 is thus not expected to have a strong length dependence.
From this it can be deduced that

$$\theta(0,\epsilon) = \theta_0\frac{1}{\cosh\sqrt{-2i\alpha\epsilon}\frac{L}{2}}, \tag{9.4}$$

which shows that in case $\sqrt{\epsilon}L \gg 1$ the value of θ in the centre of the junction is suppressed by a complex exponential with $\sqrt{\epsilon L}$.
Instead of considering what happens if L is increased, one can also consider the energy dependence of $\theta(0)$. Viewing $\theta(0)$ at a fixed L at a fixed position as a function of energy, it should be taken into account that θ_0 is energy dependent. Therefore, the energy dependence is not a simple complex hyperbolic cosine. However, from the term $\frac{1}{\cosh\sqrt{-2i\alpha\epsilon}\frac{L}{2}}$ it is clear that $\epsilon_{\mathrm{Th}} \sim \frac{1}{L^2}$ is a relevant energy scale for the problem.

In case of a nonzero phase difference the coupled equations should be considered. Again using the approximation $\sinh x \approx x$, the equations read

$$\frac{\partial^2\theta}{\partial x^2} + 2i\alpha\epsilon\theta - (\frac{\partial\chi}{\partial x})^2\theta = 0. \tag{9.5}$$

$$\frac{\partial}{\partial x}\left(\theta^2\frac{\partial\chi}{\partial x}\right) = 0. \tag{9.6}$$

The second of these equations can be written as

$$\theta^2\frac{\partial\chi}{\partial x} = \frac{j_\epsilon}{2}, \tag{9.7}$$

where j_ϵ is the position independent spectral supercurrent. Substituting this in the first equation one obtains

$$\frac{\partial^2\theta}{\partial x^2} + 2i\alpha\epsilon\theta - \frac{j_\epsilon^2}{4\theta^4}\theta = 0. \tag{9.8}$$

Now suppose that the second term completely dominates the third over the entire interval. After the calculation it will become clear under which assumptions this is a self-consistent approximation. In this approximation, the solution to the θ-equation is expression (9.3). Substituting this in the second equation, and considering that the phase difference between the ends of the intervals is $\Delta\psi$, one finds

$$\Delta\psi = \int_{-\frac{L}{2}}^{\frac{L}{2}} \frac{\partial\chi}{\partial x}dx \tag{9.9}$$

$$= \int_{-\frac{L}{2}}^{\frac{L}{2}} \frac{j_\epsilon}{2\theta^2}dx \tag{9.10}$$

$$= \frac{j_\epsilon \cosh^2\sqrt{2i\alpha\epsilon}\frac{L}{2}}{2\theta_0^2}\int_{-\frac{L}{2}}^{\frac{L}{2}} \frac{1}{\cosh^2\sqrt{2i\alpha\epsilon}x}dx. \tag{9.11}$$

As indicated, this is in the regime $\sqrt{\epsilon}L \gg 1$, so the integration limits can be replaced by $\pm\infty$ and the integral yields a factor $2\sqrt{2i\epsilon}$. Thus, the phase difference and the spectral supercurrent are related by

$$j_\epsilon \approx \frac{\Delta\psi\theta_0^2\sqrt{-2i\alpha\epsilon}}{\cosh^2\sqrt{2i\alpha\epsilon}\frac{L}{2}}. \tag{9.12}$$

From this two main conclusions can be drawn:

- $(\frac{\partial\chi}{\partial x})_{\max} \approx \frac{j_\epsilon}{2\theta(0)^2} \approx \frac{\Delta\psi\theta_0^2\sqrt{-2i\alpha\epsilon}}{\cosh^2\sqrt{2i\alpha\epsilon}\frac{L}{2}}\frac{\cosh^2\sqrt{2i\alpha\epsilon}\frac{L}{2}}{2\theta_0^2} = \frac{\Delta\psi}{2}\sqrt{-2i\alpha\epsilon}$. Thus, the approximation to neglect the third term is valid if $|2i\alpha\epsilon| \gg (\frac{\Delta\psi}{4}\sqrt{-2i\alpha\epsilon})^2$, which is equivalent to $\frac{(\Delta\psi)^2}{4} \ll 1$. This should be taken into account when analysing the results.
- For $\Delta\psi$ in the considered regime, the spectral supercurrent is exponentially suppressed at large ϵL^2.

9.2.2 Code

In Josephson junctions, there are two relevant energy scales, the gap energy Δ of the superconductor and the Thouless energy $E_{\text{Th}} = \frac{\hbar D}{L^2}$ [96], [97]. The Thouless energy is, apart from a factor $\hbar$, equal to the inverse of the diffusion time of the system. For short Josephson junctions the induced minigap in the normal material is of the order of Δ, but in long junctions the induced minigap at

the centre of the junction is of the order of E_{Th} [98]. This is directly related to the considerations in section 9.2.1. From the analytical approximations it can be inferred that E_{Th} is the energy such that for $\epsilon >> E_{\text{Th}}$ the argument of the hyperbolic cosine is large, that is, for $\epsilon >> E_{\text{Th}}$ the exponential suppression of θ and j_E is significant. To test whether the code reproduces this result the energy of the peak in the local density of states at the centre of the junction was calculated as a function of the junction length.This energy will be referred to as the peak energy
The results for $L = 8$ are shown in figure 6. The figures for other lengths are shown in appendix A.1. As introduced before, the local density of states $\nu = \cosh\theta$ is the density of states. The results compare well with the results in [90]. Near the electrodes, at $\frac{x}{L} \in \{\frac{1}{8}, \frac{7}{8}\}$, the local density of states is peaked around $E = \Delta$, as expected from the influence of a superconducting electrode [53], [23], [52]. Further from the electrodes, the local density of states is maximal at an energy $E < \Delta$. The length dependence of the peak energy is shown in figure 7a. The energies in this figure are expressed in units of Δ. For small junction lengths the peak energy is close Δ, as expected. For large junctions the peak energy drops.

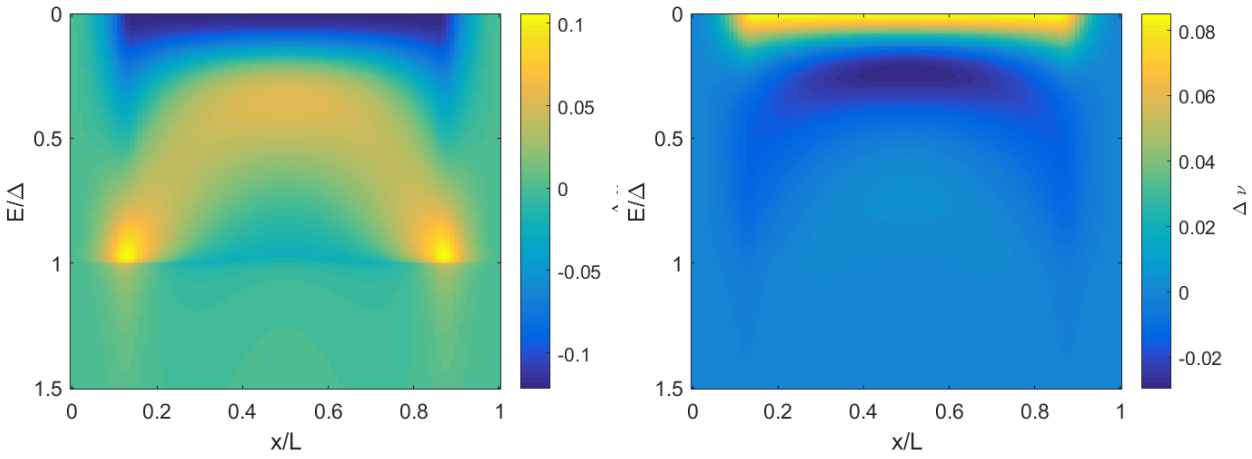

(a) S-wave.

(b) P-wave.

Figure 6: The local density of states as a function of position and energy in the VT-junction for s-wave (left) and p-wave (right) electrodes for a junction length $L = 8$. In the s-wave electrodes the Tanaka Nazarov boundary conditions with $\Delta = \Delta_0$ were implemented, for the p-wave electrodes the Tanaka Nazarov boundary conditions with $\Delta = \Delta_0 \cos\phi$ was used. For both, the parameters were set to $(\gamma_B, z) = (1, 0.2)$. For p-wave electrodes there is a peak at $E = 0$ and a dip in the local density of states at an energy that is a function of position. For s-wave electrodes there is a peak in the local density of states whose energy is position dependent and satisfies $\frac{E_{\text{peak}}}{\Delta} \approx 1$ above the electrodes. This is in good correspondence with the results in [90]. For clarity of presentation $\delta\nu$ was calculated, so that the zero-point corresponds to a normal state.

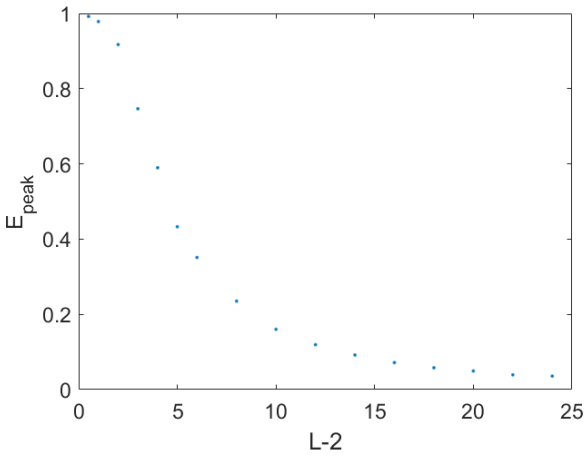

(a) The energy of the peak at the centre of the junction as a function of the junction length L, in units of Δ. S-wave superconductors were used in the calculation of these results.

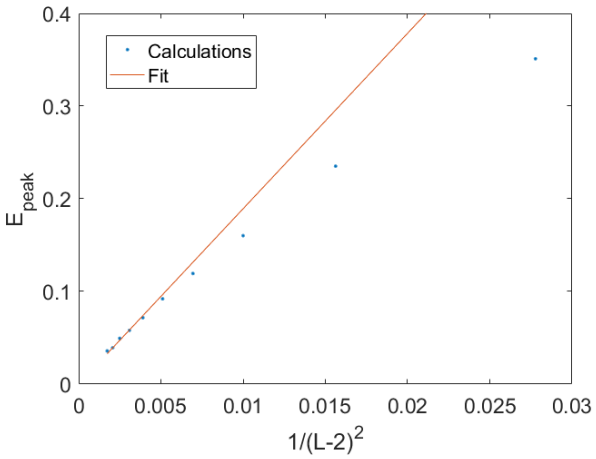

(b) The energy of the peak at the centre of the junction as a function of $(L-2)^{-2}$, in units of Δ for s-wave superconductors. For long junctions, the peak energy depends linearly on the inverse length squared.

Figure 7: The energy of the peak in the density of states at the centre of the junction as a function of the length of the junction. The s-wave superconducting electrodes have been placed with their centre one coherence length from the reservoirs, which means that the distance between the centres of the electrodes is $L-2$. The phase difference between the electrodes is set to 0. A linear fit was used on the results of the longest junctions. This fit corresponds well to the data, showing that in the long junction limit $E_{\text{peak}} \propto \frac{1}{(L-2)^2}$.

Because the Thouless energy is inversely proportional to $(L-2)^2$, the peak energy is shown as a function of $(L-2)^{-2}$ in figure 7b, together with a linear fit. Only the results for $L \geq 8$ are shown. In the calculations the boundary parameters were set to $(\gamma, z) = (1, 0.2)$, for the numerical model 100 spatial grid intervals were used. Calculations were performed for 221 values of E, in the range $\frac{E}{\Delta} = (0, 1.5)$. The linear fit approximates the data well for large L. This means that the code reproduces the expected results in this respect.

The test was repeated for the case of p-wave electrodes. The local density of states is shown in appendix A.2. In the case of p-wave electrodes there is a zero energy peak. Thus, instead of the location of the peak, the energy of the dip E_{valley} was investigated. The results are shown in figures 8a and 8b. The energy of the dip shows a linear dependence on $(L-2)^{-2}$ for large L, as expected. For small $L-2$ the peak is of the order of Δ. The limit as $L \to 2$ is not Δ, but rather a value $E \approx \frac{3}{4}\Delta$. This is due to the gap in p-wave superconductors being $\Delta \cos\phi$ rather than Δ.

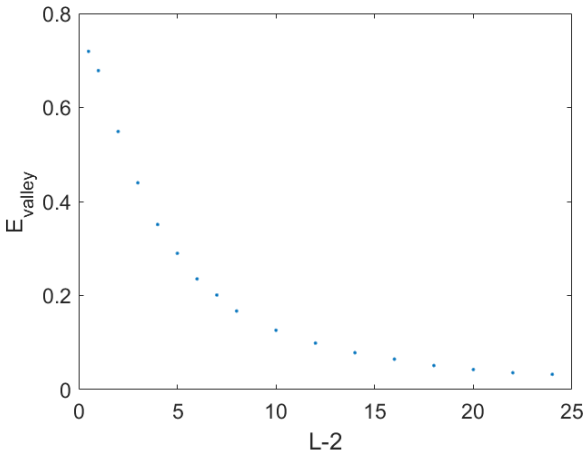

(a) The energy of the dip at the centre of the junction as a function of the junction length L, in units of Δ. P-wave electrodes were used in the calculation of these results.

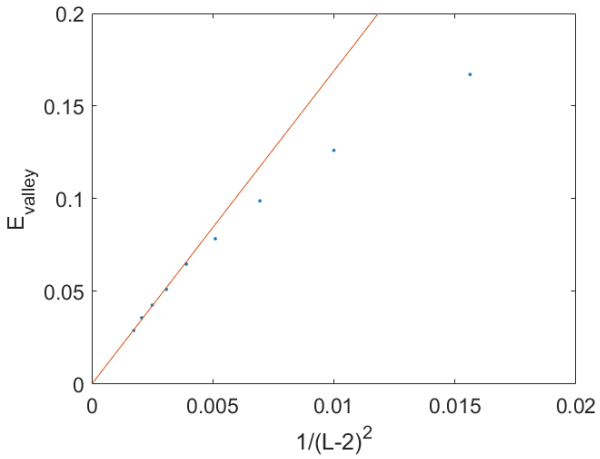

(b) The energy of the dip at the centre of the junction as a function of $(L-2)^{-2}$, in units of Δ for p-wave electrodes. For long junctions, the valley energy depends linearly on the inverse length squared.

Figure 8: The energy of the dip in the density of states at the centre of the junction. The p-wave superconducting electrodes have been placed with their centre one coherence length from the reservoirs, which means that the distance between the centres of the electrodes is $L-2$. The phase difference between the electrodes is set to 0. A linear fit was used on the results of the longest junctions. This fit corresponds well to the data, showing that in the long junction limit $E_{\text{valley}} \propto \frac{1}{(L-2)^2}$.

9.3 Code for Keldysh part

For the Keldysh component, the equation in the normal metal ignoring the electrodes is linear. The main feature of the system is that when no voltage is applied to the system and there is no phase difference between the electrodes, the current through the junction should be zero. In this section it will be shown that in case no bias voltage is applied to the reservoirs the solution to the Keldysh equation of the Usadel equation using the Tanaka Nazarov boundary conditions is

$$f_L(E,x) = f_{L0}(E) \tag{9.13}$$

$$f_T(E,x) = 0. \tag{9.14}$$

This shows that the model does indeed satisfy the requested feature, since the latter equation implies that no dissipative current flows, while the former equation implies that the equilibrium Fermi-Dirac distribution is attained.
To obtain this result, a lemma is needed. A statement of this lemma was given in [99], [100].
Let $X, Y \in \mathbf{C}^{4x4}$ with retarded, Keldysh and advanced components. If there exists $h \in \mathbf{C}^{2x2}$ such that

$$X = \begin{bmatrix} X^R & X^R h - h X^A \\ 0 & X^A \end{bmatrix}, Y = \begin{bmatrix} Y^R & Y^R h - h Y^A \\ 0 & Y^A, \end{bmatrix} \tag{9.15}$$

then

1. $(XY)^K = (XY)^R h - h(XY)^A$.
2. $(X^{-1})^K = (X^R)^{-1} h - h(X^A)^{-1}$.

The first statement is proven as follows:

$$\begin{aligned}(XY)_K &= X^R Y^K + X^K Y^A = X^R Y^R h - X^R h Y^A + X^R h Y^A - h X^A Y^A \\ &= X^R Y^R h - h X^A Y^A = (XY)^R h - h (XY)^A.\end{aligned} \tag{9.16}$$

The second equation can be found using that the Keldysh component of the identity matrix is actually 0.

$$0 = (XX^{-1})^K = X^R (X^{-1})^K + X^K (X^{-1})_A = X^R (X^{-1})^K + X^K (X^A)^{-1}. \tag{9.17}$$

From this it follows that

$$(X^{-1})^K = -(X^R)^{-1} X^K (X^A)^{-1} = -(X^R)^{-1} X^R h (X^A)^{-1} + (X^R)^{-1} h X^A (X^A)^{-1} = (X^R)^{-1} h - h (X^A)^{-1}. \tag{9.18}$$

This proves the lemma.

Now the claim that $f_L(E,x) = f_{L0}$ and $f_T(E,x) = 0$ solves the Keldysh equations can be proved. Recall from equations (B.33) and (B.34) that the Keldysh equations read

$$\begin{aligned}&\nabla(D_L \nabla f_L) + \nabla(C_L \nabla f_T) + \mathrm{Im Is} \nabla f_T = 0 + \mathrm{Tr}(S), \\ &\nabla(D_T \nabla f_T) + \nabla(C_T \nabla f_L) + \mathrm{Im Is} \nabla f_L + \mathrm{Tr}(\tau_3 S) = 0,\end{aligned} \tag{9.19}$$

and the boundary conditions read $f_L(E,0) = f_L(E,L) = f_{L0}$ and $f_T(E,0) = f_T(E,L) = 0$. In the proposed solution, f_L and f_T are independent of position, so all derivatives vanish. This means that it is enough to show that S vanishes. Recall from equation (B.18) that

$$\begin{aligned}S &= 2([G,B]^K - [G,B]^R h + h[G,B]^A)\Theta_s(x), \\ B &= D^{-1} N, \\ N &= T_{1n} H_+^{-1} H_- - T_{1n} H_+^{-1} + T_{1n}^2 H_+^{-1} H_- G_1 H_-^{-1} H_+, \\ D &= -T_{1n} H_+^{-1} H_- G_1 H_-^{-1} + T_{1n} H_+^{-1} G_1 + 1 - T_{1n}^2 H_+^{-1} H_- G_1 H_-^{-1} H_+ G_1.\end{aligned} \tag{9.20}$$

In this equation all quantities in the normal material have $X^K = X^R h - h X^A$ and all quantities in the superconductor have $Y^K = Y^R h_s - h_s Y^A$. However, for the proposed solution $h = h_s$, and therefore the lemma can be applied several times to the epxressions for N and D to obtain $N_K = N_R h - h N_A$ and $D_K = D_R h - h D_A$. Thus, applying the lemma to $B = D^{-1} N$, it is found that $B_K = B_R h - h B_A$. Now a last application of the lemma gives $([G,B])^K = ([G,B])^R h - h([G,B])^A$. This shows that indeed $S = 0$. Thus, $f_L(E,x) = f_{L0}(E)$ and $f_T(E,x) = 0$ solve the Keldysh equations. The numerical code should provide this solution, and it was found to do so.
This shows that the code for both the retarded and the Keldysh component is consistent with other research and analytical approximations. In the following sections the results of the code will be analysed further.

10 Effect of boundary conditions

The Tanaka-Nazarov boundary conditions are characterised by two parameters, z and γ_B, the parameter z via the transparency $T_\theta = \frac{\cos\theta^2}{\cos\theta^2+z^2}$, the parameter γ_B as $I \propto \gamma_B$. The parameters may differ per contact. Therefore, it is important to investigate the influence of these parameters on the Green's function in the normal metal. The influence of these parameters is investigated for different configurations. The short junction limit is chosen here, because in the short junction limit there are analytical calculations for the spectral supercurrent in the transparent junction limit $\gamma = \frac{L_y}{\xi}\gamma_B \ll 1$: [101]

$$\mathrm{ImIs} = \frac{\Delta^2 \sin\phi}{\sqrt{E^2-\Delta^2}\sqrt{E^2-\Delta^2\cos^2\frac{\phi}{2}}}. \tag{10.1}$$

It should be noted that this expression is calculated using Kupriyanov Luckichev boundary conditions, rather than Tanaka Nazarov boundary conditions. However, the qualitative predictions of equation (10.1) should be satisfied by the model.

10.1 SNS junction

To compare with the analytical results from [101], the conventional SNS junction was investigated for a length of $L = \frac{\xi}{5}$. A phase difference of $\frac{\pi}{5}$ was imposed between the superconducting electrodes. The density of states and the spectral supercurrent in the middle of the junction were investigated. The results depend strongly on the different parameters. In the limit of small γ the results are in accordance with the analytical calculations of [101]. There is clear gap that is slightly smaller than Δ. It was found that for small γ_B the gap value is close to the analytically predicted value of $\Delta\cos\frac{\phi}{2}$. The density of states shows a peak just above the gap energy. It should be noted that the density of states for energies in the gap is not exactly zero. However, as the density of states is 5 orders of magnitude smaller than for larger E this region will be referred to as a gap. The difference between the results obtained here and the analytic results in [101] is due to the neglect of higher order terms in analytical calculations. For large γ_B the results are distinctly different. Whereas analytically there should be no states for $E < \Delta\cos\frac{\phi}{2}$, the contribution of energies in this energy range is considerable for large γ_B, for very large γ_B the main contribution can even be found for energies close to $E = 0$.
The results indicate that a different quality of the electrodes has an influence on the density of states and spectral supercurrent that is similar to the influence of an imposed phase difference. This should be taken care of in possible experiments.

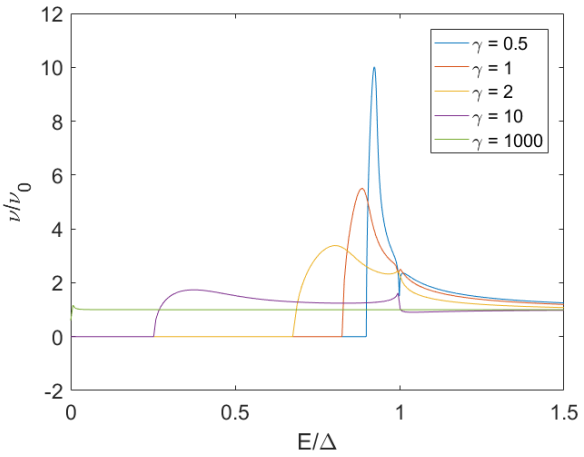

(a) The density of states. For $\gamma = 0.5$ the calculations become unstable. A smaller γ leads to a sharper peak, closer to $E = \Delta$.

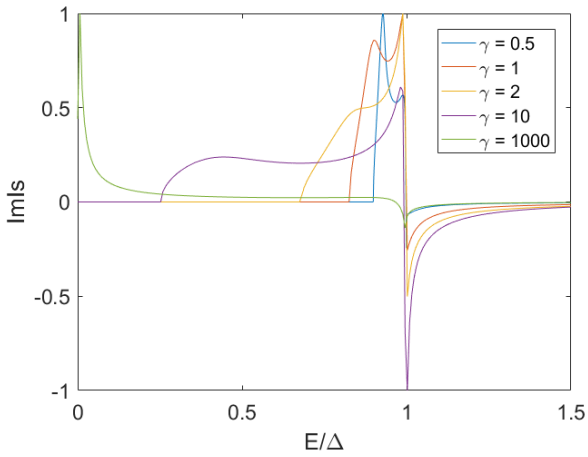

(b) The spectral supercurrent. The results are normalised to their maximum absolute to compare the results. As for the density of states a smaller γ leads to a larger minigap. The results for small γ are similar to the results predicted by equation (10.1), there are two peaks, one at $E \approx \Delta$, and one slightly below. Thus, the results are in agreement with [101].

Figure 9: Density of states and spectral supercurrent for the SNS junction. The boundary parameter z is kept constant at $z = 1$. The results show that for smaller values of γ the minigap at low energies becomes larger. For $\gamma = 0.5$ calculations for 100 spatial intervals and 221 energy values were not stable, calculations were repeated for 800 spatial intervals and 2210 energy values.

The behaviour of the spectral supercurrent is similar, for small γ the results are in good agreement with the analytical calculations in [101], for large γ the results are distinctly different. In the resolution of figure 9 it appears that the spectral supercurrent has a peak at zero energy for large γ. However, this is a purely numerical artifact, the minigap is so small that that it does not appear in the resolution of figure 9. This is confirmed in figure 10. It was found that both the minigap and the peak in the spectral supercurrent scale as $\frac{1}{\gamma}$ in the range of large γ.

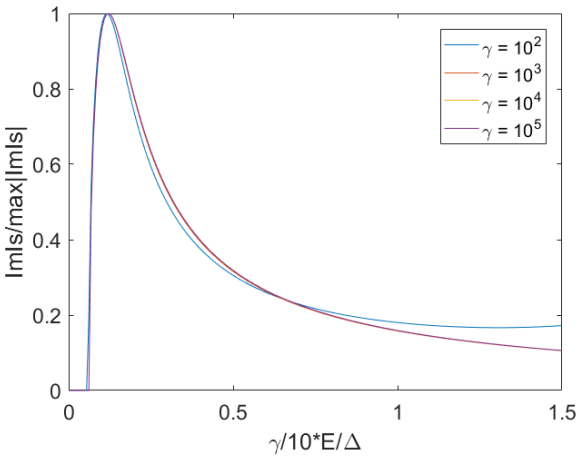

(a) The low energy spectral supercurrent in the SNS junction in the large γ range. The spectral supercurrent as been normalised to to its maximum value, energies have been scaled by γ. The profiles for large γ are very similar, indicating that both the peak energy and the minigap scale as $\frac{1}{\gamma}$ for large γ. This shows that for large γ there is still a minigap, although very small for large γ.

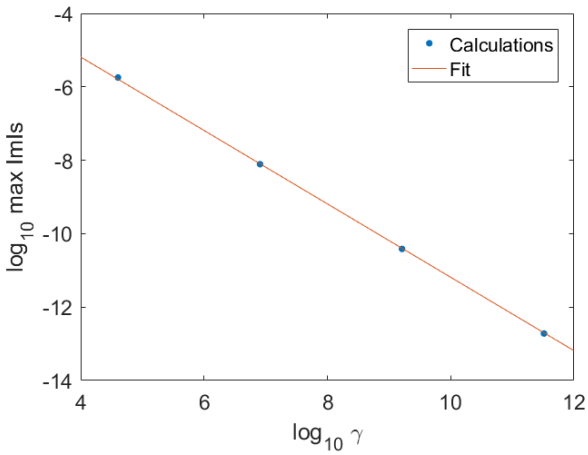

(b) The maximum spectral supercurrent in the SNS junction as a function of γ. A linear fit with slope -1 was used on the data. The good agreement between the calculations and the linear fit show that the maximum spectral supercurrent scales at $\frac{1}{\gamma}$ for large γ.

Figure 10: The low energy behaviour of the spectral supercurrent in the SNS junction for large γ. Both the location and the height of the peak scale as $\frac{1}{\gamma}$ for large γ, the function shape is approximately the same for all γ.

The parameter z has a similar influence as the parameter γ, in that low energy states become more important to the supercurrent contribution if the parameter z is increased. A distinction however, is that states around $E = \Delta$ remain important for large z-values, whereas for large γ-values states with $E \approx \Delta$ are much less pronounced compared to the results for small γ. For large z the spectral supercurrent normalised to its maximum value becomes approximately independent of z.

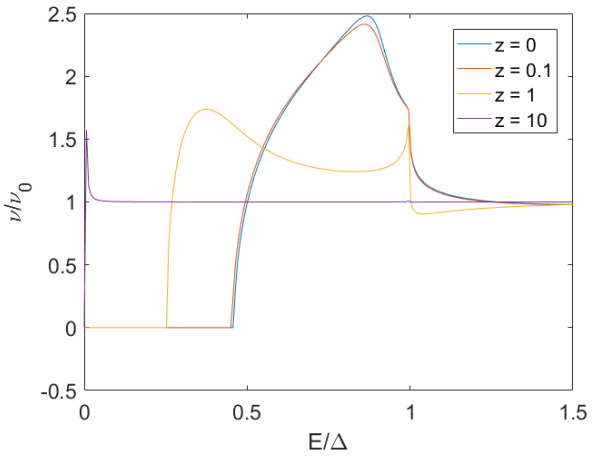

(a) The density of states for different values of z for the SNS junction. The density of states is sensitive to the z-parameter. For small values of z there is a clear gap at low energies, for large z this gap becomes smaller and smaller.

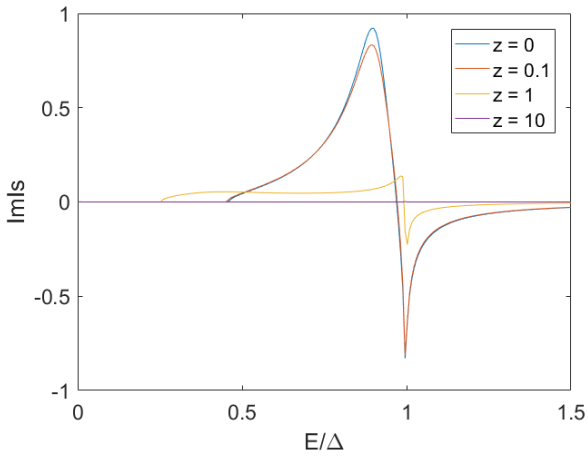

(b) The spectral supercurrent for different values of z for the SNS junction. As for the density of states, the spectral supercurrent shows a gap at low energies for small z. The result are different from equation (10.1). This is no surprise as $\gamma = 10 > 1$ is used. As expected from the decrease of transparency with z the supercurrent is smaller for larger z.

Figure 11: Density of states and spectral supercurrent for the SNS junction. The boundary parameter γ is kept constant at $\gamma = 10$.

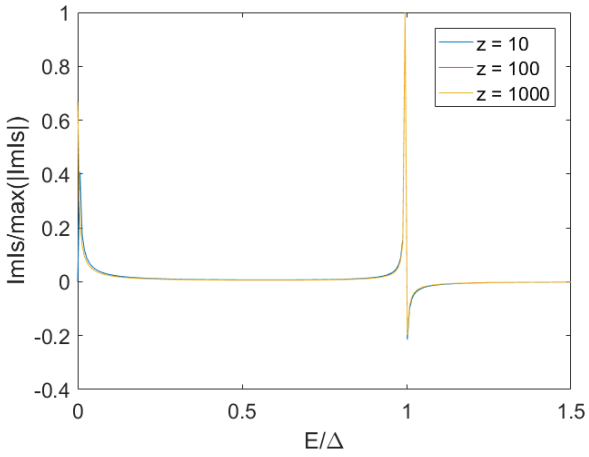

Figure 12: The spectral supercurrent for large values of z for the SNS junction. The value of γ is set to 10. To compare the results the supercurrrent is normalised to its maximum. The results for the different z-values are very similar.States with $E \approx \Delta$ remain important to the transport of current as z is increased.

10.2 VT-junction

Similar calculations have been executed for the VT-junction. However, the length of the junction was not to be set to $\frac{\xi}{5}$, as the distance between electrodes and reservoirs and the width of the electrodes is nonzero. The distance between the reservoirs and the centre of the electrodes is ξ,

the width of the electrodes is $\frac{3}{10}\xi$. Therefore the required length of the VT junction such that the region between the electrodes is $\frac{\xi}{5}$ is $L = \frac{5}{2}\xi$. The results, shown below, are different from the results for the SNS junction. For the SNS junction the density of states shows a gap at low energies, for the VT-junction there is only a suppression of the density of states in the low energy limit. The spectral supercurrent shows similarities with the spectral supercurrent in the SNS junction in that the spectral supercurrent for energies $E > \Delta$ have opposite sign compared to the spectral supercurrent for $E < \Delta$. The cause of the differences between the results for the SNS junction and the VT-junction will be investigated in the coming section.

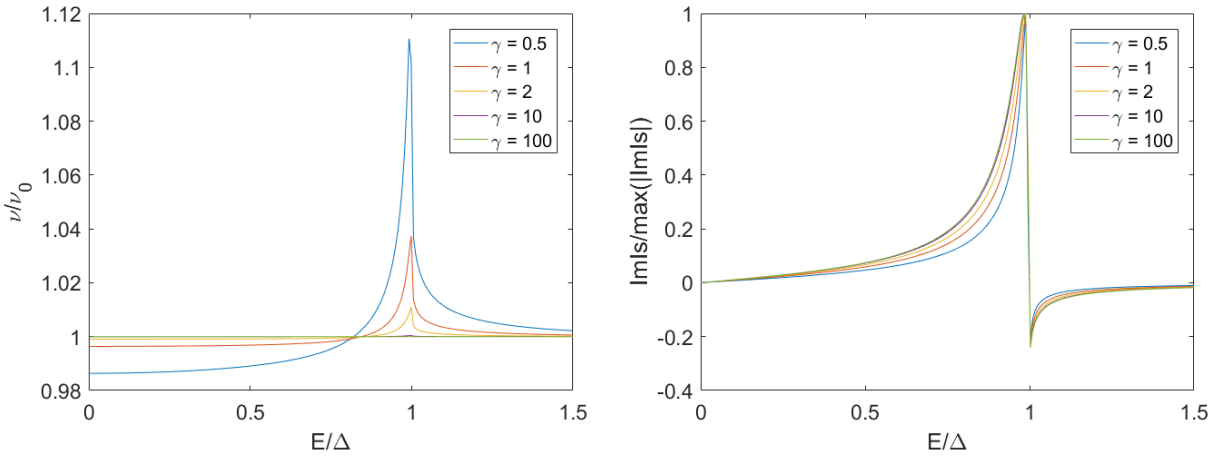

(a) Density of states. Contrary to the SNS junction, there is no gap, the density of states is only slightly suppressed. The profiles for different γ are similar, a smaller γ leads to a higher peak at $E = \Delta$ and more supression for small $\frac{E}{\Delta}$.

(b) Spectral supercurrent. Results have been normalised to highlight the similarity in energy dependence. For small γ the peak around $E = \Delta$ is slightly sharper than for large γ.

Figure 13: Density of states and spectral supercurrent as a function of energy for different values of γ for the VT-junction. In the calculations $z = 1$ was used.

For the VT-junction there is a distinct difference between the dependence on γ and the dependence on z. Whereas the dependence on γ merely increases the peak at $E = \Delta$, a decrease of z actually causes the peak to shift to lower energies.

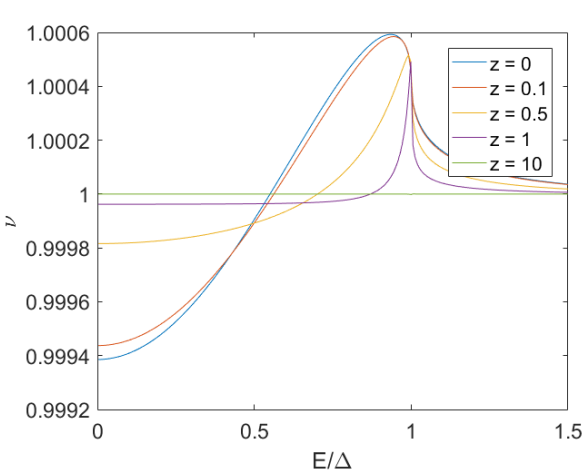

(a) Density of states. For large values of z there is a sharp peak in the density of states. For small z the peak becomes broader and is centered at $E < \Delta$.

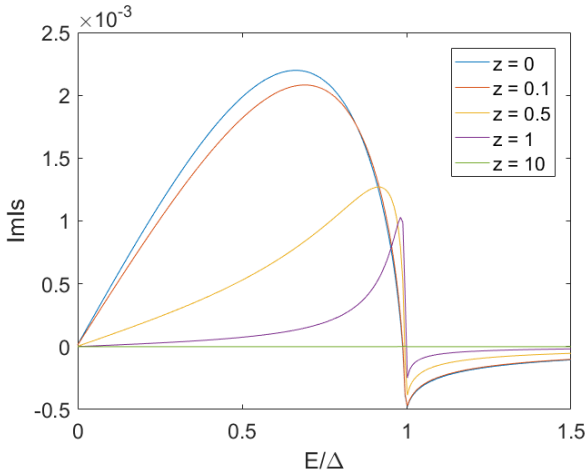

(b) The spectral supercurrent. A smaller z value gives a broader peak at lower energy. The spectral supercurrent shows no gap at zero energy, contrary to the case of the SNS junction.

Figure 14: Density of states and spectral supercurrent for the VT-junction. The boundary parameter γ is kept constant at $\gamma = 10$, the value of z is varied.

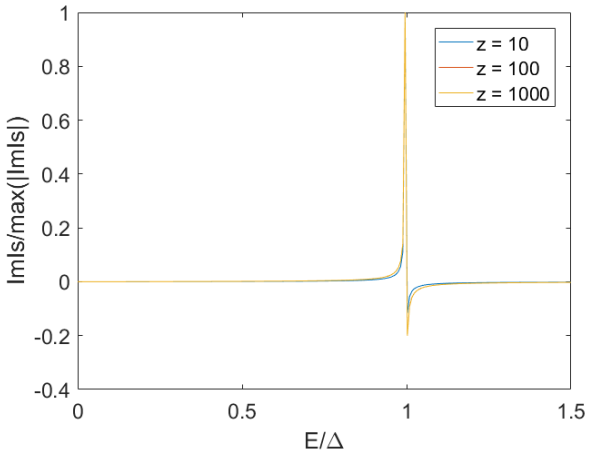

Figure 15: The spectral supercurrent normalised to its maximum absolute value for large z for the VT-junction. The value of γ was 10 for all calculations. Similar to the SNS junction, the energy dependence of supercurrent is similar for the different large values of z.

10.3 Modified VT-junction

To investigate whether the differences between the results from the SNS junction and VT-junction are to be attributed to the use of the electrodes as source term instead of a normal boundary condition or to the presence of the metallic reservoirs the calculations for the VT-junction were repeated, however, now the Dirichlet boundary condition for metallic reservoirs was replaced by the no current boundary condition for vacuum. Again, the length of the junction was set to $\frac{5}{2}\xi$. The results are shown below.

The results for the modified VT-junction are more similar to the results for the SNS junction than to the results of the VT-junction. The density of states and the spectral supercurrent do show a gap

at low energies, though smaller than for the SNS junction. Thus, the presence of metallic reservoirs is the main cause for the difference between the results of the different geometries. The vertical instead of horizontal placement of the electrodes does have some influence, but this influence is distinctively smaller.

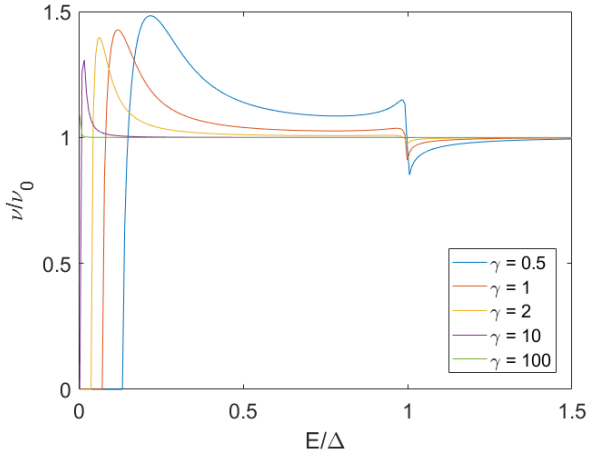

(a) Density of states. The density of states shows a gap at low energies, similar to the SNS junction and contrary to the VT-junction, however, the gap is distinctly smaller than for the SNS junction.

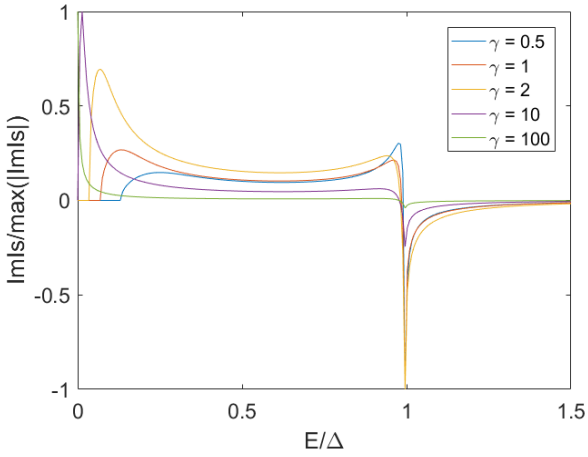

(b) The spectral supercurrent. The dependence on energy is very similar to the SNS junction, however, the gap at low energy is much smaller.

Figure 16: Density of states and spectral supercurrent for the modified VT-junction. The boundary parameter z is kept constant at $z = 1$, the value of γ is varied.

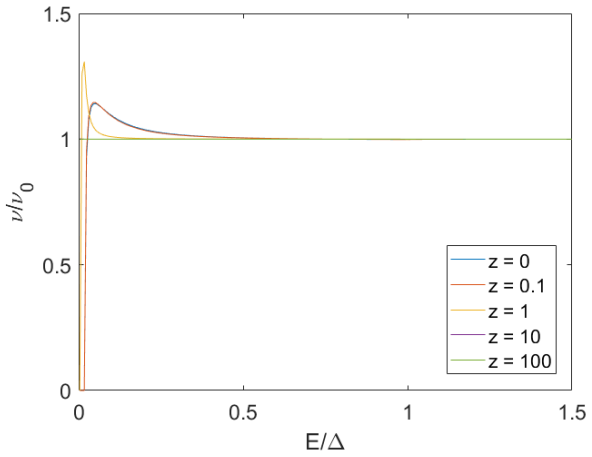

(a) Density of states. The peak at $E = \Delta$ is completely overwhelmed by the peak at low energy. Te density of states for very low energies is zero.

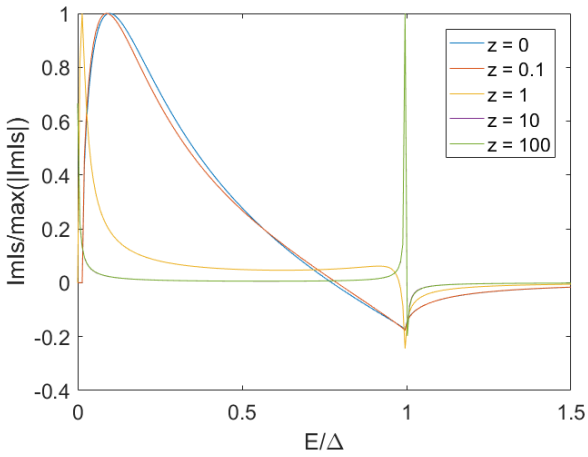

(b) The spectral supercurrent. The results are normalised to the maximum absolute value to highlight the difference in energy dependence. As is the case for SNS junctions there is a broad peak and a gap at low energy for small z, albeit the energies associated with the peak and gap are distinctly lower. For large z the peak becomes sharper and shifts towards zero energy.

Figure 17: Density of states and spectral supercurrent for the modified VT-junction. The boundary parameter γ is kept constant at $\gamma = 10$, the value of z is varied.

11 Phase difference near π

When the phase difference between the electrodes is π the supercurrent through a Josephson junction absent [23]. The model was found to reproduce this fact. This can be explained from symmetry arguments. When the phase difference is π the $(1,2)$-element of G^R, which will be called F here, describing the superconducting correlations, is antisymmetric with respect to the centre of the junction. This means that at the centre of the junction $F = 0$. Thus, at the centre of the junction the material is normal, without superconducting correlations. This explains the absence of a supercurrent. There are two ways to parametrise this state in the θ-parametrisation. One way is that the parameter θ is antisymmetric around the centre of the junction and the parameter χ is constant. The other is that the parameter is θ is symmetric around the centre of the junction and χ makes a jump of magnitude π at the centre of the junction and is constant elsewhere. In the latter description the parameters are not differentiable (θ) and not continuous (χ), so the former is the desired description at $\Delta\psi = \pi$. However, the latter description turns out to be the limiting behaviour of the parameters as $\Delta\psi \to \pi$. Figures 18 and 19 show the behaviour of the parameters used in the Usadel equation as a function of the phase difference between the electrodes. In the calculations the boundary parameters were set to $(\gamma, z) = (1, 0.2)$. Calculations were performed for 221 values of E, in the range $\frac{E}{\Delta} = (0, 1.5)$. For all phase differences θ is symmetric around the centre of the junction, whereas for χ the gradient at the centre of the junction becomes larger and larger, approaching a step function.

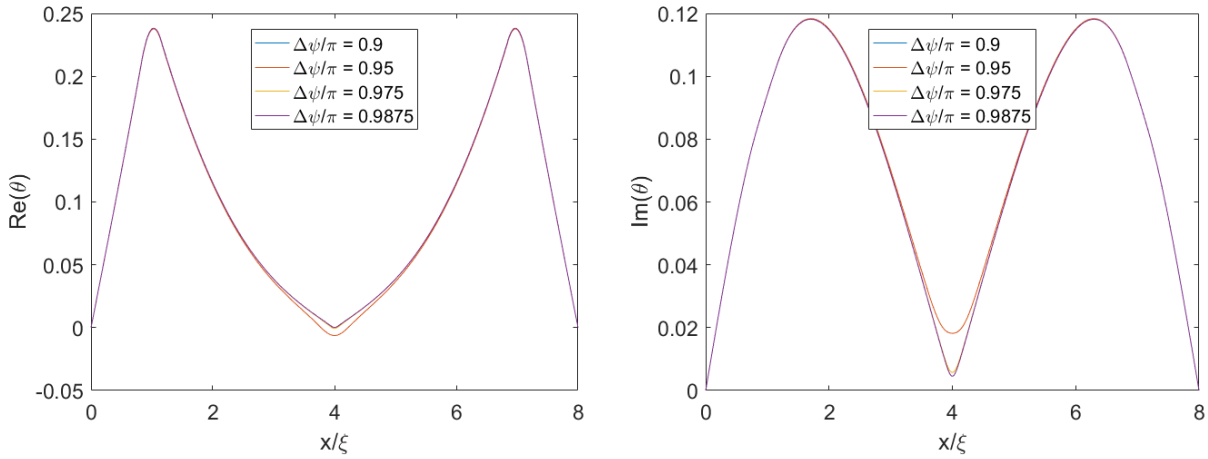

(a) Real part

(b) Imaginary part

Figure 18: The real and imaginary part of the parameter θ as a function of position for $E \approx \Delta$. The phase is varied, and is chosen successively closer to π. The figure was generated using Nx = 401.

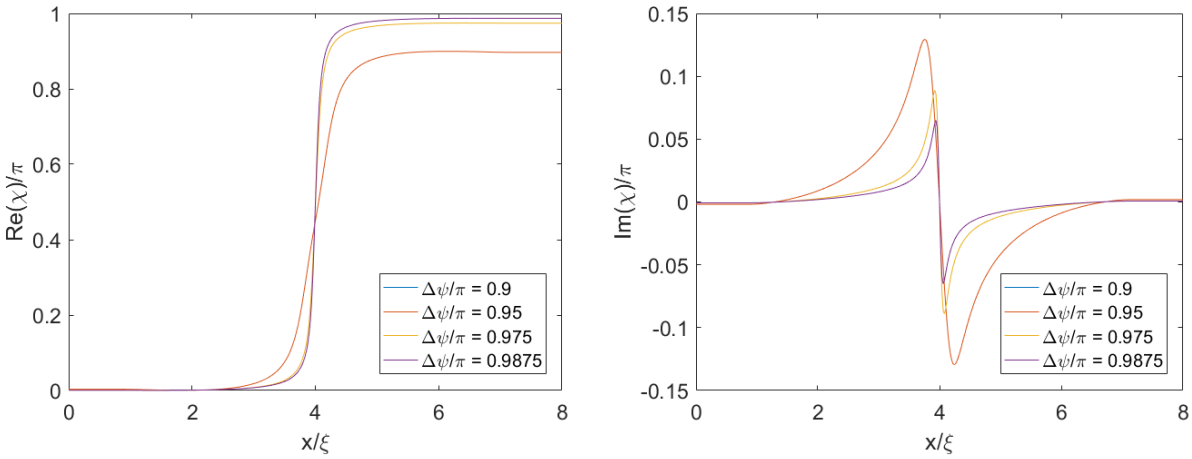

(a) Real part

(b) Imaginary part

Figure 19: The real and imaginary part of the parameter χ as a function of position for $E \approx \Delta$. As the phase difference between electrodes $\Delta\psi$ comes closer to π, the gradient in the centre of the junction is higher, a step function is approached. The imaginary part becomes smaller as $\Delta\psi \to \pi$. The figure was generated using Nx = 401.

This means that results for phase differences close to π should be used carefully. Having a sharper and sharper gradient, the number of grid points Nx needed to give an accurate description becomes larger and larger, and diverges as $\Delta\psi \to \pi$. However, as explained at the start of this section, at $\Delta\psi = \pi$, the parameter θ can be taken antisymmetric with respect to the centre of the junction. Therefore the number of grid points needed is finite for $\Delta\psi = \pi$.
The effect is illustrated in figure 20, which shows spectral supercurrent calculated using different gridsizes. For $\chi = 0.9\pi$, there is a small difference between the results for different Nx, but they are qualitatively similar. However, for $\chi = 0.9875\pi$ there is a large difference between the results for various Nx. The difference between the results with Nx = 51 and Nx = 201 is more than a factor 2. There is even a considerable difference between Nx = 201 and Nx = 401. Thus, this close to π, even smaller grid sizes than presented here are necessary for an accurate description of the system.

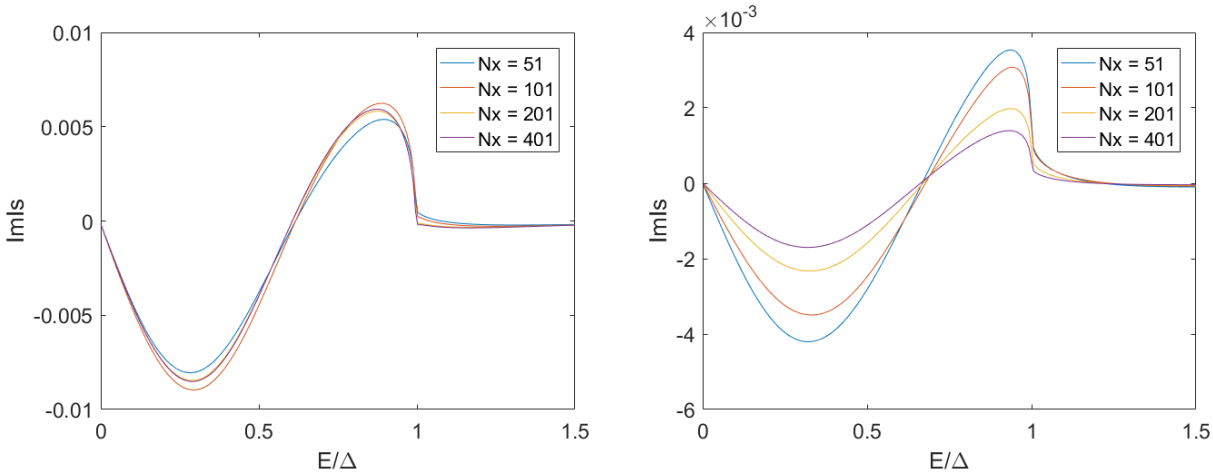

(a) $\Delta\psi = 0.9\pi$

(b) $\Delta\psi = 0.9875\pi$

Figure 20: The spectral supercurrent as a function of energy using different grid sizes. For $\chi = 0.9\pi$, the results are relatively similar, and the difference between Nx = 201 and Nx = 401 is small. However, for $\chi = 0.9875\pi$, the differences between the different calculations are large. The results are still qualitatively the same, however, quantitatively there is a factor of more than two difference between the results for Nx = 101 and Nx = 401.

12 Shapiro steps

A famous technique to investigate Josephson junctions is the study of Shapiro steps [76]. First, a short introduction to Shapiro steps will be given, then it will be considered how Shapiro steps can be found using the model. As discussed, a Josephson junction can carry a free current, this is called the DC Josephson effect [24]. Next to the DC Josephson effect, there is also an AC Josephson effect. If a DC voltage is applied across the Josephson junction, the resulting current will not only be a DC current. The current will also have an AC component. In an SNS-junction, the current phase relation can be described as follows

$$I = \frac{V}{R} + I_c \sin\psi \tag{12.1}$$

$$\frac{\partial\psi}{\partial t} = eV. \tag{12.2}$$

If $I < I_c$ then there exists a ψ such that $I_c \sin\phi = I$, and hence $V = 0$, there is a DC current and no alternating current. However, if $I > I_c$ a voltage needs to be generated, and ψ becomes time dependent. This means that V and I cannot both be constant, one has to choose to keep either V or I or neither constant.
Now, to generate Shapiro steps a slightly more difficult procedure is needed. Instead of applying a DC voltage or a DC current, a modulated voltage or current is applied, that is, next to the DC component, there is also an AC component:

$$V = V_0 + V_1 \cos\omega t$$

or

$$I = I_0 + I_1 \cos\omega t.$$

In case a modulated voltage is applied, the time averaged current is zero, except at a discrete set of voltages [76]. These are called Shapiro spikes. If the current is modulated, the average voltage will show steps, that is, the average voltage is a discontinuous function of the current [76]. In experiment conventionally Shapiro steps are measured rather than Shapiro spikes [102]. Shapiro steps have gained more interest since it was discovered that in topological insulators there are missing Shapiro steps [1]. Recently though, missing Shapiro steps were found as well in a material in a topological trivial state [103]. This marks the importance of a good model for the calculation of Shapiro steps.
In the code, it is simpler to modulate the voltage then to modulate the current, as the voltage is an input of the model, whereas the current is an output. For a current modulated Shapiro calculation, an iterative scheme is thus needed. However, the implementation of voltage modulation has a pitfall. As indicated, the time averaged voltage is only nonzero at a discrete set of voltages. Because in the calculation only a finite time width is possible, the voltage peak will have a finite, but small, width. There is thus a chance that the calculation will miss a Shapiro spike not because it does not exist, but because the calculation could not find it. Therefore, a time modulation is deemed more convenient.
Time modulation also has a significant problem. Because an iterative scheme is needed for many time steps, the process is very time consuming. It is that much time consuming that brute force calculation is not possible for us. Therefore, a different strategy was pursued. The dependence of $I(t)$ on $V(t)$ and $\psi(t)$ was calculated for a number of fixed (V, ψ). The data obtained in this way was approximated using a fit. It was found that the dependence of $I(t)$ on $V(t)$ could well be described by a linear relation in the VT-junction, just as in the SNS-junction. The current-phase relation however is not perfectly sinusoidal, as shown in figure the peak was find to be at $\chi > \frac{\pi}{2}$, although $|\chi_{\max} - \frac{\pi}{2}|$ is small. With this, the current can be described a

$$I(t) = \frac{V(t)}{R} + I_c f(\psi), \tag{12.3}$$

$$\frac{\partial \psi}{\partial t} = eV, \tag{12.4}$$

where f is the function displayed in figure 21a. Note that the latter equation is the same as for SNS-junctions because it only depends on the superconducting electrodes and not on the junction between them. With this relation, the Shapiro steps can be calculated using a much simpler iterative scheme.
The Shapiro steps using the function as shown above have been calculated. The result is shown in figure 21b. The steps are clearly visible and have a height of $2 \cdot 10^{-6} \frac{\Delta}{e}$.

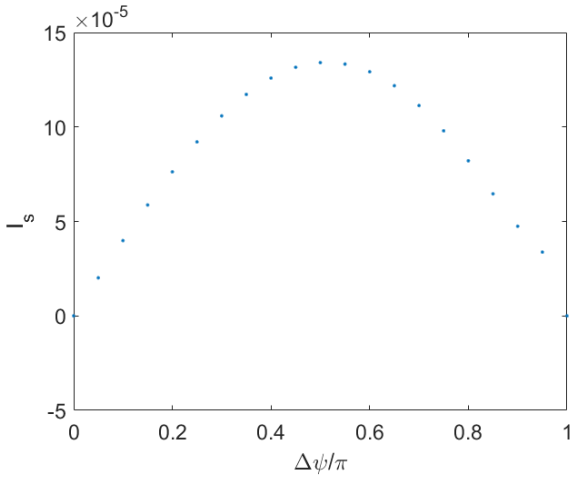

(a) The total supercurrent through the junction as a function of the phase difference accross the electrodes for s-wave electrodes.

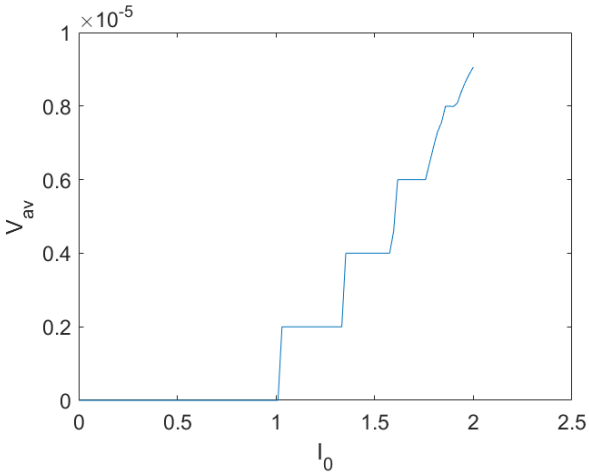

(b) The voltage between electrodes for the VT-junction as a function of the total supercurrent through the junction. The current has been normalised so that the first discontinuity occurs at $I_0 = 1$. The Shapiro steps are clearly visible.

Figure 21: Total supercurrent through the junction and Shapiro steps for the VT-junction with s-wave electrodes.

The big advantage of this method is that it is much less time consuming. A disadvantage is that a fitting procedure is needed to obtain f, and therefore some details may be lost. One should be careful only to apply this model in the limit of slow time dependence, as the adiabatic approximation is inherent to the theory behind the model used.

13 S-TI-S

As discussed in previous sections, the type of superconducting electrode can be varied in the VT junction. However, the material between the electrodes can also be varied. The normal metal can be replaced by a ferromagnet, an insulator or a topological insulator. Here the focus will be on topological insulators.
The junction between topological insulators and superconductors has been subject to interest since Fu and Kane predict the existence of Majorana fermions in topological insulators in which superconductivity was introduced using the proximity effect [1]. In this section, the concept of topological insulators will first be introduced. Then, the application of the Green's function formalism to topological insulators is introduced and some results are highlighted. The focus will be on the junction with s-wave superconductors. A schematic of the VT junction with a topological insulator is shown in figure 22.

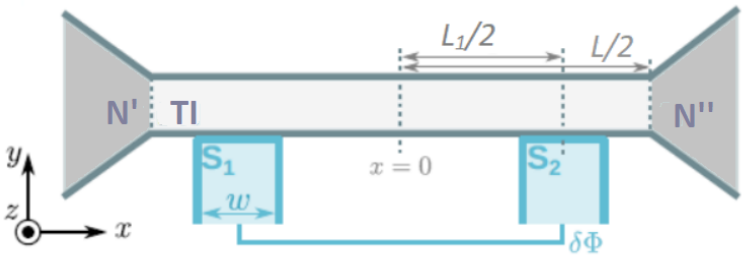

Figure 22: The VT junction modified to have a topological insulator. Figure adapted from [90]. The electrodes are applied in the vertical y-direction, the plane in which the topological insulator lies is an xz-plane. Similar to the regular VT junction, the topological insulator is assumed to have a small width in the z-direction, so that a quasi-onedimensional model can be used.

13.1 Topological insulators

A crude way to describe a topological insulator is as an insulator with conducting edge states. Insulators can classified using Chern numbers [104], which are defined as

$$C_m = \frac{1}{2\pi} \int dk \nabla \times \langle u_m | \nabla_k u_m \rangle \,, \tag{13.1}$$

where m is the band index, $u_m(k)$ is the wavefunction in band m with wavenumber k and C_m is called the Chern number of band m. It can be shown that the Chern number of a band is always an integer [1]. The Chern number of an insulator is then the sum of all Chern numbers of filled bands. Insulators for which the total Chern number is 0 are normal insulators. Insulators for which the Chern number is nonzero are topological insulators. To see why topological insulators have conducting edge states, note that because of the quantisation of Chern number, the Chern number can not change continuously, but should rather jump. As the Chern number of a single band fixed, this is only possible if a filled band and a non-filled band merge and new separate bands emerge. Thus, between the air with $C = 0$, and the topological insulator with $C \neq 0$, there should be a location, where the bands merge. If the bands merge the highest occupied band is not fully occupied. Therefore, there is conductance at the edges.
These edge states can be described using the following Hamiltonian [105], [106]:

$$H = -i\alpha(\nabla \times \hat{y})\hat{\sigma} + h \cdot \sigma - \mu. \tag{13.2}$$

In this formula α is the spin orbit coupling strength, $\hat{y}$ is the unit vector in the direction that is normal to the surface, $\sigma = (\sigma_1, \sigma_2, \sigma_3)$, where $\sigma_i, i = 1, 2, 3$ are the Pauli matrices, h is the exchange coupling and μ is the Fermi level.

13.2 Green's function for topological insulators

For topological insulators, a Green's function approach has been developed, similar to the theory for metals [105], [106], [107]. An important difference with the approach for normal metals is that the Hamiltonian is now spin dependent, which means that each entry in the Green's function is now a 2 by 2 matrix. Similar to the case for normal metals, a quasiclassical approximation can be made, which results in the following Eilenberger equation for topological insulators [106]:

$$\frac{\alpha}{2}\{\eta, \nabla g\} = [g, iE\tau_3 + ih \cdot \sigma\tau_3 + i\mu\eta \cdot n_F + \frac{1}{\tau} < g >], \tag{13.3}$$

where $\eta = (-\sigma_2, \sigma_1)$, h and α are as defined in the Hamiltonian above, μ is the chemical potential, E is the energy, n_F is the direction of the Fermi velocity and g is the Green's function. In general, this equation is much harder than the Eilenberger equation for normal metals. However, if $|h| << \mu$, an important simplification can be made. It can be shown [106], [105], that in that case, the dominant term in the Green's function has the form

$$g = G\frac{1}{2}(1 + n_F \cdot \eta), \tag{13.4}$$

where G is a spin independent Green's function. This is a projection in spin space, and couples direction of motion and spin, as expected in the presence of strong spin orbit coupling.
The Green's function G satisfies an Eilenberger equation very similar to the Green's function in a normal metal, only with the derivatives replaced by the following 'derivative' [106]:

$$\hat{\nabla} = \nabla - i\frac{1}{\alpha}(h_x\hat{z} - h_z\hat{x})[\tau_3, \cdot], \tag{13.5}$$

where $\hat{x}$ and $\hat{z}$ are unit vectors in the horizontal x and z directions respectively. From here the dirty limit analysis carries through from the normal metal case, which means that the Usadel equation for a topological insulator reads

$$\frac{1}{3}v_F^2\tau\hat{\nabla}(G_0\hat{\nabla}G_0) = [-iE\tau_3 + \Delta, G_0]. \tag{13.6}$$

$$G_0^2 = 1. \tag{13.7}$$

The difference between the Usadel equation for the topological insulator and the normal metal is thus the exchange coupling. In the VT-junction, the one dimensional approximation is made, which means that only h_y is of influence. This will be denoted by h. For simplicity of notation, the parameter B is defined such that $B = \frac{h}{\alpha}$. An important note here is that whereas the function G_0 here is isotropic the Green's function is not isotropic due to the spin dependence described in equation (13.4).

13.3 Boundary conditions

It is not immediately clear how the Tanaka Nazarov boundary conditions should be generalised to topological insulators. One could argue that because the Tanaka Nazarov boundary conditions are based on the solution of the Eilenberger equation [84], which we have seen remains the same in the limit of no exchange coupling, the Tanaka Nazarov boundary conditions need not be modified. However, there are two issues that plays a role for topological insulators that did not come up in the case of a normal metal. In the derivation of the Tanaka Nazarov boundary condition there is an intermediate region in the vertical y-direction, which was perfectly sensible in the case of a normal metal. The edge states of the topological insulator however are two-dimensional, with no y-component. The second issue is that the Green's function in the topological insulator is projected using $\frac{1}{2}(1 + n_F\sigma)$, whereas the Green's function in the superconductor is not.
This suggests that the Tanaka Nazarov boundary conditions are a good starting point for suitable boundary conditions, but that some adjustments are necessary in the case of a topological insulator.

A second approach is to follow the approach used in the Bogoliubov de Gennes equations. Here the region above the superconductors is described as an STI, at topological insulator with an effective superconducting potential. In this approach there is no y-component needed. However, what is less appealing about this method is that this approach does not consider the current conservation from electrodes to the topological insulators.
Thus, there are two different approaches that focus. The results of the different approaches are shown in figure 23. In the calculations the boundary parameters were set to $(\gamma_B, z) = (1, 0.2)$, for the numerical model 100 spatial grid intervals were used. Calculations were performed for 221 values of E, in the range $\frac{E}{\Delta} = (0, 1.5)$. The results of the two methods do have some similarity, but there are also differences between the methods. This means that the required boundary conditions should be investigated further.

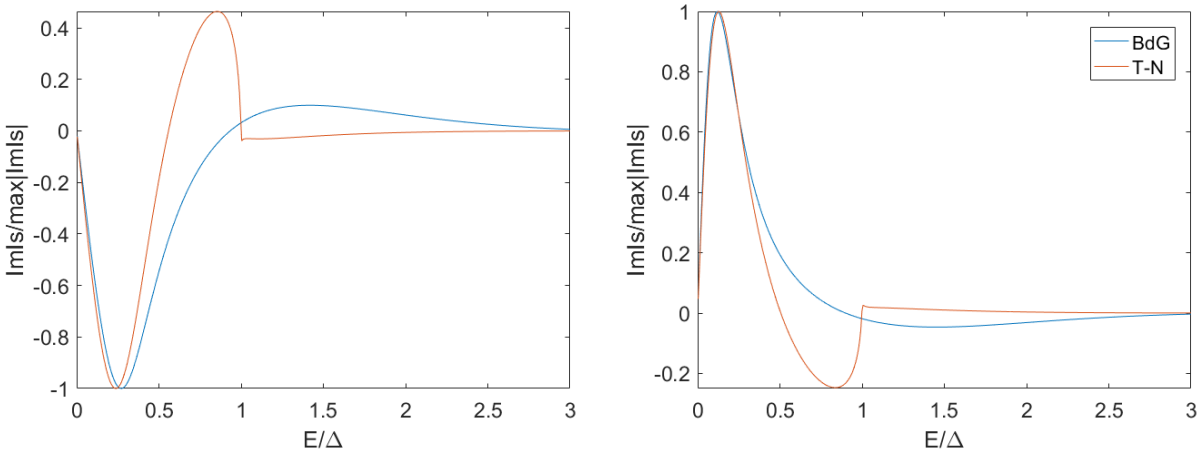

(a) $\Delta\psi = \frac{\pi}{2}$, $B = 0$.

(b) $\Delta\psi = 0$, $B = 0.01$

Figure 23: The spectral supercurrent as a function of energy for the Bogoliubov de Gennes approach and the Tanaka Nazarov approach, for both a nonzero phase difference and nonzero exchange coupling. The results between the two methods are different, for the Tanaka Nazarov boundary conditions the spectral super current changes sign for some $E < \Delta$, for the Bogoliubov de Gennes approach the spectral super current has a uniform sign for $E < \Delta$.

13.4 Effect of exchange coupling

The effect of turning on the exchange coupling is most easily seen at zero phase difference. To investigate only the effect of the exchange coupling, the Tanaka Nazarov boundary conditions were used as for the normal metal. Without exchange coupling, the phase was found to be constant throughout the junction, and thus, there is no supercurrent. If the exchange coupling is turned on, the spectral supercurrent becomes nonzero, as shown in figure 24a. The effect of having a nonzero exchange coupling is very similar to the effect of having a phase difference across the junction, in both cases the spectral supercurrent has different sign for $E << \Delta$ then for E just below Δ. For $\Delta\psi = \frac{\pi}{2}$ the results for small $B < 0.01$ are very similar to the case $B = 0$. For $B = 0.1$ however, the current due to exchange coupling is comparable to the current generated by the phase difference, and the results are considerably different.

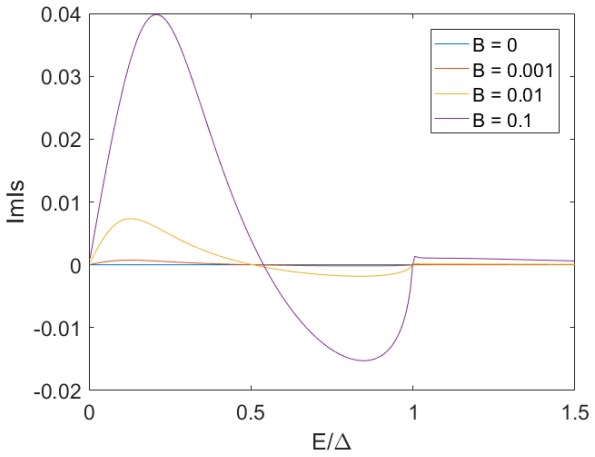

(a) $\Delta\psi = 0$. In absence of exchange coupling, $B = 0$, there is no spectral supercurrent. As B is increased, the spectral supercurrent appears.

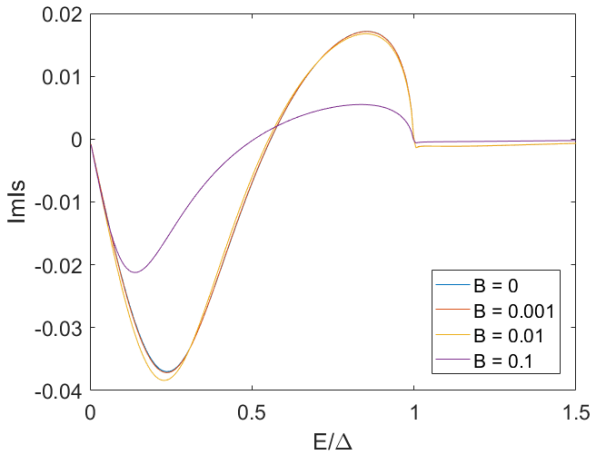

(b) $\Delta\psi = 0.5\pi$. For $B = 0.001$ and $B = 0.01$ the current due to the exchange coupling is much smaller than the current generated by a phase difference, the results are similar to the result without exchange coupling. For $B = 0.1$ the current deviates considerably from the limit in which there is no exchange coupling.

Figure 24: The spectral supercurrent as a function of energy for three different values of $B = \frac{h}{\alpha}$. As for a nonzero phase difference, the spectral supercurrent changes sign as energy is increased. Tanaka Nazarov boundary conditions have been used.

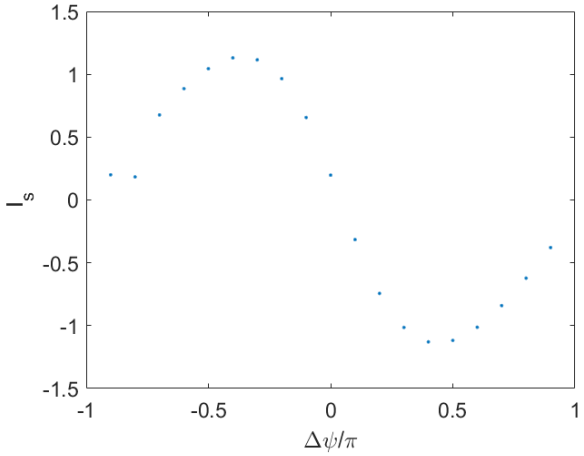

Figure 25: The supercurrent as a function of the phase difference between the electrodes for $B = 0.01$. The junction behaves as a ϕ_0-junction, that is, the phase at which there is no supercurrent is nonzero. Here, $\phi_0 > 0$. The result for $\Delta\psi = -0.9\pi$ is attributed to the near π discussed in section 11. That it appears more clearly for $\Delta\psi = -0.9\pi$ than for $\Delta\psi = 0.9\pi$ is because $\phi_0 > 0$ here.

14 Differential conductance

Next to the supercurrent through the junction, also the differential conductance of the junction can be calculated, that is, the voltage derivative of the dissipative current. Similar to [108], the diferential conductance was calculated for the junction. The differential conductance is given by [109]:

$$R_N \frac{\partial I}{\partial V} = \int_0^\infty \frac{\partial}{\partial V} f_T(E) D(E) dE, \tag{14.1}$$

where R_N is the normal state resistance of the junction and

$$D(E) = \left(\frac{1}{L} \int_{-\frac{L}{2}}^{\frac{L}{2}} \frac{1}{D_T(E,x)} dx \right)^{-1}. \tag{14.2}$$

The expression $D_T = \mathrm{Tr}(1 - \tau_3 G_R \tau_3 G_A)$ can be calculated in the θ-parametrisation. The result is

$$D_T(E,x) = \frac{1}{2} |\cosh\theta|^2 + \frac{1}{2} |\sinh\theta|^2 \cosh \mathrm{Im}\chi. \tag{14.3}$$

In the limit where $\mathrm{Im}\chi = 0$, this reduces to the expression found in [109].
In the zero temperature limit, $\frac{\partial}{\partial V} f_T(E) = \delta(E - \frac{eV}{2}) + \delta(E + \frac{eV}{2})$, and the expression reduces to

$$R_N \frac{\partial I}{\partial V} = \left(\frac{1}{L} \int_0^L \frac{1}{D_T(\frac{eV}{2}, x)} dx \right)^{-1} \tag{14.4}$$

The phase between the electrodes of the junction was varied. In the calculations the boundary parameters were set to $(\gamma_B, z) = (1, 0.2)$, for the numerical model 100 spatial grid intervals were used. Calculations were performed for 221 values of V, in the range $\frac{eV}{\Delta} = (0, 1.5)$. The results are shown in figure 26. The behaviour is qualitatively different for p-wave superconducting electrodes compared to s-wave superconducting electrodes. In the case of s-wave electrodes, the differential conductance is lowest at $E = 0$, where it approaches the normal state value 1. The differential conductance increases with energy in a range from $E = 0$ to just below Δ. Around $E = \Delta$ there is a sharp decrease of the differential conductance, though the differential conductance remains larger than for the normal state. For $E > \Delta$ the differential conductance approaches the normal state value. With an increase of $\Delta\psi$ peak in the differential conductance becomes less broad and shifts to higher energies. The differential conductance for $E > \Delta$ has a much weaker dependence on $\Delta\psi$. For p-wave electrodes the differential conductance is highest at $E = 0$ and decreases towards the normal state value as energy is increased. This peak at $E = 0$ is notably higher than the peak for s-wave electrodes. With increasing phase difference between the electrodes the peak at $E = 0$ becomes lower. The width of the peak has no appreciable dependence on the phase of the junction. The results for $\Delta\psi = 0$ are in good agreement with the results published in [108] for a T-shaped geometry, as expected.

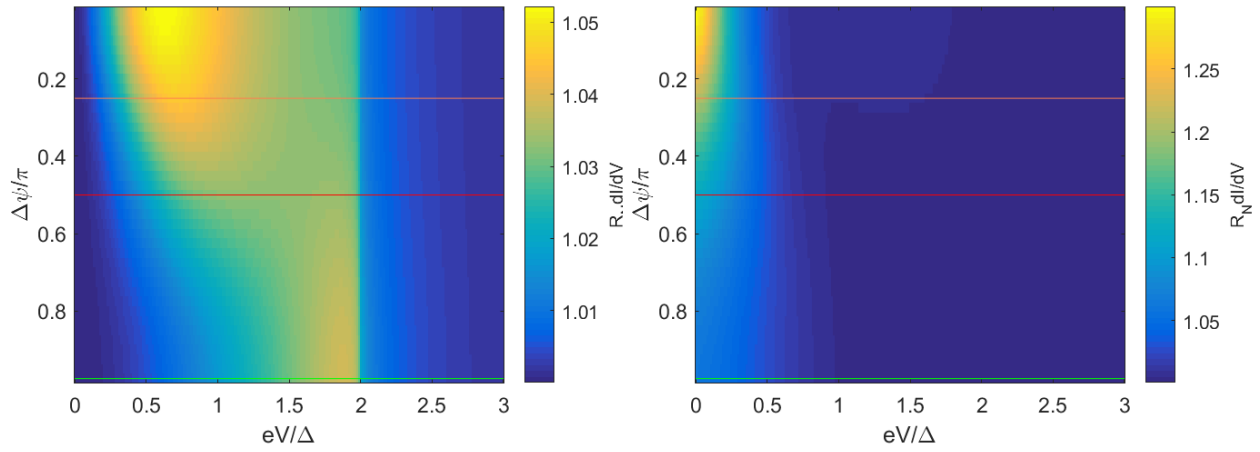

(a) S-wave.

(b) P-wave.

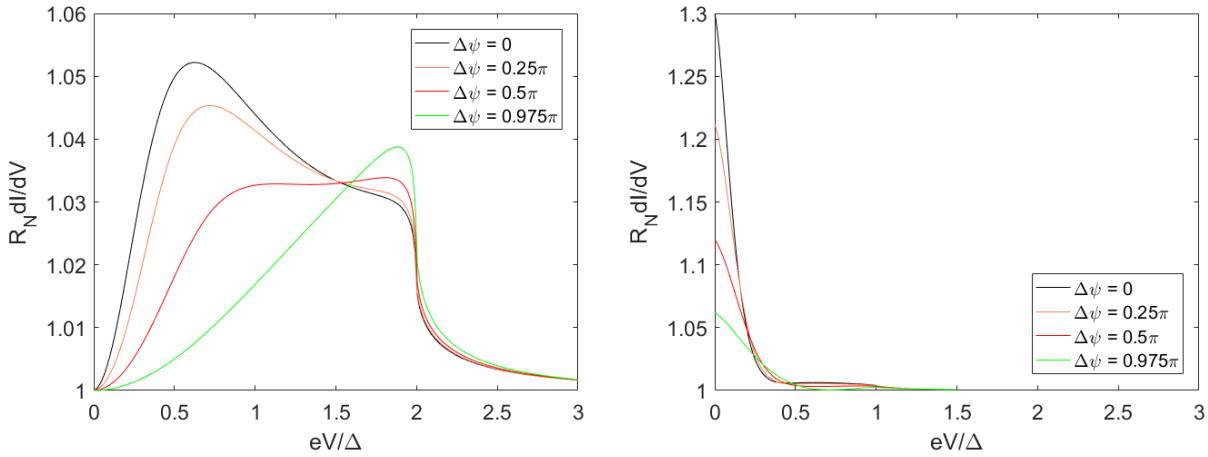

(c) S-wave, selection of results.

(d) P-wave, selection of results.

Figure 26: The differential conductance of the VT-junction as a function of energy for s-wave (left) and p-wave (right) electrodes. For s-wave electrodes, the differential conductance assumes a minimum at $E = 0$, for p-wave electrodes the normal state differential is reached at $E = 0$ and the dip in the differential conductance occurs at nonzero energy.

15 Supercurrent through the junction

In this section the supercurrent through the junction will be discussed. First, the spectral supercurrent ImIs is calculated for both s-wave and p-wave superconductors. Afterwards, the total supercurrent $I = \int f_L(E)\text{ImIs}dE$ is calculated. The distribution function f_L is manipulated by applying a voltage between the reservoirs, the superconducting electrodes are kept at ground in order to keep the phase difference between the electrodes constant. The dependence of the supercurrent on the reservoir voltage is shown to be different for s-wave and p-wave electrodes. The results will also be published in an article. In all calculations for this section the boundary parameters were set to $(\gamma, z) = (1, 0.2)$, for the numerical model 100 spatial grid intervals were used. Calculations were performed for 221 values of E, in the range $\frac{E}{\Delta} \in (0, 1.5)$.

15.1 Spectral Supercurrent

As indicated in equation 5.54, the spectral supercurrent is defined in θ-parametrisation as $\text{ImIs} = -4\text{Im}(\sinh^2\theta\frac{\partial\chi}{\partial x})$. This quantity can thus be calculated using only the retarded equation. It can be interpreted as the net current carrying density of states. The spectral supercurrent has been calculated for both s-wave and p-wave superconductors as a function of energy and phase. The results are shown in figure 27. A clear distinction between s-wave and p-wave is that there is a sign difference between the two cases. However, the sign of spectral supercurrent for p-wave electrodes is arbitrary, a rotation of π of the electrodes will introduce an extra minus sign in the spectral supercurrent. This can thus not be used to distinguish s-wave and p-wave electrodes. For both s-wave and p-wave superconductors, there are two peaks, the low energy peak being clearly higher than the higher energy peak. The two peaks have opposite sign. The energy of both peaks was investigated for s-wave and p-wave. The results are shown in figure 28. There is a difference in these results, for p-wave electrodes the energy of the first peak becomes independent of the phase difference for $\psi > \frac{\pi}{2}$, whereas for s-wave electrodes the energy of the first peak is increasing also for $\psi > \frac{\pi}{2}$. For the second peak there is also a distinction between s-wave and p-wave electrodes. For s-wave electrodes the energy of the second peak is non decreasing, whereas for p-wave electrodes the energy of the second peak attains a minimum for a phase difference $0.3 < \frac{\Delta\psi}{\pi} < 0.4$.
There is another distinction between the results for the s-wave and p-wave superconductor, the discontinuity in the derivative of the spectral supercurrent at $E \approx \Delta$ is much smaller for p-wave superconductors than for s-wave superconductors.

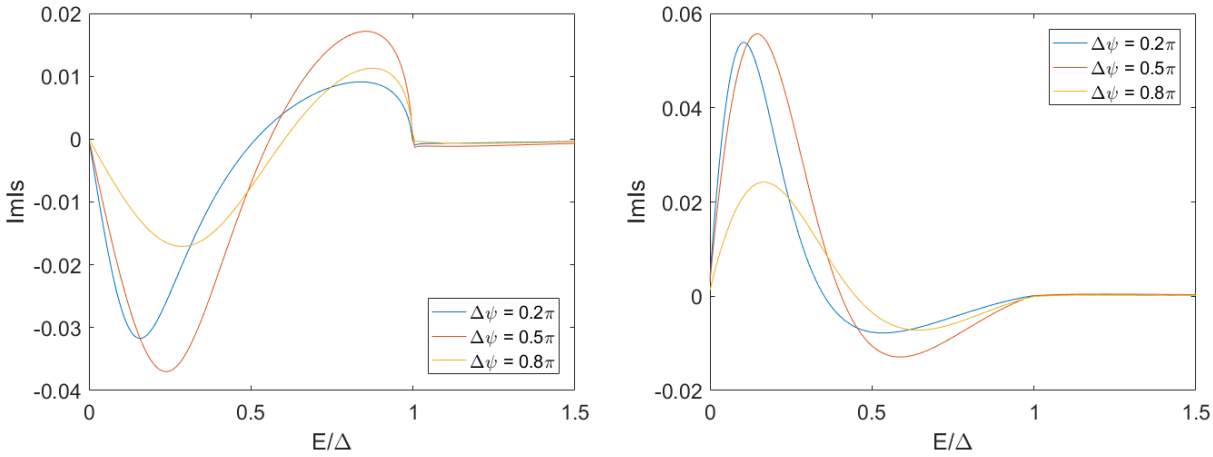

(a) S-wave.

(b) P-wave.

Figure 27: The spectral supercurrent through the VT-junction as a function of energy for s-wave and p-wave electrodes. The spectral supercurrent changes sign as energy is increased for both s-wave and p-wave electrodes. For clarity of presentation, a selection of the results is shown. A larger selection of the results is shown in the appendix.

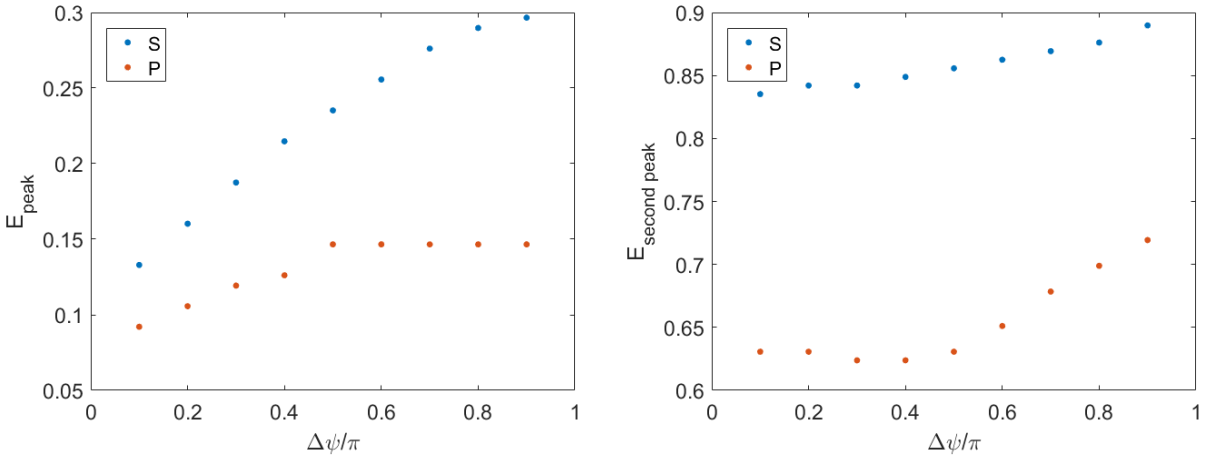

(a) S-wave.

(b) P-wave.

Figure 28: The energy of the first (left) and second (right) peak in the spectral supercurrent as a function of phase for the VT-junction using s-wave and p-wave electrodes. There is a qualitative difference between the results. Calculations for $\Delta\psi > \frac{\pi}{2}$ were also calculated using Nx = 401, giving the same peak locations.

15.2 Total supercurrent

Apart from the spectral supercurrent also the total supercurrent was calculated. The advantage of the total supercurrent is that it is easier to measure than the spectral supercurrent.The reason for this is that the occupation of the states is not taken into account for the spectral supercurrent, whereas it is taken into account for the total supercurrent. The total supercurrent can be expressed

as

$$I_s = \int_0^\infty f_L(E)\text{ImIs}(E)dE, \tag{15.1}$$

where f_L is the parameter used in the parametrisation of the Keldysh equation, it describes the occupation of the current-carrying states.
The boundary conditions for f_L depend on the voltage between the reservoirs as explained in section 6. This is a clear advantage of the VT-junction compared to an SNS-junction, the supercurrent through the junction can be manipulated by applying a voltage between the reservoirs. The Keldysh equation has been solved for both s-wave and p-wave superconductors. As shown in the previous subsection, the results for different values of $\Delta\psi$ are qualitatively the same. Therefore, focus will be on $\Delta\psi = \frac{\pi}{2}$ in the coming analysis. The results for the total supercurrent is shown for both s-wave and p-wave in figure 29.

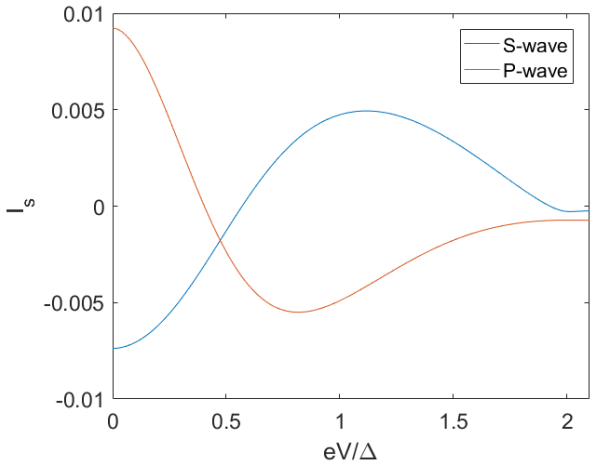

Figure 29: The supercurrent as a function of voltage for the VT-junction in case of s-wave and p-wave electrodes. As for the spectral supercurrent there is a sign difference in the supercurrent between the case of s-wave and p-wave electrodes.

The supercurrent changes sign as the voltage between the reservoirs is increased, which is in good correspondence with the results as found in [110]. The results are clearly different from the results for the spectral supercurrent, mainly around $E \approx \Delta$. This is not a surprise, as integration smoothens the kink. However, the quantity $\sigma = \frac{\partial I_s}{\partial \frac{eV}{\Delta}}$ does resemble the spectral supercurrent, as shown in figure 30. This can be explained from the distribution functions for the normal reservoirs. At temperatures $T << \Delta$, the hyperbolic tangent is very similar to the sign function, being -1 for negative arguments and 1 for positive arguments. This means that f_L is zero in the range $|E| < eV$, and nonzero outside this range. In the region between the superconductors the exact form of f_L will be different. Therefore f_L will not be an exact step function. Still, the supercurrent can be approximated by

$$I_s \approx \int_{\frac{eV}{\Delta}}^\infty \text{ImIs}(\frac{E}{\Delta})d\frac{E}{\Delta}, \tag{15.2}$$

$$\sigma \approx -\text{ImIs}. \tag{15.3}$$

From this it is clear that at low temperatures, the spectral supercurrent can be approximated by σ.

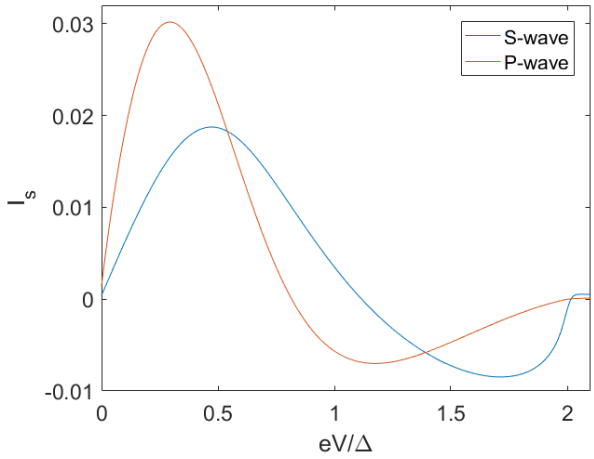

Figure 30: The derivative of the supercurrent with respect to the voltage for the VT-junction for both s-wave and p-wave electrodes. The results for the p-wave superconductors have been negated to highlight the differences.

In figure 31 the total supercurrent and σ is shown for p-wave superconducting electrodes for three different temperatures. The results confirm that σ approximately equals ImIs in the low temperature regime. The results for $T = 0.01$ and $T = 0.001$ are indistinguishable from the figure. To investigate the temperature dependence of I_s in this very low temperature limit, the difference in I_s compared to $T = 0.001$ was investigated. The results are shown in figure 32. It is confirmed that the difference ΔI_s is much smaller than I_s, there is a difference of more than 2 orders of magnitude. The energy dependence of ΔI_s is similar to the energy dependence of I_s.

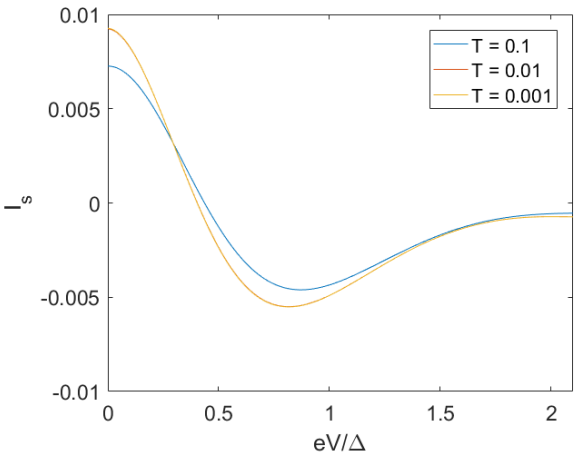

(a) The total supercurrent as a function of the voltage applied between the reservoirs for p-wave superconductors. The results for $T = 0.01$ and $T = 0.001$ are almost indistinguishable, the results for $T = 0.1$ are clearly different.

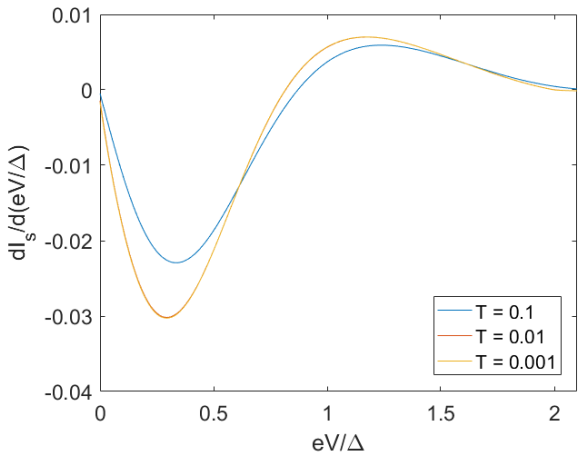

(b) Derivative of the total supercurrent as a function of the voltage applied between the reservoirs with respect for p-wave superconductors. The results for $T = 0.01$ and $T = 0.001$ are almost indistinguishable and resemble the spectral supercurrent, confirming the theory.

Figure 31: Total supercurrent and its derivative with respect to the applied voltage between reservoirs for p-wave superconductors.

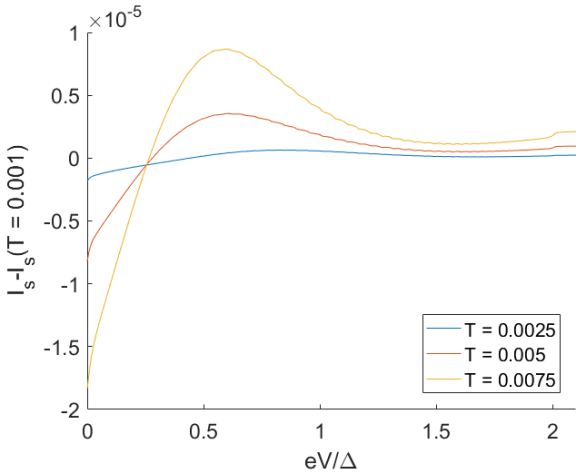

Figure 32: The difference in total supercurrent compared to $T = 0.001$ in the very low temperature regime. The difference in total supercurrent is two orders of magnitude lower than the total supercurrent.

16 Length dependence

In this section the length dependence of the solutions to the Usadel equation in the VT-junction is investigated using the spectral supercurrent and the imaginary part of the parameter χ.

16.1 Length dependence of spectral supercurrent

The dependence of the spectral supercurrent on the length of the junction was investigated for both s-wave and p-wave superconductors. The results for a phase difference of $\frac{\pi}{2}$ between the electrodes are shown in figure 33. Here a logarithmic axis was chosen for the spectral supercurrent for clarity of presentation. For both s-wave electrodes and p-wave electrodes, the number of energies for which the supercurrent is zero increases, that is, the spectral supercurrent changes sign as a function of energy more and more often. This can be qualitatively understood from the analytical considerations discussed in section 9.2. The spectral supercurrent equals $\mathrm{Im}(j_E) \propto \mathrm{Im}\left(\cosh^2\sqrt{2i\epsilon}x\right)^{-1} = \mathrm{Im}\left(\cosh^2(1+i)\sqrt{\epsilon}\frac{L}{2}\right)^{-1}$. This is the inverse of a complex, rather than real hyperbolic sinusoid. Complex hyperbolic sinusoids have an oscillatory decay. This is in good correspondence with the results in figure 33. The behaviour can be qualitatively understood from a physics point of view as well. In long junctions, a large set of Andreev bound states, rather than a single pair appears in the junction [111], [112], [113]. In the clean limit, these appear as δ-peaks in the energy spectrum. These peaks need not all carry current in the same direction. In the dirty limit however, the Andreev bound states do not appear as δ-peaks, but rather as broad peaks. It is this set of multiple bound states that is responsible for the oscillatory behaviour observed.
Another remark with respect to the results in figure 33 is that successive peaks in ImIs have considerably smaller magnitude. In the low energy range, the spectral super current only changes slightly as the length of the junction is increased, whereas for high energies there is a difference of several orders of magnitude between long junctions and short junctions, even far away from the zero crossings. This is illustrated in figure 34, which shows a section of figure 33 at $E \approx 1.5\Delta$ for s-ave and p-wave electrodes. The zero crossings are clearly visible in this figure, and the maxima correspond well to exponential decay, in good correspondence with the discussion in section 9.2.1. In figure 33, the results for s-wave and p-wave electrodes look qualitatively similar. The only notable difference is that the location of zeros for energies just below $E = \Delta$ has a stronger length dependence for s-wave electrodes and for p-wave electrodes. Also the derivative of the spectral supercurrent is investigated as a function of length. The results are shown in figure 35. There is a difference between the junctions with s-wave electrodes and p-wave electrodes. For s-wave electrodes the discontinuity at $E = \Delta$ is much more pronounced. Moreover, for p-wave electrodes, the zeros of the derivative of the spectral supercurrent occur at lower energies than for s-wave electrodes. This is in good correspondence with the results found in figure 28.

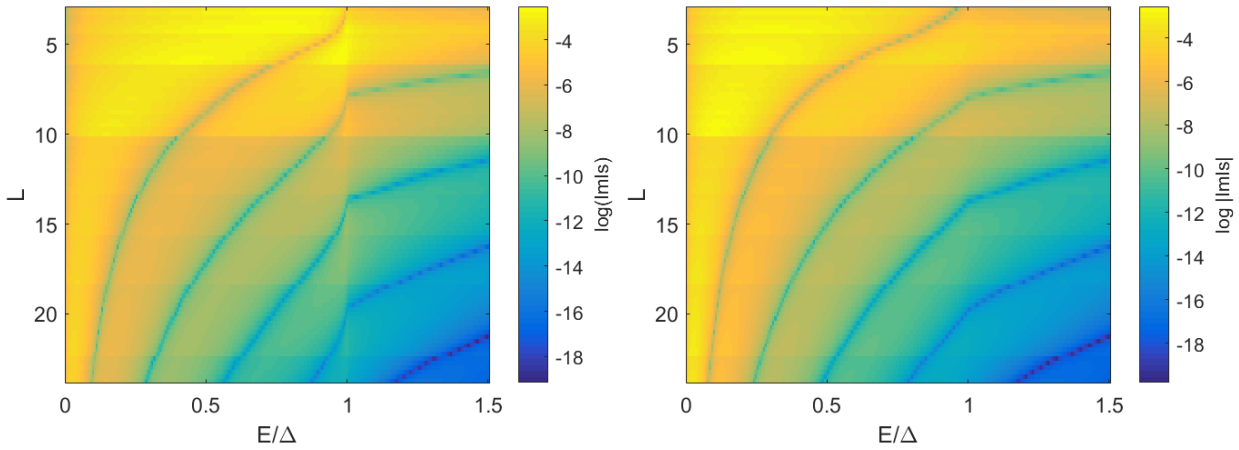

(a) S-wave. (b) P-wave.

Figure 33: The spectral supercurrent as a function of energy and the length of the junction for s-wave electrodes (left) and p-wave electrodes (right). As the length of the junction is increased, the spectral supercurrent changes sign at more different energies $E < \Delta$. The results for s-wave and p-wave electrodes are qualitatively the same, although the results for E just below Δ are different.

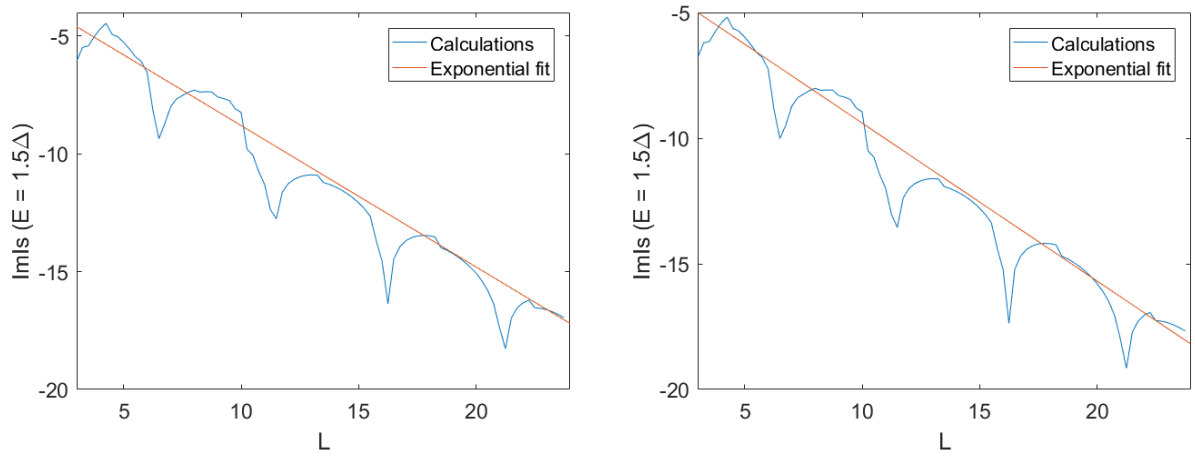

(a) S-wave. (b) P-wave.

Figure 34: The dependence of the spectral super current on length for $E \approx 1.5\Delta$ for s-wave (left) and p-wave (right) superconductors. The results are very similar, though the spectral supercurrent is slightly higher for s-wave electrodes. This can be explained from the fact that for p-wave superconductors, the contributions of angles for which $\cos\phi$ is small, is much more suppressed, as $\frac{E}{\Delta_0 \cos\phi}$ is large for those angles. For both types of electrodes, the peaks in the spectral supercurrent correspond well to an exponential fit.

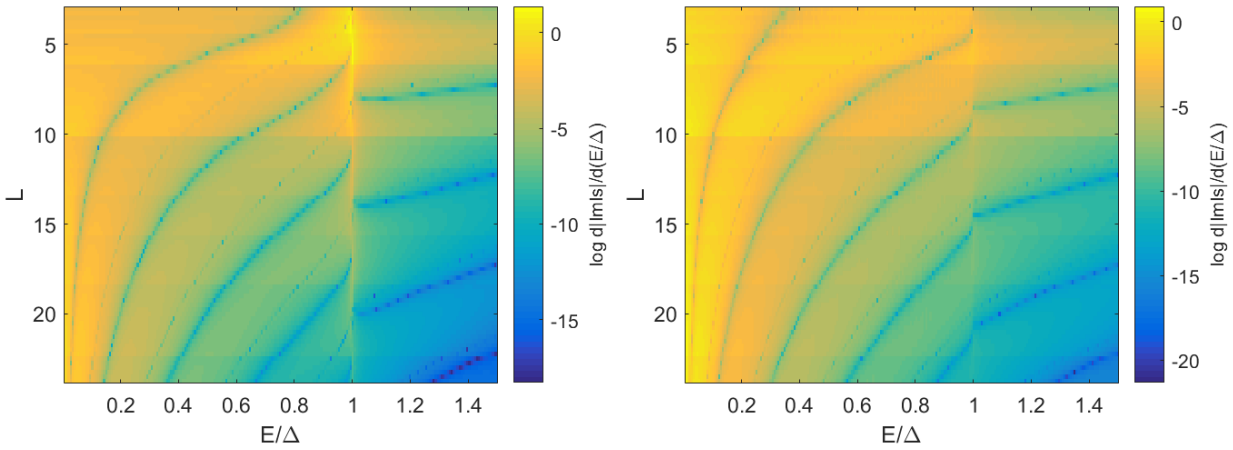

(a) S-wave.

(b) P-wave.

Figure 35: The derivative of the spectral supercurrent with respect to energy for junctions with s-wave electrodes (left) and p-wave electrodes (right). For both types of electrodes there is a discontinuity at $E = \Delta$, although more pronounced for s-wave electrodes. For p-wave electrodes, there is an extra discontinuity at $E \approx \frac{\Delta}{4}$. The energy at which this discontinuity occurs is independent of the length of the junction.

16.2 Length dependence of the imaginary part of the phase

In the discussion of the equations for the Keldysh component of the Green's function and the expression for conductivity it was noted that the conventional expressions need to be modified if the superconducting phase is complex rather than real. In short junctions, this term should be negligible. This assertion was tested by investigating the length dependence of the maximum of the imaginary part of the phase $\max_{x,E} \mathrm{Im}\chi$ as a function of the length of the junction L. The calculations were performed for $\Delta\psi = \frac{\pi}{2}$. The results are shown in figure 36. It was found that for short junctions $L - 2 \approx \xi$, the imaginary part indeed becomes vanishingly small. For $L > 10$, $\max_{x,E} \mathrm{Im}\chi$ becomes approximately independent of length.

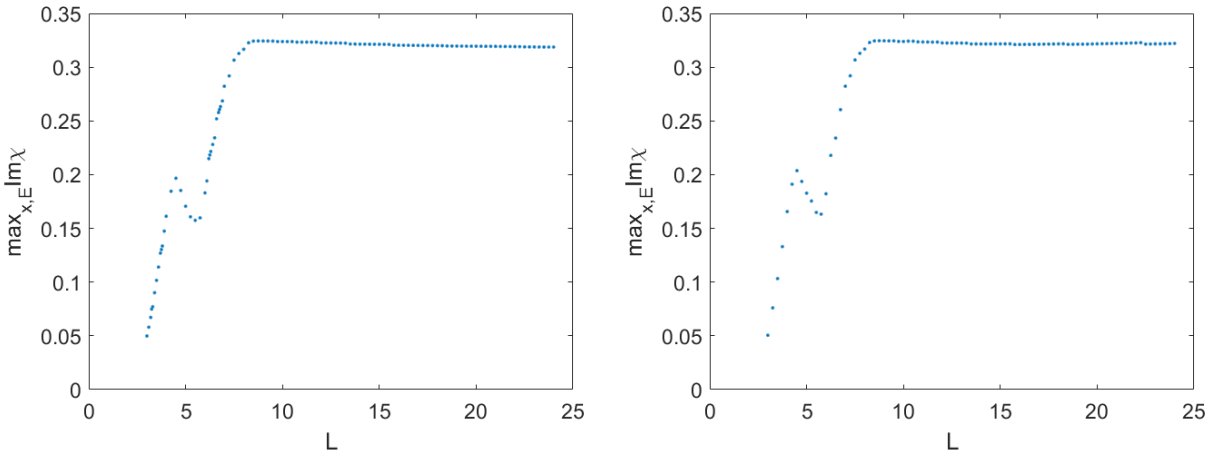

(a) S-wave.

(b) P-wave.

Figure 36: The maximum of the imaginary part of χ over both energy and position as a function of the length L of the VT-junction. As the length of the VT-junction decreases, the imaginary part of χ becomes negligible. For long VT-junctions, the maximum of $\mathrm{Im}\chi$ approaches a constant value, for the parameter settings under considerations this is approximately 0.3. Interestingly enough, $\max_{x,E} \mathrm{Im}\chi$ does not increase monotonically as a function of L, but shows a dip around $L \approx 6$. The results for s-wave and p-wave electrodes are similar.

In figure 37 this dependence is studied further. It is shown that the functional dependence of $\max_{x,E} \mathrm{Im}\chi$ is similar for the different lengths, but that the energy at which $\max_{x,E} \mathrm{Im}\chi$ is attained scales with $(L-2)^{-2}$, similar to the peak in the density of states.

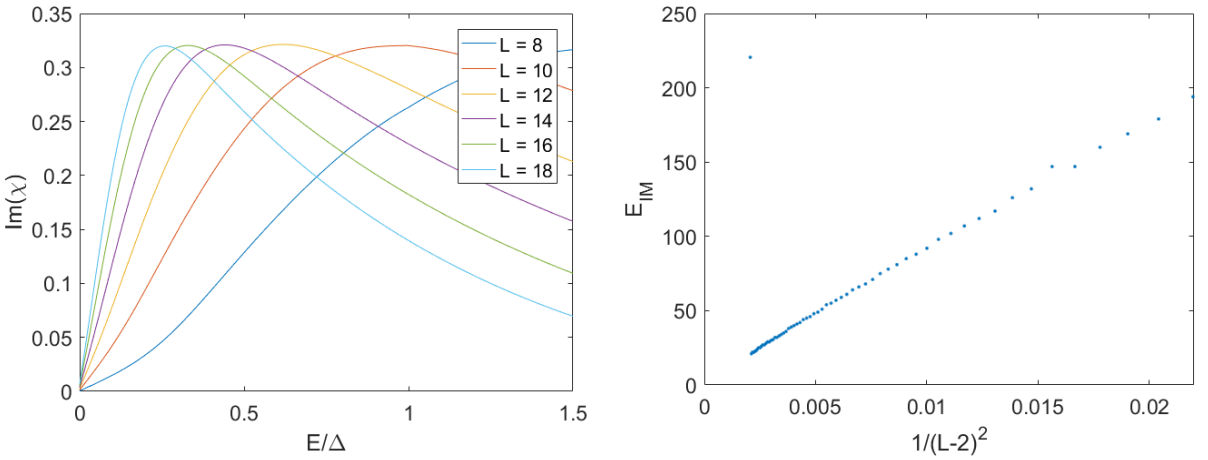

(a) The imaginary part of the phase at the location at which $\max_{x,E} \mathrm{Im}\chi$ is attained. The functional dependence of $\mathrm{Im}\chi$ is similar for all lengths, the energy E_{IM} at which $\max_{x,E} \mathrm{Im}\chi$ is attained decreases with increasing length.

(b) The energy E_{IM} is proportional to $(L-2)^{-2}$, in good agreement with the length dependence of θ.

Figure 37: Imaginary part of the phase parameter χ.

17 Conclusion

In this thesis a four-terminal Josephson junction was investigated. More specifically, the VT junction, with two superconducting terminals and two normal metal reservoirs, was considered. The system was described using the non-equilibrium Green's function method. Using the quasiclassical approximation and the dirty limit approximation, the Gorkov equations, which give a complete description of the system, were simplified to the Usadel equations.
The Usadel equation was derived in most general form for non-equilibrium superconductivity, allowing for a complex parameter χ. New terms were identified in the equations for the Keldysh components. It was shown that the equations reduce to the known equations if the parameter χ can be assumed real. It was shown numerically that in the VT junction the imaginary part of χ does not vanish in general, showing the necessity of these terms.
The Usadel equation was supplemented by the Tanaka Nazarov boundary conditions, which can be used for both conventional (s-wave) and unconventional (p-wave) superconductors. The equations resulting from these boundary conditions were derived in the θ-parametrisation. Also the boundary conditions were derived in general form, allowing for a complex parameter χ, and a discontinuity of both parameters along the interface. The expressions found were cast in such a form that the computation is stable. The implementation boundary conditions were tested on a few problems for which analytical approximations are known. The results compared favourably to known theory.
An iterative scheme was developed to solve the nonlinear Usadel equation. The scheme developed solves the θ and χ equation simultaneously and can thus be applied not only in equilibrium, but also in quasistationary non-equilibrium settings.

The code developed was used to reproduce known results in equilibrium and to produce new results in non-equilibrium settings, and to compare the difference in results between the VT-junction and the well-known SNS-junction. The dependence of the differential conductance of the VT-junction phase difference between the electrodes was shown to be different for s-wave and p-wave superconductors. The spectral supercurrent, on the other hand, was shown to be qualitatively similar for s-wave and p-wave superconductors. It was found that the spectral supercurrent changes sign as a function of energy more and more often if the length of the junction is increased, in good agreement with analytical approaches. It was confirmed that by varying the voltages applied to the normal reservoirs, the spectral supercurrent can be found using measurements of the total supercurrent.
It was shown that Shapiro steps, an important experimental tool in the study of Josephson junctions could be calculated using the calculations of the spectral supercurrent in the VT junction. The effect of using a topological insulator was investigated by allowing an exchange coupling. It was shown that the exchange coupling has a significant influence on the spectral supercurrent.
The thesis provides predictions on the outcomes of realisable experiments, that can be used to distinguish p-wave superconductivity from s-wave superconductivity, and thereby provides a test for possible host materials of Majorana particles, a promising direction for a quantum computer.

18 Outlook

The code developed allows for several extensions. Apart from s-wave and p-wave superconductors, also d-wave and f-wave superconductors can be investigated. Moreover, the normal metal in the can be replaced by a ferromagnetic material or a topological insulator. For this latter adjustment the Tanaka Nazarov boundary conditions need to be adjusted to give a good description of the spin-orbit coupling. This is an interesting direction for future research. If the normal metal is replaced by a ferromagnetic material adjustment of the Tanaka Nazarov boundary conditions is not needed.
The code allows as well for an adjustment of the geometry to multiterminal junctions with more than four terminals. This would allow for a more elaborated investigation of the influence of the geometry on the local density of states and the supercurrent. An extension of the code to solve the two-dimensional Usadel equation would provide an even larger flexibility in the geometry.
Another interesting research direction is to drop the dirty limit assumption and use the Eilenberger equation, the quasiclassical equation that is valid also beyond the dirty limit approximation. In this way a greater variety of junctions can be considered. It would be interesting to show that the results of the Eilenberger do coincide with the results of the Usadel equation in the dirty limit for the VT-junction. Next to this, one might consider to solve the full Gorkov equation and investigate in detail the error of the quasiclassical approximation.
In the calculation of Shapiro steps, the current method has the limitation that it is only valid in the adiabatic limit, that is, for slowly varying oscillations. It would be good to have a solution method for the equations that do not need the adiabatic limit.
The code developed in this thesis can be used to compare with measurements on this geometry. An interesting approach for future research is to build the VT-junction and validate the parameter dependencies as found in this thesis. This would be a good test for the model.

19 Acknowledgements

First of all, I would like to thank my daily supervisors, Alexander Golubov and Bernard Geurts. I would like to thank Alexander for the help in understanding the background material and for valuable discussions regarding the interpretation of the results. I would like to thank Bernard for useful discussions on the obtained results and for his guidance on the presentation of the background material.

Next to this, I would like to thank all other members of the ICE/QTM and MMS research groups. Due to the ongoing Covid measurements we have not often met in person. However, it was a pleasure to attend the online meetings of both groups. It was interesting to listen to the updates on progress of all group members, from the presentations on more experimental works in ICE/QTM and the stochastic differential equations in MMS to the presentations on works that were closely related to my thesis. Moreover, the questions that arose during my presentation were very useful, they helped me to find new interesting results, and to get a clearer idea of the presented results or the theory behind those results.

Lastly, I would like to thank Yukio Tanaka and Shu Suzuki for useful discussions regarding the mechanisms behind the boundary conditions used in this thesis.

Bibliography

[1] L. Fu and C.L. Kane. Superconducting proximity effect and Majorana fermions at the surface of a topological insulator. Physical review letters, 100(9):096407, 2008.

[2] W. Belzig, F. K. Wilhelm, C. Bruder, G. Schön, and A.D. Zaikin. Quasiclassical Green's function approach to mesoscopic superconductivity. Superlattices and microstructures, 25(5-6):1251–1288, 1999.

[3] V. Chandrasekhar. An introduction to the quasiclassical theory of superconductivity for diffusive proximity-coupled systems. In K.-H. Bennemann and J.B. Ketterson, editors, The Physics of Superconductors, pages 55–110. Springer, Berlin Heidelberg, 2004.

[4] Y. V. Nazarov. Novel circuit theory of Andreev reflection. Superlattices and microstructures, 25(5-6):1221–1231, 1999.

[5] T.N. Theis and H.-S. Wong. The end of Moore's law: A new beginning for information technology. Computing in Science & Engineering, 19(2):41–50, 2017.

[6] G.E. Moore. Cramming more components onto integrated circuits. Proceedings of the IEEE, 86(1):82–85, 1998.

[7] R. Landauer. Dissipation and noise immunity in computation and communication. Nature, 335(6193):779–784, 1988.

[8] I.L. Markov. Limits on fundamental limits to computation. Nature, 512(7513):147–154, 2014.

[9] J. R. Powell. The quantum limit to Moore's law. Proceedings of the IEEE, 96(8):1247–1248, 2008.

[10] R. Landauer. Irreversibility and heat generation in the computing process. IBM journal of research and development, 5(3):183–191, 1961.

[11] C.C. Mann. The end of Moore's law? Technology Review, 103(3):42–42, 2000.

[12] L.B. Kish. End of Moore's law: Thermal (noise) death of integration in micro and nano electronics. Physics Letters A, 305(3-4):144–149, 2002.

[13] E. Masanet, A. Shehabi, N. Lei, S. Smith, and J. Koomey. Recalibrating global data center energy-use estimates. Science, 367(6481):984–986, 2020.

[14] A. Shehabi, S. Smith, D. Sartor, R. Brown, M. Herrlin, J. Koomey, E. Masanet, N. Horner, I. Azevedo, and W. Lintner. United states data center energy usage report. 2016.

[15] M. Avgerinou, P. Bertoldi, and L. Castellazzi. Trends in data centre energy consumption under the European code of conduct for data centre energy efficiency. Energies, 10(10):1470, 2017.

[16] J. Preskill. Lecture notes for physics 229: Quantum information and computation. California Institute of Technology, 16, 1998.

[17] R. De Wolf. Quantum computing: Lecture notes. arXiv preprint arXiv:1907.09415, 2019.

[18] P.W. Shor. Algorithms for quantum computation: discrete logarithms and factoring. In Proceedings 35th Annual Symposium on Foundations of Computer Science, pages 124–134, 1994.

[19] R.L. Rivest, A. Shamir, and L. Adleman. A method for obtaining digital signatures and public-key cryptosystems. Communications of the ACM, 21(2):120–126, 1978.

[20] S. J. Lomonaco. A talk on quantum cryptography or how Alice outwits Eve. In Coding Theory and Cryptography, pages 144–174. Springer, Berlin Heidelberg, 2000.

[21] R.P. Feynman. Simulating physics with computers. International Journal of Theoretical Physics, 21(6):467–488, 1982.

[22] N. Wiebe, D.W. Berry, P. Høyer, and B.C. Sanders. Simulating quantum dynamics on a quantum computer. Journal of Physics A: Mathematical and Theoretical, 44(44):445308, 2011.

[23] V.V. Schmidt. The Physics of Superconductors, edited by P. Müller and A.V. Ustinov. Springer, Berlin Heidelberg, 1997.

[24] B.D. Josephson. Possible new effects in superconductive tunnelling. Physics letters, 1(7):251–253, 1962.

[25] B.D. Josephson. Supercurrents through barriers. Advances in Physics, 14(56):419–451, 1965.

[26] T. Yokoyama. Odd frequency superconductivity in symmetry breaking systems. PhD thesis, Nagoya University, 2008.

[27] J.R. Williams, A.J. Bestwick, P. Gallagher, S. S. Hong, Y. Cui, A.S. Bleich, J.G. Analytis, I.R. Fisher, and D. Goldhaber-Gordon. Unconventional Josephson effect in hybrid superconductor-topological insulator devices. Physical review letters, 109(5):056803, 2012.

[28] J. Clarke and A.I. Braginski. The SQUID handbook, volume 1. Wiley Online Library, 2004.

[29] P.A.M. Dirac. The quantum theory of the electron. Proceedings of the Royal Society of London. Series A, Containing Papers of a Mathematical and Physical Character, 117(778):610–624, 1928.

[30] E. Majorana and L. Maiani. A symmetric theory of electrons and positrons. In Ettore Majorana Scientific Papers, pages 201–233. Springer, Berlin Heidelberg, 2006.

[31] S.M. Bilenky. Neutrinos: Majorana or Dirac? Universe, 6(9):134, 2020.

[32] A. B. Balantekin, A. de Gouvêa, and B. Kayser. Addressing the Majorana vs. Dirac question with neutrino decays. Physics Letters B, 789:488–495, 2019.

[33] R.D. Mattuck. A guide to Feynman diagrams in the many-body problem, Second edition. Dover, New York, 1992.

[34] H. Zhang, C.-X. Liu, S. Gazibegovic, D. Xu, J.A. Logan, G. Wang, N. Van Loo, J.D.S. Bommer, M. W.A. De Moor, D. Car, et al. Quantized Majorana conductance. Nature, 556(7699):74–79, 2018.

[35] H. Zhang, C.-X. Liu, S. Gazibegovic, D. Xu, J.A. Logan, G. Wang, N. van Loo, J.D.S. Bommer, M.W.A. de Moor, D. Car, et al. Retraction note: Quantized Majorana conductance. Nature, pages 1–1, 2021.

[36] V. Mourik, K. Zuo, S.M. Frolov, S.R. Plissard, E.P.A.M. Bakkers, and L.P. Kouwenhoven. Signatures of Majorana fermions in hybrid superconductor-semiconductor nanowire devices. Science, 336(6084):1003–1007, 2012.

[37] Z. Wang, J. O. Rodriguez, L. Jiao, S. Howard, M. Graham, G.D. Gu, T.L. Hughes, D. K. Morr, and V. Madhavan. Evidence for dispersing 1D Majorana channels in an iron-based superconductor. Science, 367(6473):104–108, 2020.

[38] M. Kayyalha, D. Xiao, R. Zhang, J. Shin, J. Jiang, F. Wang, Y.-F. Zhao, R. Xiao, L. Zhang, K.M. Fijalkowski, et al. Absence of evidence for chiral Majorana modes in quantum anomalous Hall-superconductor devices. Science, 367(6473):64–67, 2020.

[39] D.J. Griffiths. Introduction to quantum mechanics, second edition. Cambridge University Press, Cambridge, 2010.

[40] F. Steglich, J. Aarts, C.D. Bredl, W. Lieke, D. Meschede, W. Franz, and H. Schäfer. Superconductivity in the Presence of Strong Pauli Paramagnetism: $cecu_2si_2$. Physical Review Letters, 43(25):1892, 1979.

[41] J.G. Bednorz and K.A. Müller. Possible high T_c superconductivity in the Ba- La- Cu- O system. Zeitschrift für Physik B Condensed Matter, 64(2):189–193, 1986.

[42] M. Sigrist. Review on the chiral p-wave phase of Sr_2RuO_4. Progress of Theoretical Physics Supplement, 160:1–14, 2005.

[43] Y. Maeno, S. Kittaka, T. Nomura, S. Yonezawa, and K. Ishida. Evaluation of spin-triplet superconductivity in Sr_2RuO_4. Journal of the Physical Society of Japan, 81(1):011009, 2011.

[44] H. Hilgenkamp, H.-J. H. Smilde, D.H.A. Blank, G. Rijnders, H. Rogalla, J.R. Kirtley, C.C. Tsuei, et al. Ordering and manipulation of the magnetic moments in large-scale superconducting π-loop arrays. Nature, 422(6927):50–53, 2003.

[45] T. Maier, M. Jarrell, T. Pruschke, and J. Keller. D-wave superconductivity in the Hubbard model. Physical review letters, 85(7):1524, 2000.

[46] A.Y. Kitaev. Unpaired Majorana fermions in quantum wires. Physics-Uspekhi, 44(10S):131, 2001.

[47] C.W.J. Beenakker. Search for Majorana fermions in superconductors. Annual Review of Condensed Matter Physics, 4(1):113–136, 2013.

[48] C. Nayak, S. H. Simon, A. Stern, M. Freedman, and S. D. Sarma. Non-Abelian anyons and topological quantum computation. Reviews of Modern Physics, 80(3):1083, 2008.

[49] H. Kamerlingh Onnes. Further experiments with liquid helium. In Proceedings of the KNAW, volume 13, pages 1910–1911, 1911.

[50] F. London and H. London. Supraleitung und diamagnetismus. Physica, 2(1):341–354, 1935.

[51] V. L. Ginzburg. On superconductivity and superfluidity (what i have and have not managed to do), as well as on the'physical minimum'at the beginning of the xxi century (december 8, 2003). Physics-Uspekhi, 47(11):1155–1170, 2004.

[52] J.B. Ketterson and S.N. Song. Superconductivity (2nd edition). Cambridge University Press, Cambridge, 1999.

[53] A. A. Abrikosov, L.P. Gorkov, and I.E. Dzyaloshinski. Methods of quantum field theory in statistical physics (English version). Courier Corporation, 1963.

[54] A. A. Abrikosov. Fundamental theory of metals (English version). North-Holland, Amsterdam, 1988.

[55] L.N. Cooper. Bound electron pairs in a degenerate Fermi gas. Physical Review, 104:1189–1190, Nov 1956.

[56] J. Bardeen, L. N. Cooper, and J. R. Schrieffer. Microscopic theory of superconductivity. Phyical Review, 106:162–164, Apr 1957.

[57] J. Bardeen, L. N. Cooper, and J. R. Schrieffer. Theory of superconductivity. Physical Review, 108:1175–1204, Dec 1957.

[58] H. Fröhlich. Theory of the superconducting state. I. The ground state at the absolute zero of temperature. Physical Review, 79(5):845, 1950.

[59] N. W. Ashcroft, N. D. Mermin, et al. Solid state physics, volume 2005. holt, rinehart and winston, new york London, 1976.

[60] N.N. Bogoljubov, V. V. Tolmachov, and D.V. Širkov. A new method in the theory of superconductivity. Fortschritte der physik, 6(11-12):605–682, 1958.

[61] T.K. Worthington, W.J. Gallagher, and T.R. Dinger. Anisotropic nature of high-temperature superconductivity in single-crystal $Y_1Ba_2Cu_3O_{7-x}$. Physical review letters, 59(10):1160, 1987.

[62] Y. Maeno, S. NishiZaki, and Z.Q. Mao. Experimental evidence for spin-triplet superconductivity in Sr_2RuO_4. Journal of superconductivity, 12(4):535–541, 1999.

[63] H.G. Suh, H. Menke, P.M.R. Brydon, C. Timm, A. Ramires, and D.F. Agterberg. Stabilizing even-parity chiral superconductivity in Sr_2RuO_4. Physical Review Research, 2(3):032023, 2020.

[64] C. Kallin and A.J. Berlinsky. Is Sr_2RuO_4 a chiral p-wave superconductor? Journal of Physics: Condensed Matter, 21(16):164210, 2009.

[65] L.P. Gorkov. On the energy spectrum of superconductors. Soviet Physics JETP, 7(505):158, 1958.

[66] J. Rammer and H. Smith. Quantum field-theoretical methods in transport theory of metals. Reviews of modern physics, 58(2):323, 1986.

[67] A.L. Shelankov. On the derivation of quasiclassical equations for superconductors. Journal of low temperature physics, 60(1):29–44, 1985.

[68] G. Eilenberger. Transformation of Gorkov's equation for type II superconductors into transport-like equations. Zeitschrift für Physik A Hadrons and nuclei, 214(2):195–213, 1968.

[69] A.I. Larkin and Y.N. Ovchinnikov. Quasiclassical method in the theory of superconductivity. Sov Phys JETP, 28(6):1200–1205, 1969.

[70] K. D. Usadel. Generalized diffusion equation for superconducting alloys. Physical Review Letters, 25(8):507, 1970.

[71] V. Somà, T. Duguet, and C. Barbieri. Ab initio self-consistent Gorkov-Green's function calculations of semimagic nuclei: Formalism at second order with a two-nucleon interaction. Physical Review C, 84(6):064317, 2011.

[72] V. Somà, C. Barbieri, and T. Duguet. Ab initio self-consistent Gorkov-Green's function calculations of semi-magic nuclei: Numerical implementation at second order with a two-nucleon interaction. Physical Review C, 89(2):024323, 2014.

[73] E. Snider, N. Dasenbrock-Gammon, R. McBride, M. Debessai, H. Vindana, K. Vencatasamy, K.V. Lawler, A. Salamat, and R.P. Dias. Room-temperature superconductivity in a carbonaceous sulfur hydride. Nature, 586(7829):373–377, 2020.

[74] A.I. Larkin and Y.U.N. Ovchinnikov. Nonlinear conductivity of superconductors in the mixed state. Soviet Physics JETP, 41(5):960–965, 1975.

[75] J.W. Serene and D. Rainer. The quasiclassical approach to superfluid 3He. Physics Reports, 101(4):221–311, 1983.

[76] S. Shapiro. Josephson currents in superconducting tunneling: The effect of microwaves and other observations. Physical Review Letters, 11(2):80, 1963.

[77] E.B. Saff and A.D. Snider. Fundamentals of Complex Analysis, Engineering, Science and Mathematics, 3rd edition. Pearson, Edinburgh, 2014.

[78] A. Schmid. Kinetic equations for dirty syperconductors. In K.E. Gray, editor, Nonequilibrium superconductivity, phonons, and Kapitza boundaries, chapter 14, pages 423–481. Plenum Press, New York, 1981.

[79] S.-I. Suzuki, A.A. Golubov, Y. Asano, and Y. Tanaka. Effects of phase coherence on local density of states in superconducting proximity structures. Physical Review B, 100(2):024511, 2019.

[80] A.F. Volkov and H. Takayanagi. Effect of gate voltage on critical current in controllable superconductor–normal-metal–superconductor Josephson junctions. Physical Review B, 53(22):15162, 1996.

[81] A.F. Volkov and H. Takayanagi. Long-range phase-coherent effects in the transport properties of mesoscopic superconductor–normal-metal structures. Physical Review B, 56(17):11184, 1997.

[82] E. Toyoda, H. Takayanagi, and H. Nakano. Systematic gate-controlled reentrant conductance of a superconductor-semiconductor two-dimensional electron gas junction. Physical Review B, 59(18):R11653, 1999.

[83] R Shaikhaidarov, A.F. Volkov, H. Takayanagi, V.T. Petrashov, and P. Delsing. Josephson effects in a superconductor–normal-metal mesoscopic structure with a dangling superconducting arm. Physical Review B, 62(22):R14649, 2000.

[84] Y. Tanaka, Y.V. Nazarov, and S. Kashiwaya. Circuit theory of unconventional superconductor junctions. Physical review letters, 90(16):167003, 2003.

[85] Y. Tanaka, Y. V. Nazarov, A.A. Golubov, and S. Kashiwaya. Theory of charge transport in diffusive normal metal/unconventional singlet superconductor contacts. Physical Review B, 69(14):144519, 2004.

[86] E. : Italian Fermi. On the quantisation of the monatomic ideal gas. Rendiconti Lincei, 3(145):9, 1926. Translated to English by Zannoni, A.

[87] P. A. M. Dirac. On the theory of quantum mechanics. Proceedings of the Royal Society of London. Series A, Containing Papers of a Mathematical and Physical Character, 112(762):661–677, 1926.

[88] T.T. Heikkilä, T. Vänskä, and F.K. Wilhelm. Supercurrent-induced Peltier-like effect in superconductor/normal-metal weak links. Physical Review B, 67(10):100502, 2003.

[89] Y. Tanaka. personal communication.

[90] S.-I. Suzuki, A.A. Golubov, Y. Asano, and Y. Tanaka. Quasiparticle spectrum in mesoscopic superconducting junctions with weak magnetization. In Proceedings of the International Conference on Strongly Correlated Electron Systems (SCES2019), page 011045, 2020.

[91] M.Y. Kuprianov and V.F. Lukichev. Influence of boundary transparency on the critical current of dirty SS'S structures. Zh. Eksp. Teor. Fiz, 94:149, 1988.

[92] J. Van Kan, A. Segal, and F. Vermolen. Numerical Methods in Scientific Computing. Department of Applied Mathematics. Delft University of Technology, The Netherlands, 2008.

[93] S. Pilgram, W. Belzig, and C. Bruder. Excitation spectrum of mesoscopic proximity structures. Physical Review B, 62(18):12462, 2000.

[94] A. A. Golubov, Y.M. Kupriyanov, and E. Il'Ichev. The current-phase relation in Josephson junctions. Reviews of modern physics, 76(2):411, 2004.

[95] P. Dubos, H. Courtois, O. Buisson, and B. Pannetier. Coherent low-energy charge transport in a diffusive SNS junction. Physical review letters, 87(20):206801, 2001.

[96] A.N. Tahvildar-Zadeh, J.K. Freericks, and B.K. Nikolić. Thouless energy as a unifying concept for josephson junctions tuned through the Mott metal-insulator transition. Physical Review B, 73(18):184515, 2006.

[97] P. Dubos, H. Courtois, B. Pannetier, F.K. Wilhelm, A.D. Zaikin, and G. Schön. Josephson critical current in a long mesoscopic SNS junction. Physical Review B, 63(6):064502, 2001.

[98] J. Reutlinger, L. Glazman, Y.V. Nazarov, and W. Belzig. Secondary "smile"-gap in the density of states of a diffusive Josephson junction for a wide range of contact types. Physical Review B, 90(1):014521, 2014.

[99] A. Kamenev. Field theory of non-equilibrium systems. Cambridge University Press, Cambridge, 2011.

[100] C. Fräßdorf and J.E.M. Mosig. Keldysh functional renormalization group for electronic properties of graphene. Physical Review B, 95(12):125412, 2017.

[101] A. Brinkman, A.A. Golubov, H. Rogalla, F.K. Wilhelm, and Y.M. Kupriyanov. Microscopic nonequilibrium theory of double-barrier Josephson junctions. Physical Review B, 68(22):224513, 2003.

[102] C.A. Hamilton, C.J. Burroughs, and S.P. Benz. Josephson voltage standard-a review. IEEE transactions on applied superconductivity, 7(2):3756–3761, 1997.

[103] M.C. Dartiailh, J.J. Cuozzo, B.H. Elfeky, W. Mayer, J. Yuan, K.S. Wickramasinghe, E. Rossi, and J. Shabani. Missing Shapiro steps in topologically trivial Josephson junction on InAs quantum well. Nature communications, 12(1):1–9, 2021.

[104] M. Z. Hasan and C.L. Kane. Colloquium: topological insulators. Reviews of modern physics, 82(4):3045, 2010.

[105] I. V. Bobkova, A. M. Bobkov, A. A. Zyuzin, and M. Alidoust. Magnetoelectrics in disordered topological insulator josephson junctions. Physical Review B, 94(13):134506, 2016.

[106] A. Zyuzin, M. Alidoust, and D. Loss. Josephson junction through a disordered topological insulator with helical magnetization. Physical Review B, 93(21):214502, 2016.

[107] F.S. Bergeret and I.V. Tokatly. Theory of diffusive φ 0 Josephson junctions in the presence of spin-orbit coupling. EPL (Europhysics Letters), 110(5):57005, 2015.

[108] Y. Asano, Y. Tanaka, A.A. Golubov, and S. Kashiwaya. Conductance spectroscopy of spin-triplet superconductors. Physical review letters, 99(6):067005, 2007.

[109] A.A. Golubov, F.K. Wilhelm, and A.D. Zaikin. Coherent charge transport in metallic proximity structures. Physical Review B, 55(2):1123, 1997.

[110] F.K. Wilhelm, G. Schön, and A.D. Zaikin. Mesoscopic superconducting–normal metal–superconducting transistor. Physical review letters, 81(8):1682, 1998.

[111] V.S. Shumeiko, E.N. Bratus, and G. Wendin. Scattering theory of superconductive tunneling in quantum junctions. Low Temperature Physics, 23(3):181–198, 1997.

[112] C. Ishii. Thermodynamical properties of Josephson junction with a normal metal barrier. Progress of Theoretical Physics, 47(5):1464–1481, 1972.

[113] N. Argaman. Nonequilibrium Josephson-like effects in wide mesoscopic SNS junctions. Superlattices and microstructures, 25(5-6):861–875, 1999.

[114] H. G. Hugdal, J. Linder, and S. H. Jacobsen. Quasiclassical theory for the superconducting proximity effect in dirac materials. Physical Review B, 95(23):235403, 2017.

A Local density of states

This section contains the calculated local density of states (LDOS) in the VT-junction as a function of the junction length L. The distance between the electrodes is $L-2$. In each of the figures $z = 0.2$ and $\gamma = 1$ is used.

A.1 S-wave

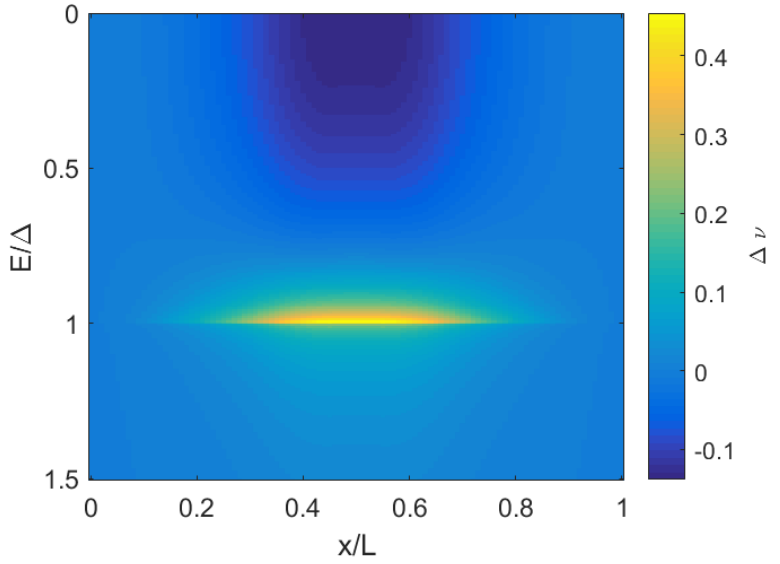

Figure 38: The LDOS as a function of position and energy as calculated using the Usadel equation for a junction length of 2.5.

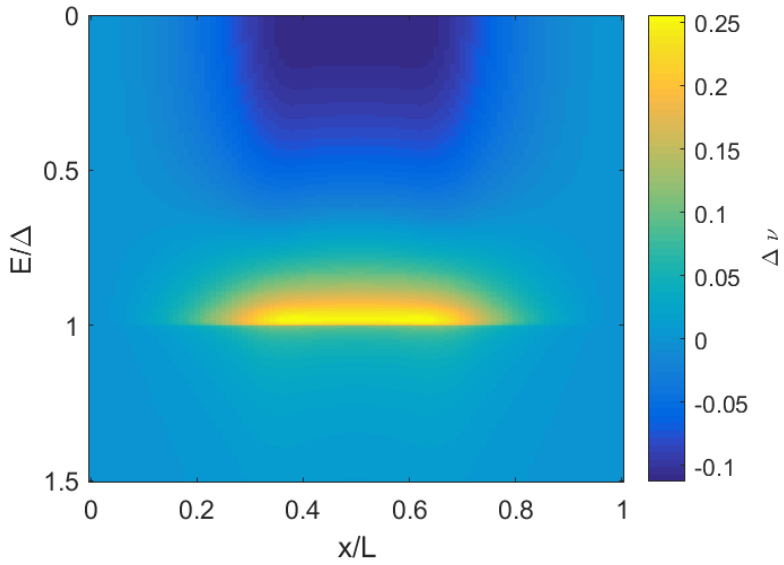

Figure 39: The LDOS as a function of position and energy as calculated using the Usadel equation for a junction length of 3.

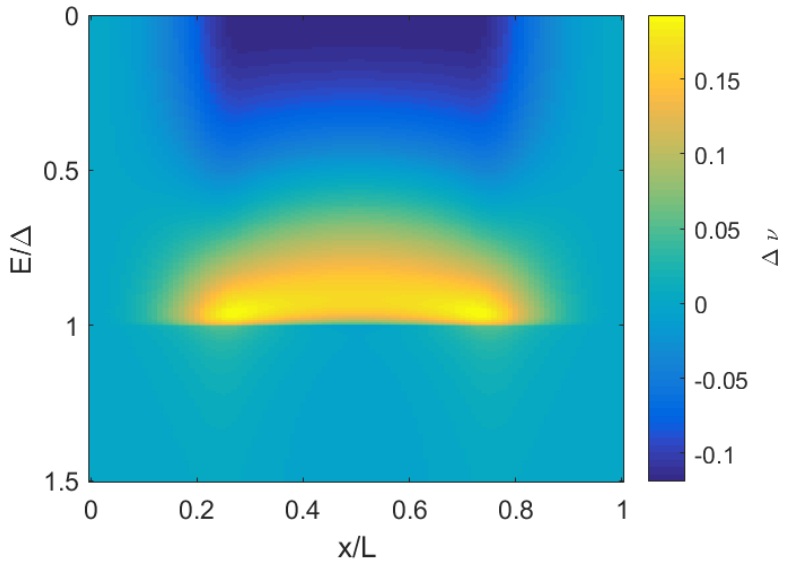

Figure 40: The LDOS as a function of position and energy as calculated using the Usadel equation for a junction length of 4.

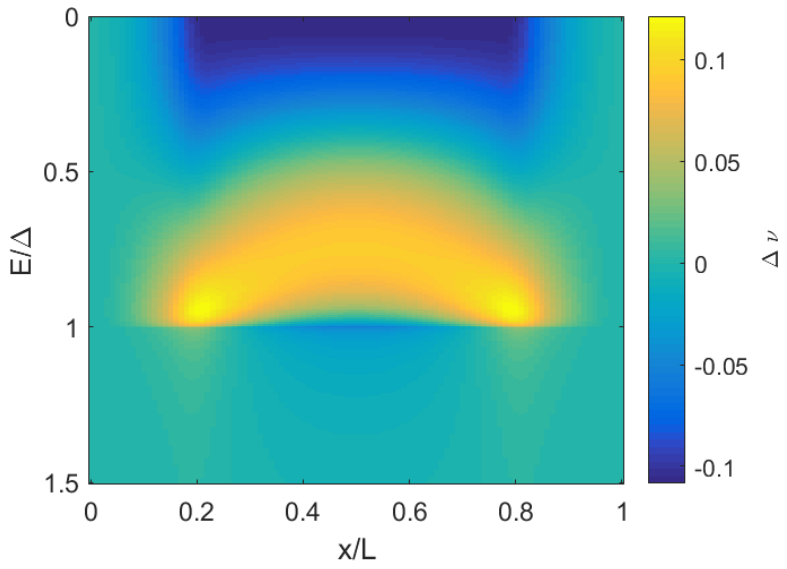

Figure 41: The LDOS as a function of position and energy as calculated using the Usadel equation for a junction length of 5.

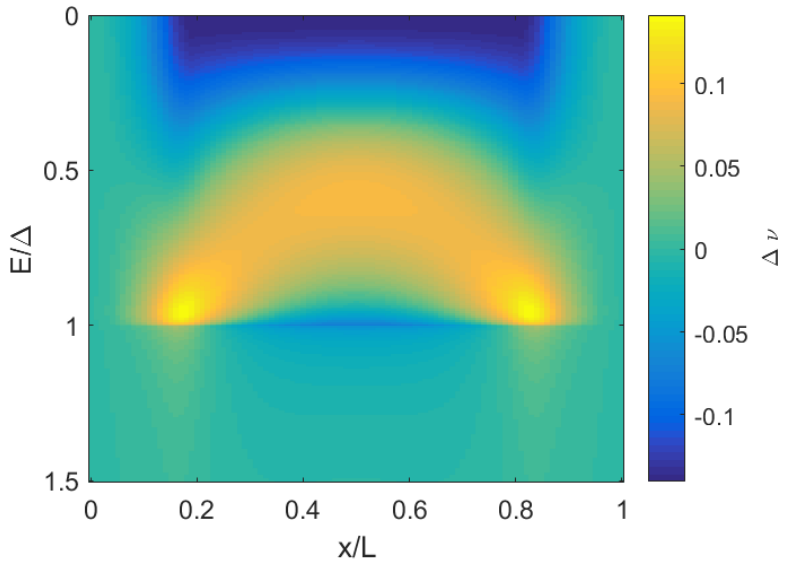

Figure 42: The LDOS as a function of position and energy as calculated using the Usadel equation for a junction length of 6.

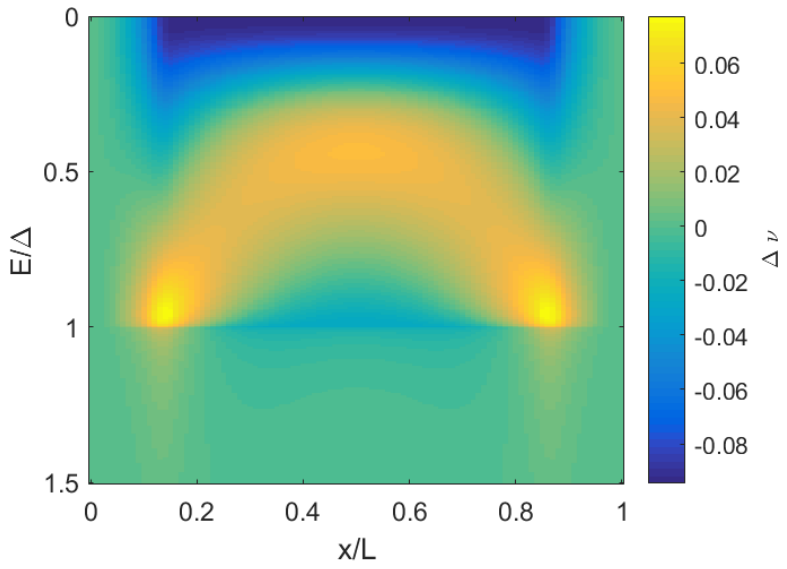

Figure 43: The LDOS as a function of position and energy as calculated using the Usadel equation for a junction length of 7.

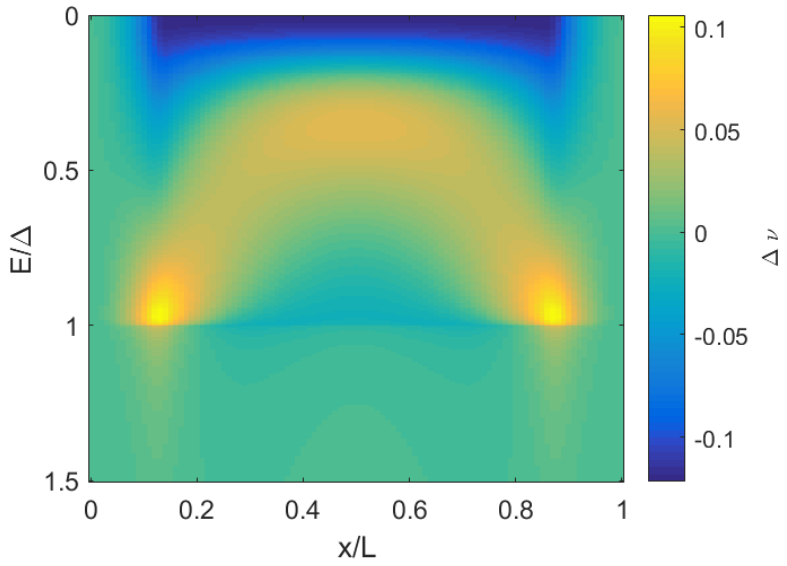

Figure 44: The LDOS as a function of position and energy as calculated using the Usadel equation for a junction length of 8.

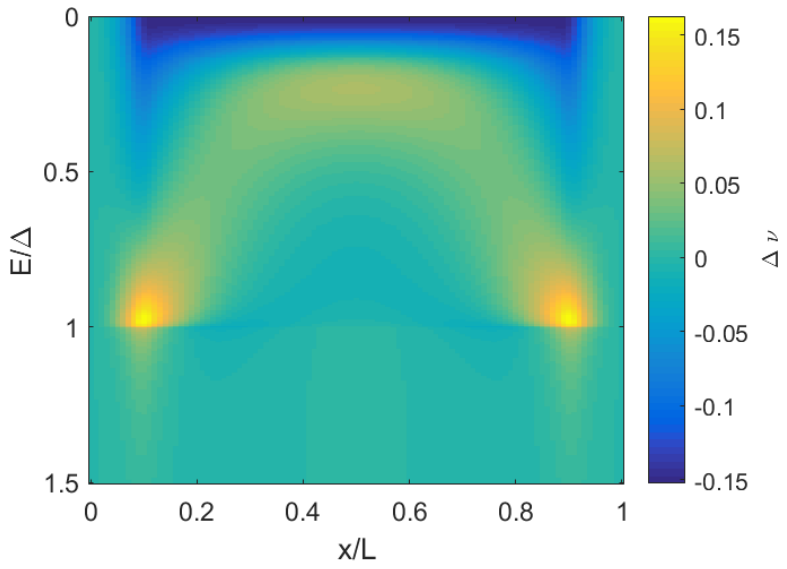

Figure 45: The LDOS as a function of position and energy as calculated using the Usadel equation for a junction length of 10.

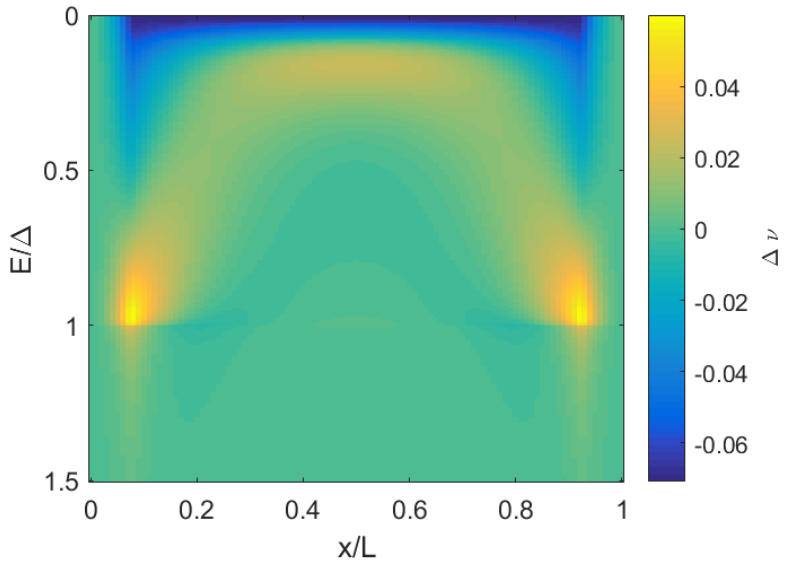

Figure 46: The LDOS as a function of position and energy as calculated using the Usadel equation for a junction length of 12.

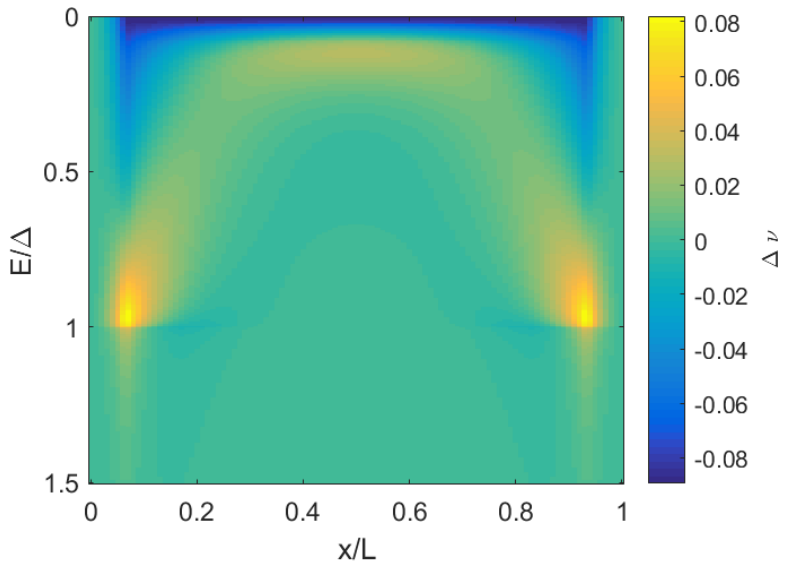

Figure 47: The LDOS as a function of position and energy as calculated using the Usadel equation for a junction length of 14.

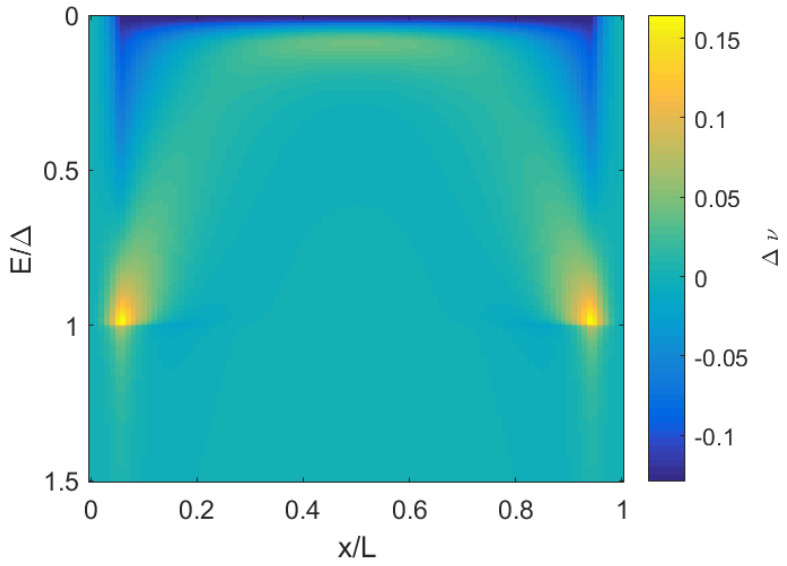

Figure 48: The LDOS as a function of position and energy as calculated using the Usadel equation for a junction length of 16.

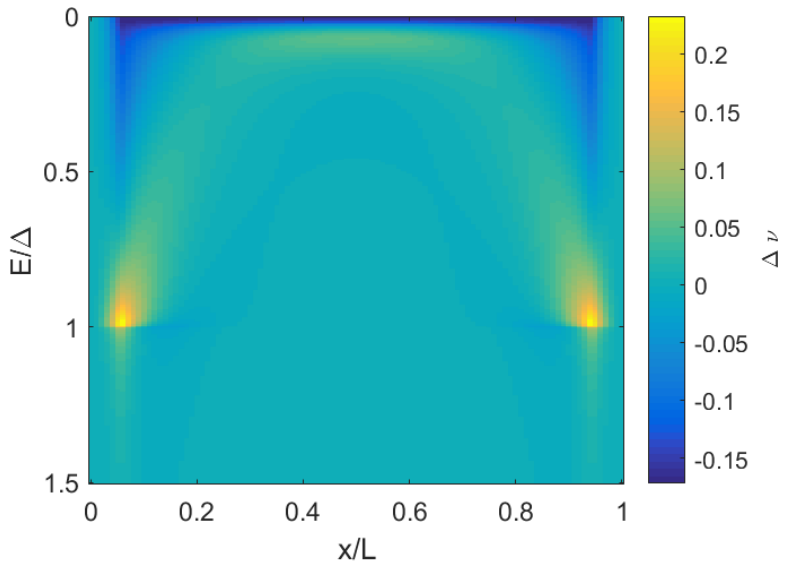

Figure 49: The LDOS as a function of position and energy as calculated using the Usadel equation for a junction length of 18.

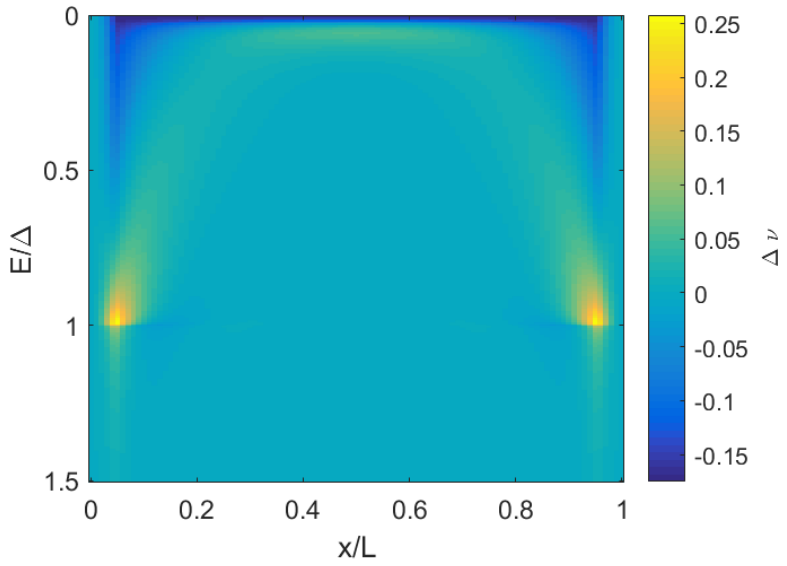

Figure 50: The LDOS as a function of position and energy as calculated using the Usadel equation for a junction length of 20.

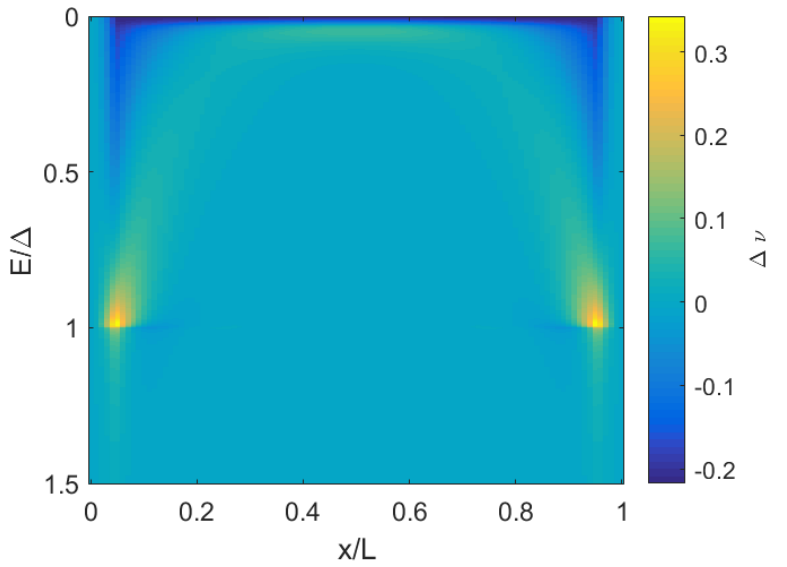

Figure 51: The LDOS as a function of position and energy as calculated using the Usadel equation for a junction length of 22.

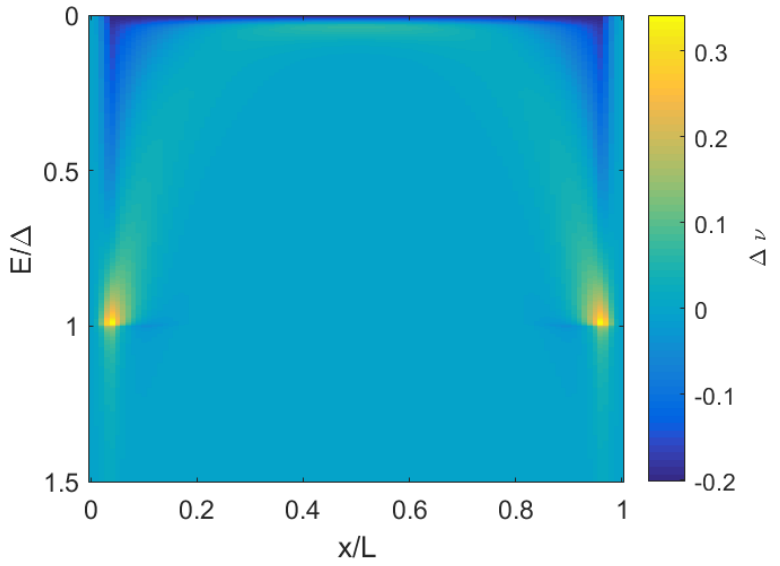

Figure 52: The LDOS as a function of position and energy as calculated using the Usadel equation for a junction length of 24.

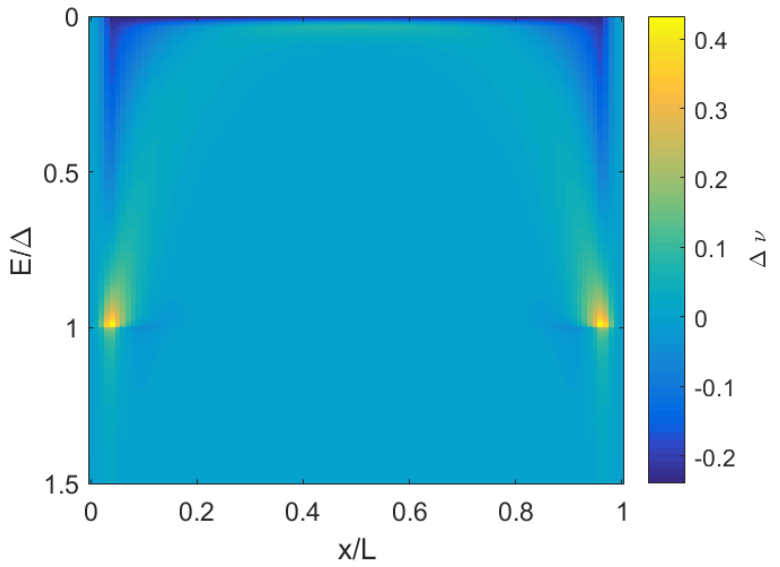

Figure 53: The LDOS as a function of position and energy as calculated using the Usadel equation for a junction length of 26.

A.2 P-wave

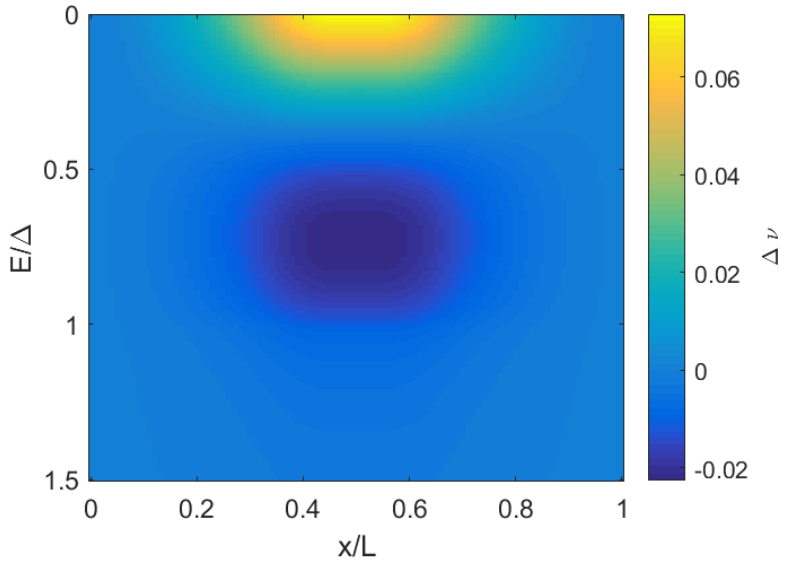

Figure 54: The LDOS as a function of position and energy as calculated using the Usadel equation for a junction length of 2.5.

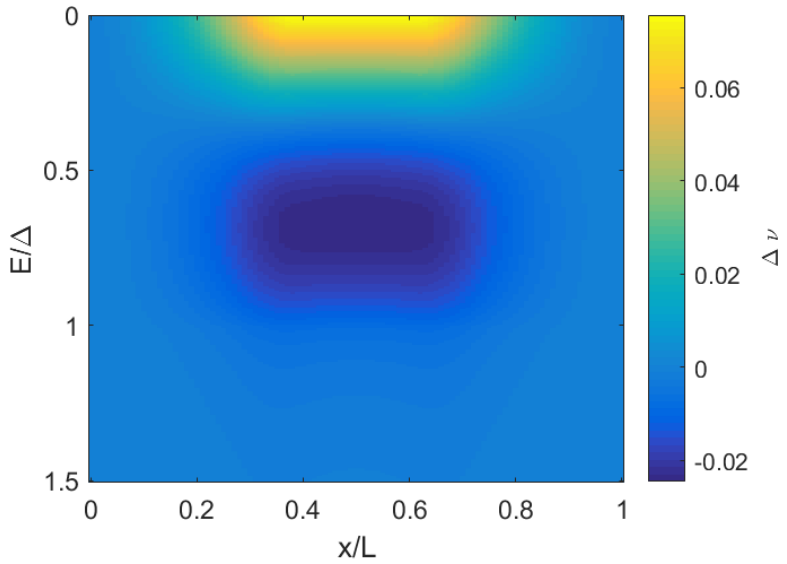

Figure 55: The LDOS as a function of position and energy as calculated using the Usadel equation for a junction length of 3.

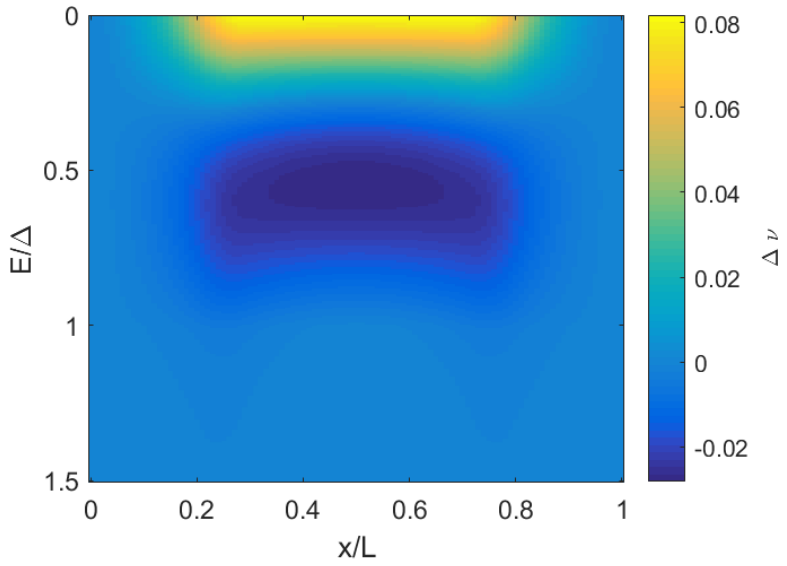

Figure 56: The LDOS as a function of position and energy as calculated using the Usadel equation for a junction length of 4.

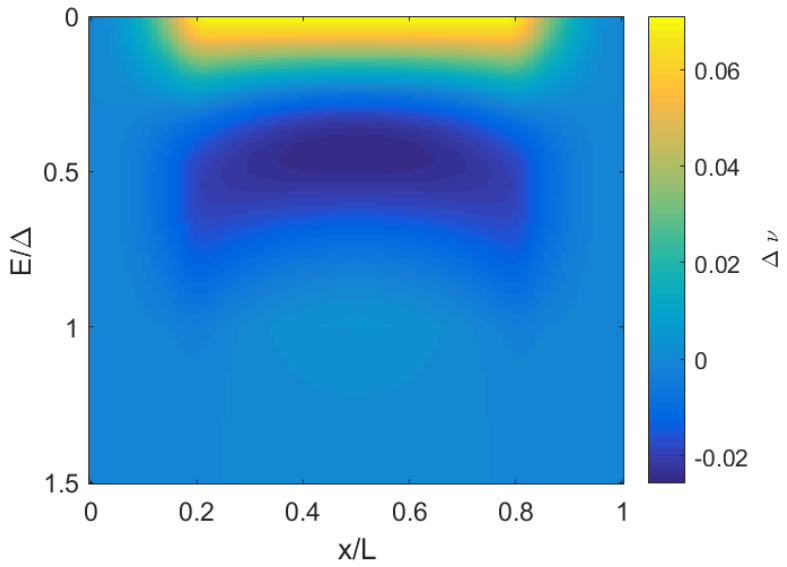

Figure 57: The LDOS as a function of position and energy as calculated using the Usadel equation for a junction length of 5.

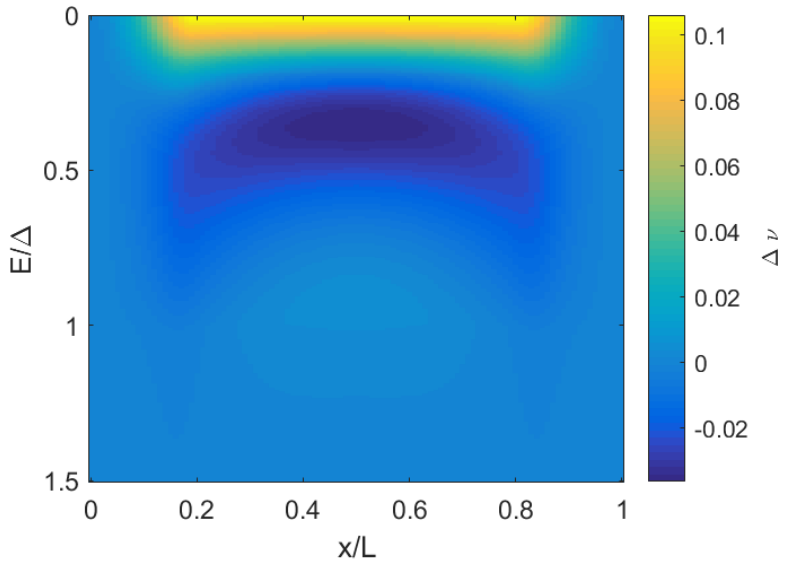

Figure 58: The LDOS as a function of position and energy as calculated using the Usadel equation for a junction length of 6.

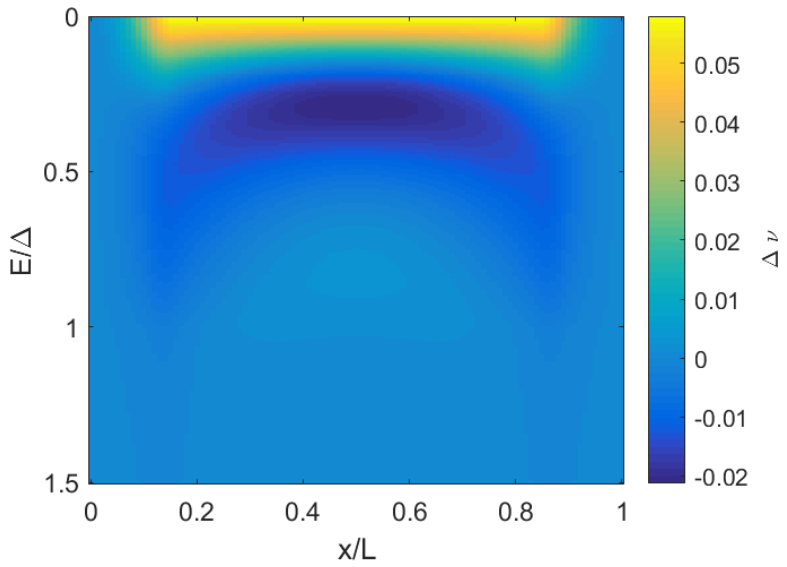

Figure 59: The LDOS as a function of position and energy as calculated using the Usadel equation for a junction length of 7.

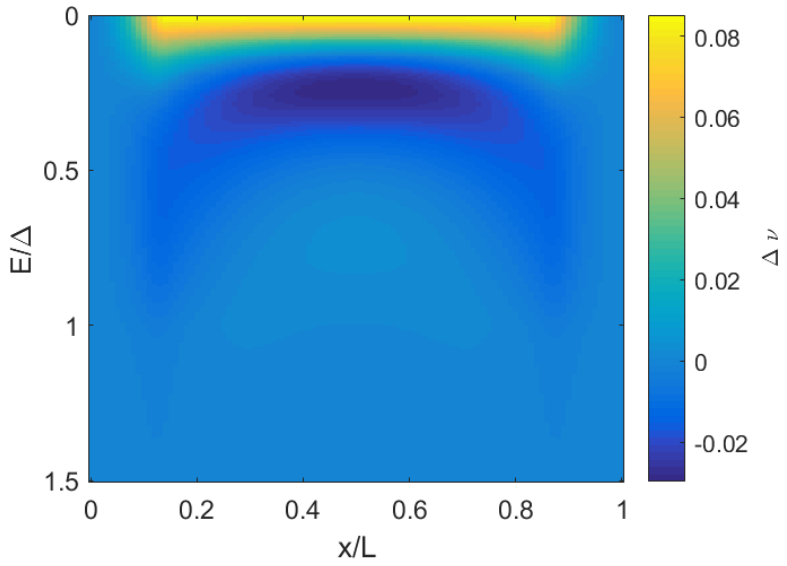

Figure 60: The LDOS as a function of position and energy as calculated using the Usadel equation for a junction length of 8.

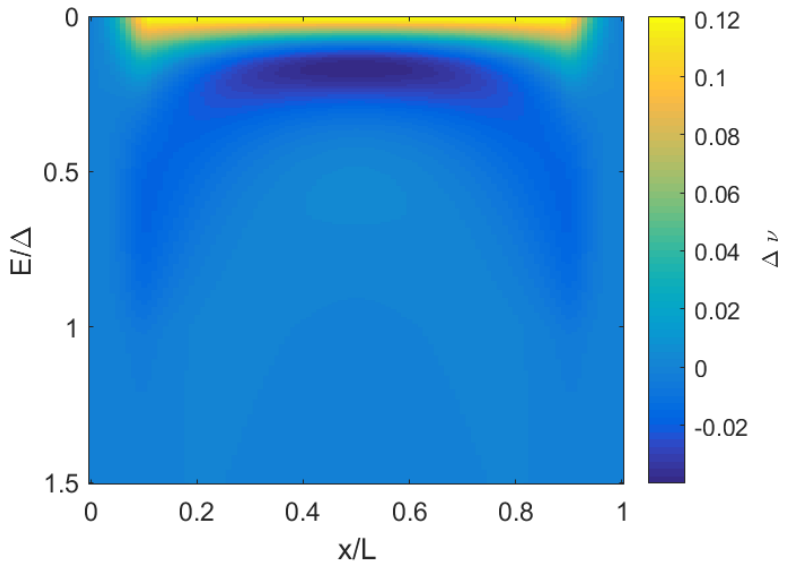

Figure 61: The LDOS as a function of position and energy as calculated using the Usadel equation for a junction length of 10.

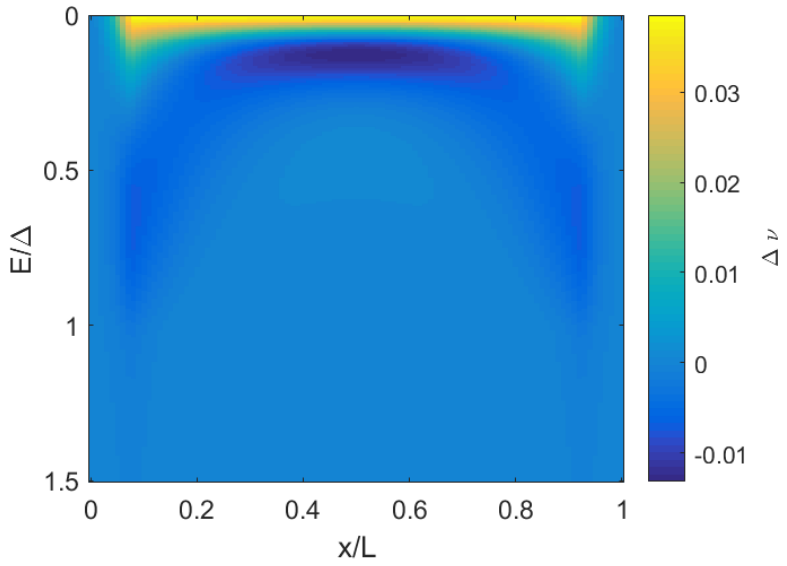

Figure 62: The LDOS as a function of position and energy as calculated using the Usadel equation for a junction length of 12.

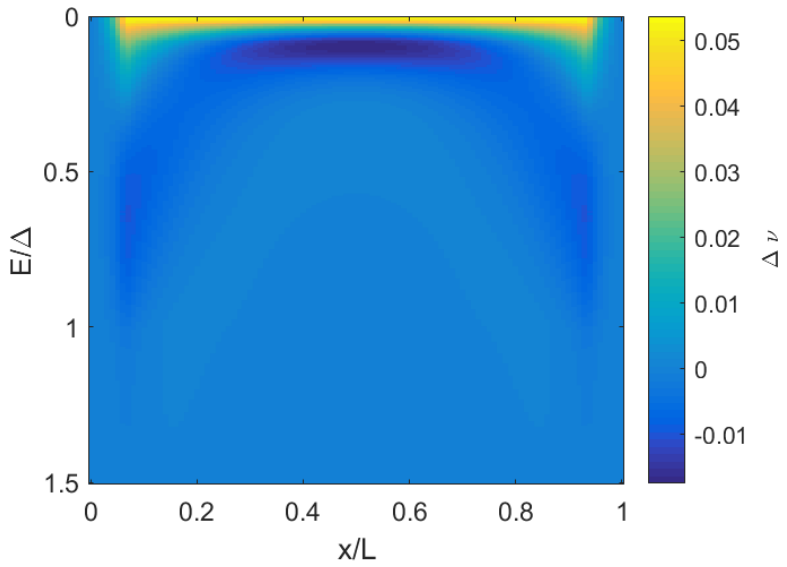

Figure 63: The LDOS as a function of position and energy as calculated using the Usadel equation for a junction length of 14.

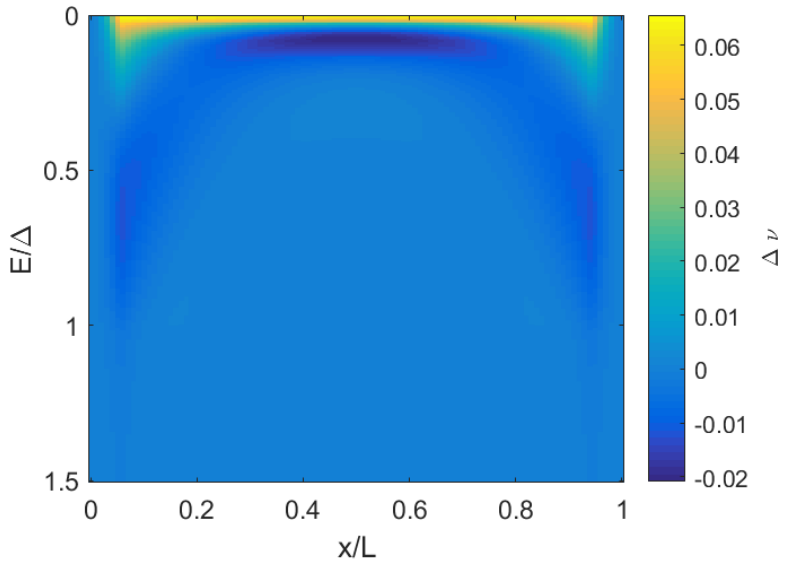

Figure 64: The LDOS as a function of position and energy as calculated using the Usadel equation for a junction length of 16.

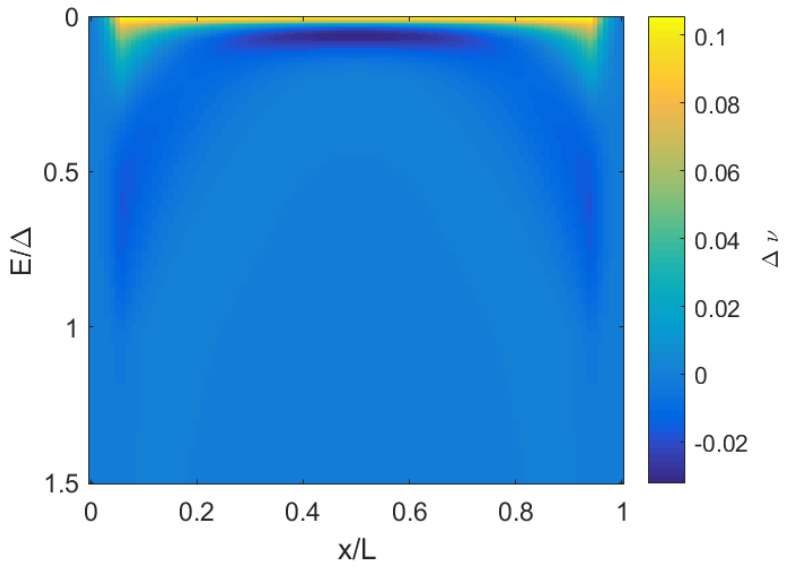

Figure 65: The LDOS as a function of position and energy as calculated using the Usadel equation for a junction length of 18.

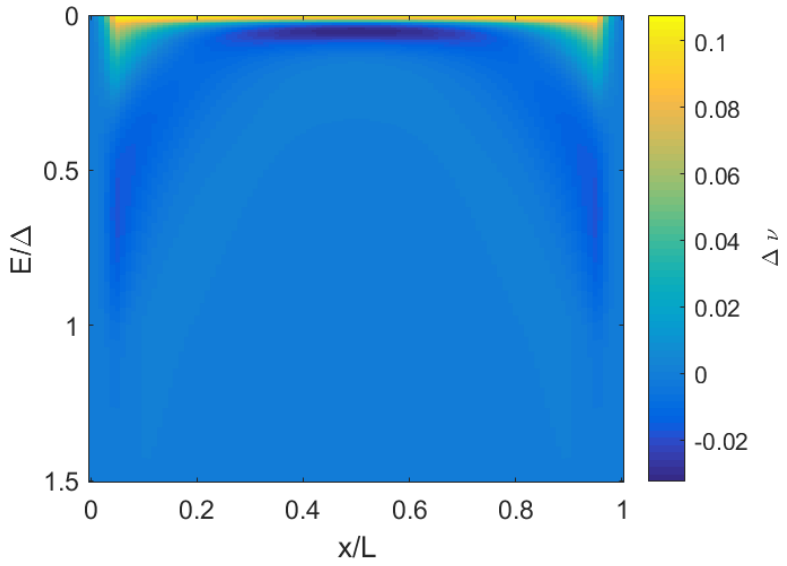

Figure 66: The LDOS as a function of position and energy as calculated using the Usadel equation for a junction length of 20.

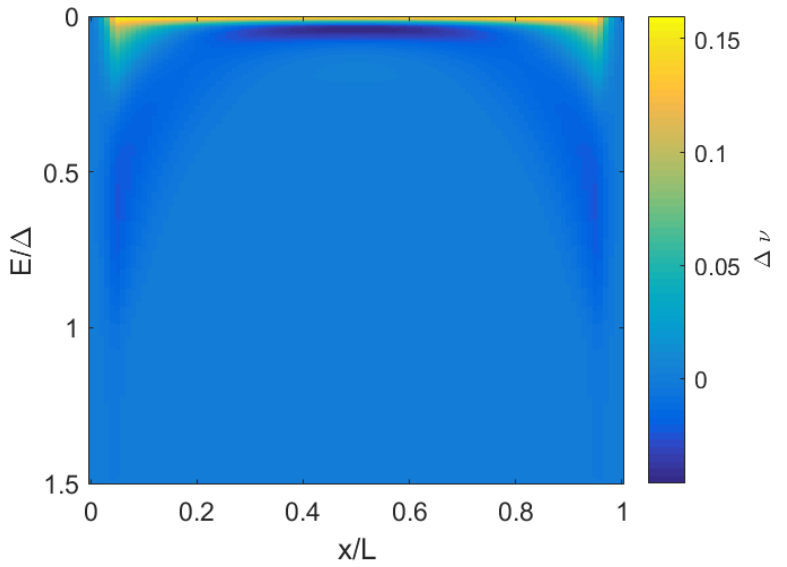

Figure 67: The LDOS as a function of position and energy as calculated using the Usadel equation for a junction length of 22.

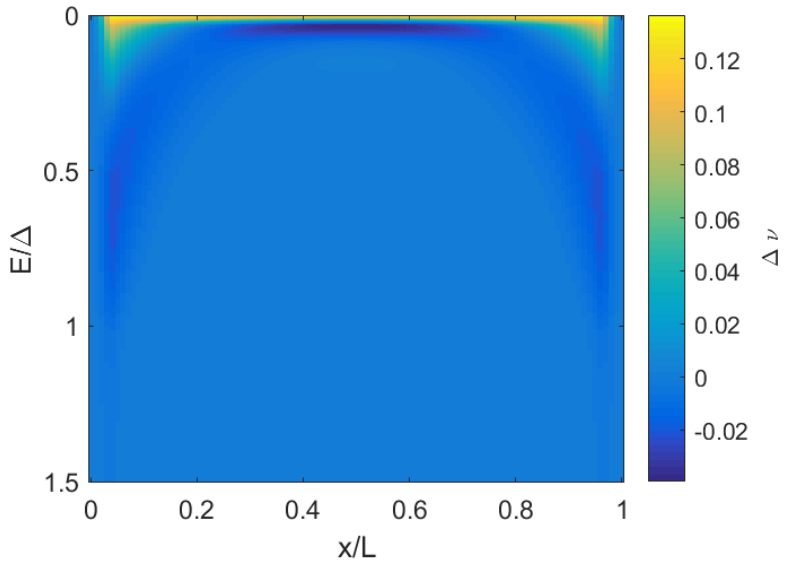

Figure 68: The LDOS as a function of position and energy as calculated using the Usadel equation for a junction length of 24.

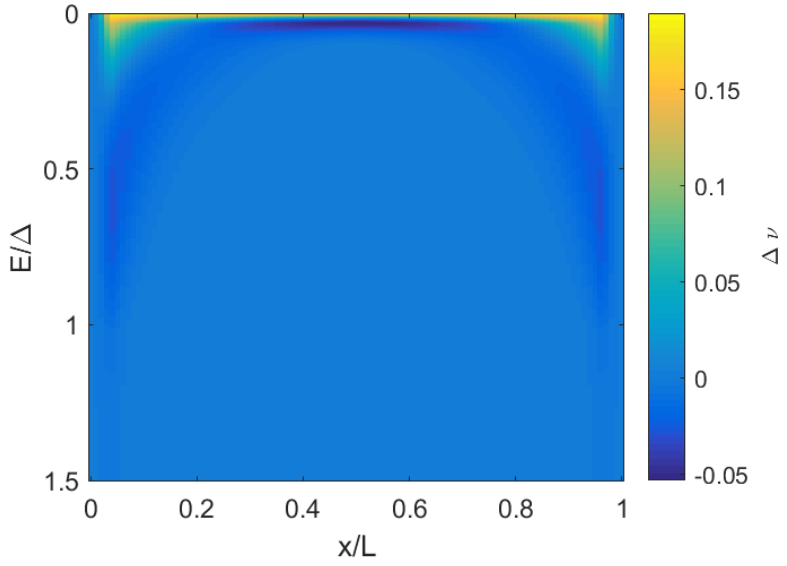

Figure 69: The LDOS as a function of position and energy as calculated using the Usadel equation for a junction length of 26.

B Derivations

B.1 Retarded equations in parametrisation

In this section it will be explained how the Usadel equation in the θ-parametrisation can be derived from the Usadel equation. The Usadel equation as introduced in equation (13.6) reads:

$$G^R \nabla G^R + i\epsilon[\tau_3, G] + S(G, x) = 0. \tag{B.1}$$

The θ-parametrisation reads:

$$G^R = \begin{bmatrix} \cosh\theta & \sinh\theta e^{i\chi} \\ -\sinh\theta e^{-i\chi} & -\cosh\theta \end{bmatrix}. \tag{B.2}$$

This means that

$$\begin{aligned} \nabla G^R &= \begin{bmatrix} \sinh\theta & \cosh\theta e^{i\chi} \\ -\cosh\theta e^{-i\chi} & -\sinh\theta \end{bmatrix} \nabla\theta + \begin{bmatrix} 0 & i\sinh\theta e^{i\chi} \\ i\sinh\theta e^{-i\chi} & 0 \end{bmatrix} \nabla\chi, \\ G^R \nabla G^R &= \begin{bmatrix} 0 & e^{i\chi} \\ e^{-i\chi} & 0 \end{bmatrix} \nabla\theta + \begin{bmatrix} i\sinh\theta^2 & i\cosh\theta\sinh\theta e^{i\chi} \\ -i\cosh\theta\sinh\theta e^{-i\chi} & -i\sinh\theta^2 \end{bmatrix} \nabla\chi. \end{aligned} \tag{B.3}$$

Moreover

$$[\tau_3, G^R] = \begin{bmatrix} 0 & 2\sinh\theta e^{i\chi} \\ 2\sinh\theta e^{-i\chi} & 0 \end{bmatrix}. \tag{B.4}$$

Because there are two independent parameters θ and χ, two equations should be extracted from this. The first is found taking the $(1,1)$-component of each term. Defining $S_\chi = -iS_{1,1}$, this yields

$$\nabla(i\sinh\theta^2\nabla\chi) + iS_\chi = 0, \tag{B.5}$$

which is the χ-equation. The θ-equation is found by multiplying the $(1,2)$-components by $\frac{1}{2}e^{-i\chi}$, the $(2,1)$-components by $\frac{1}{2}e^{i\chi}$ and adding the results. The contribution of the $\nabla(G^R\nabla G^R)$-term is

$$\begin{aligned} &\frac{1}{2}e^{-i\chi}\nabla(e^{i\chi}\nabla\theta) + \frac{1}{2}e^{-i\chi}\nabla(i\cosh\theta\sinh\theta e^{i\chi}\nabla\chi) \\ &+ \frac{1}{2}e^{i\chi}\nabla(e^{-i\chi}\nabla\theta) + \frac{1}{2}e^{i\chi}\nabla(-i\cosh\theta\sinh\theta e^{-i\chi}\nabla\chi) \\ =&\frac{1}{2}\nabla^2\theta + \frac{1}{2}i\nabla\chi\nabla\theta - \frac{1}{4}\sinh 2\theta(\nabla\chi)^2 + \frac{1}{2}i\cosh 2\theta\nabla\theta\nabla\chi + \frac{1}{4}i\sinh 2\theta\nabla^2\chi \\ &+ \frac{1}{2}\nabla^2\theta - \frac{1}{2}i\nabla\chi\nabla\theta - \frac{1}{4}\sinh 2\theta(\nabla\chi)^2 - \frac{1}{2}i\cosh 2\theta\nabla\theta\nabla\chi - \frac{1}{4}i\sinh 2\theta\nabla^2\chi \\ =&\nabla^2\theta - \frac{1}{2}\sinh 2\theta(\nabla\chi)^2. \end{aligned} \tag{B.6}$$

Defining $S_\theta = \frac{1}{2}e^{-i\chi}S(1,2) + \frac{1}{2}e^{i\chi}S(2,1)$, the θ-equation is

$$\nabla^2\theta - \frac{1}{2}\sinh 2\theta(\nabla\chi)^2 + 2i\epsilon\sinh\theta + S_\theta = 0. \tag{B.7}$$

B.1.1 Consistency

In the previous section, two equations in the θ-parametrisation have been derived. In this subsection, it will be shown that these two equations are enough to satisfy the Usadel equation in $\mathbb{C}^{2x2}$. To show this, the equations for the $(1,1)$-component plus the $(2,2)$-component and the $e^{-i\chi}(1,2) - e^{i\chi}(2,1)$ component will be investigated. Note that this is enough as matrices in C^{2x2} have four components. The first of these two equations is the simplest. All terms have zero trace, therefore all terms

vanish and the equation is thus satisfied. Note that also the trace of the S-term vanishes as the S-term may be written as $S = [G, B]$ [84], and the trace of a commutator always vanishes.
The second of these equations is a bit harder. From equation (B.6) it can be read of that the contribution of $\nabla(G^R \nabla G^R)$ is

$$i\nabla\chi\nabla\theta + i\cosh 2\theta \nabla\theta\nabla\chi + \frac{1}{2} i \sinh 2\theta \nabla^2\chi. \tag{B.8}$$

When divided by i, this can be rewritten as

$$\begin{aligned} &2\cosh\theta^2 \nabla\theta\nabla\chi + \sinh\theta\cosh\theta\nabla^2\chi \\ &= \coth\theta\left(2\sinh\theta\cosh\theta\nabla\theta\nabla\chi + \sinh\theta^2\nabla^2\chi\right) \\ &= \coth\theta\nabla\left(\sinh\theta^2\nabla\chi\right), \end{aligned} \tag{B.9}$$

which is just the $(1,1)$-component multiplied by $\coth\theta$. Thus, if it can be shown that $\frac{1}{2}e^{-i\chi}S(1,2) - \frac{1}{2}e^{i\chi}S(2,1) = \coth\theta S(1,1)$ this equation is satisfied whenever the $(1,1)$-equation is satisfied, and the validation has been accomplished. Now, as indicated $S = [G, B]$. The components of S thus read:

$$\begin{aligned} S(1,1) &= \sinh\theta\left(e^{i\chi}B(2,1) + e^{-i\chi}B(1,2)\right) \\ S(1,2) &= 2\cosh\theta B(1,2) - \sinh\theta e^{i\chi}(B(1,1) - B(2,2)) \\ S(2,1) &= -2\cosh\theta B(1,2) - \sinh\theta e^{-i\chi}(B(1,1) - B(2,2)) \\ \frac{1}{2}e^{-i\chi}S(1,2) - \frac{1}{2}e^{i\chi}S(2,1) &= \cosh\theta\left(e^{i\chi}B(2,1) + e^{-i\chi}B(1,2)\right) = \coth\theta S(1,1). \end{aligned} \tag{B.10}$$

This concludes the proof.

B.2 Topological insulator

In the case of a topological insulator, the ordinary derivatives in the Usadel equation should be replaced by

$$\hat{\nabla}G = \nabla G - i\frac{h}{v_F}[\tau_3, G], \tag{B.11}$$

where h is the exchange coupling and v_F is the Fermi velocity [106],[114]. This means there are extra terms.

$$\begin{aligned} G\hat{\nabla}G &= G\nabla G - i\frac{h}{v_F}[\tau_3, G], \\ \hat{\nabla}(G\hat{\nabla}G) &= \nabla(G\nabla G) - i\frac{h}{v_F}[\tau_3, G\nabla G] - i\frac{h}{v_F}\nabla(G\tau_3 G - \tau_3) - (\frac{h}{v_F})^2[\tau_3, G\tau_3 G - \tau_3], \end{aligned} \tag{B.12}$$

where it was used that $G[\tau_3, G] = G\tau_3 G - G^2\tau_3 = G\tau_3 G - \tau_3$. The extra term in $G\hat{\nabla}G$ equals

$$-2i\frac{h}{v_F}\begin{bmatrix} \sinh\theta^2 & \cosh\theta\sinh\theta e^{i\chi} \\ -\cosh\theta\sinh\theta e^{-i\chi} & -\sinh\theta^2, \end{bmatrix}$$

which implies that the expression for the spectral supercurrent ImIs changes to

$$\text{ImIs} = \sinh\theta^2\frac{\partial\chi}{\partial x} - 2B\sinh\theta^2. \tag{B.13}$$

The extra terms in $\hat{\nabla}(G\hat{\nabla}G)$ are

$$\begin{aligned} -i\frac{h}{v_F}[\tau_3, G\nabla G] &= -i\frac{h}{v_F}\begin{bmatrix} 0 & 2i\cosh\theta\sinh\theta e^{i\chi} \\ -2i\cosh\theta\sinh\theta e^{-i\chi} & 0. \end{bmatrix}\nabla\chi - 2i\frac{h}{v_F}\begin{bmatrix} 0 & e^{i\chi} \\ -e^{-i\chi} & 0 \end{bmatrix} \\ -i\frac{h}{v_F}\nabla(G\tau_3 G - \tau_3) &= -2i\frac{h}{v_F}\begin{bmatrix} 0 & e^{i\chi} \\ -e^{-i\chi} & 0 \end{bmatrix}\nabla\theta + 2\frac{h}{v_F}\begin{bmatrix} 0 & \sinh\theta\cosh\theta e^{i\chi} \\ \sinh\theta\cosh\theta e^{-i\chi} & 0 \end{bmatrix}\nabla\chi. \\ -(\frac{h}{v_F})^2[\tau_3, G\tau_3 - G] &= -4(\frac{h}{v_F})^2\begin{bmatrix} 0 & \sinh\theta\cosh\theta e^{i\chi} \\ \sinh\theta\cosh\theta e^{-i\chi} & 0 \end{bmatrix}. \end{aligned}$$

Using this, the χ-equation has only one extra term, $-2i\frac{h}{v_F}\sinh 2\theta\nabla\theta$, whereas all three terms contribute to the θ equation, which now has extra terms $2\frac{h}{v_F}\sinh 2\theta\nabla\chi - 2(\frac{h}{v_F})^2\sinh 2\theta$.

B.3 Keldysh equation

In this section the equations for the Keldysh equations will be derived. It will be shown that, in case a complex superconducting phase χ in the normal layer is allowed, additional terms occur compared to expressions previously noted in literature [101], [2]. First the Keldysh equation will be written using the parametrisation for the Keldysh Green's function, then the coefficients of the terms in this expression will be calculated using the θ-parametrisation for the retarded and advanced components.
Recall that the Usadel equation reads

$$\frac{\partial}{\partial x}\left(G\frac{\partial G}{\partial x}\right) + i\epsilon[G,\tau_3] + 2\Theta_S[G,B] = 0. \tag{B.14}$$

Recall that for any matrix Z consisting of retarded, advanced and Keldysh components the Keldysh component can be written $Z^K = Z^R h - hZ^A$ where h is a diagonal matrix. In the following section, h will be used in the normal metal, whereas h_s will be used in the superconducting electrodes. First the Keldysh component of the first term will be calculated.

$$\begin{aligned}(G\nabla G)^K &= G^R\nabla G^K + G^K\nabla G^A = G^R\nabla(G^Rh - hG^A) + (G^Rh - hG^A)\nabla G^A \\ &= G^R\nabla G^Rh + (G^R)^2\nabla h - G^R\nabla hG^A - G^Rh\nabla G^A + G^Rh\nabla G^A - hG^A\nabla G^A \\ &= \nabla h - G^R\nabla hG^A + G^R\nabla G^Rh - hG^A\nabla G^A.\end{aligned} \tag{B.15}$$

Thus, the Keldysh equation reads

$$\begin{aligned}&\nabla(\nabla h - G^R\nabla hG^A) + \nabla(G^R\nabla G^R)h + G^R\nabla G^R\nabla h - h\nabla(G^A\nabla G^A) - \nabla hG^A\nabla G^A \\ &+ i\epsilon([G^R,\tau_3]h - h[G^A,\tau_3]) + 2[G,B]^K\Theta_S(x) = 0.\end{aligned} \tag{B.16}$$

Now, adding and subtracting $2([G,B]^Rh - h[G,B]^A)\Theta_s(x)$ and rearranging the terms this can be written as

$$\begin{aligned}&\nabla(\nabla h - G^R\nabla hG^A) + \left(\nabla(G^R\nabla G^R) + i\epsilon[G^R,\tau_3] + 2[G,B]^R\Theta_s(x)\right)h + G^R\nabla G^R\nabla h \\ &- h\left(\nabla(G^A\nabla G^A) + i\epsilon[G^A,\tau_3] + 2[G,B]^A\right) - \nabla hG^A\nabla G^A + 2([G,B]^K - [G,B]^Rh + h[G,B]^A)\Theta_s(x) = 0.\end{aligned} \tag{B.17}$$

Now, using the retarded and advanced components two of these expressions can be seen to vanish, and the equation left is

$$\begin{aligned}0 =&\nabla(\nabla h - G^R\nabla hG^A) + G^R\nabla G^R\nabla h - \nabla hG^A\nabla G^A + 2([G,B]^K - [G,B]^Rh + h[G,B]^A)\Theta_s(x). \\ =&\nabla(\nabla h - G^R\nabla hG^A) + G^R\nabla G^R\nabla h - \nabla hG^A\nabla G^A + S = 0, \\ S =&2([G,B]^K - [G,B]^Rh + h[G,B]^A)\Theta_s(x).\end{aligned} \tag{B.18}$$

Using that h is diagonal to write $h = f_L\tau_0 + f_T\tau_3$ this becomes

$$\begin{aligned}&\nabla\left((1 - G^RG^A)\nabla f_L\right) + \nabla\left((\tau_3 - G^R\tau_3G^A)\nabla f_T\right) + \nabla f_L(G^R\nabla G^R - G^A\nabla G^A) \\ &+ \nabla f_T(G^R\nabla G^R\tau_3 - \tau_3G^A\nabla G^A) + S = 0.\end{aligned} \tag{B.19}$$

Now, the coefficients in equation (B.19) need to be calculated.

B.3.1 Calculation of terms

In the previous section the Keldysh equation has been expressed in the distribution functions f_L and f_T and the retarded and advanced Green's function. Now, all coefficients will be expressed in the θ-parametrisation. The first term in equation (B.19) is $1 - G^R G^A = 1 + G^R \tau_3 (G^R)^\dagger \tau_3$. Using that

$$G^R = \begin{bmatrix} \cosh\theta & \sinh\theta e^{i\chi} \\ -\sinh\theta e^{-i\chi} & -\cosh\theta \end{bmatrix}, \tag{B.20}$$

it follows that

$$\tau_3 (G^R)^\dagger \tau_3 = \begin{bmatrix} \cosh\theta^* & \sinh\theta^* e^{i\chi^*} \\ -\sinh\theta^* e^{-i\chi^*} & -\cosh\theta^* \end{bmatrix}, \tag{B.21}$$

and therefore that

$$G^R \tau_3 (G^R)^\dagger \tau_3 = \begin{bmatrix} |\cosh\theta|^2 - |\sinh\theta|^2 e^{-2\mathrm{Im}\chi} & \cosh\theta \sinh\theta^* e^{i\chi^*} - \cosh\theta^* \sinh\theta e^{i\chi} \\ \cosh\theta \sinh\theta^* e^{-i\chi^*} - \cosh\theta^* \sinh\theta e^{-i\chi} & |\cosh\theta|^2 - |\sinh\theta|^2 e^{2\mathrm{Im}\chi} \end{bmatrix} \tag{B.22}$$

In the following expressions it will be convenient to use

$$D_L = \mathrm{Tr}(1 - G^R G^A) = 2 + 2|\cosh\theta|^2 - 2|\sinh\theta|^2 \cosh 2\mathrm{Im}\chi, \tag{B.23}$$

and

$$C_T = \mathrm{Tr}(\tau_3 - \tau_3 G^R G^A) = 2|\sinh\theta|^2 \sinh 2\mathrm{Im}\chi. \tag{B.24}$$

For the second term note that $-G^R \tau_3 G^A = G^R (G^R)^\dagger \tau_3$. This can be calculated and yields

$$\begin{aligned} G^R (G^R)^\dagger \tau_3 &= \begin{bmatrix} \cosh\theta & \sinh\theta e^{i\chi} \\ -\sinh\theta e^{-i\chi} & -\cosh\theta \end{bmatrix} \begin{bmatrix} \cosh\theta^* & \sinh\theta^* e^{i\chi^*} \\ \sinh\theta^* e^{-i\chi^*} & \cosh\theta^* \end{bmatrix} \\ &= \begin{bmatrix} |\cosh\theta|^2 + |\sinh\theta|^2 e^{-2\mathrm{Im}\chi} & \cosh\theta \sinh\theta^* e^{i\chi^*} + \cosh\theta^* \sinh\theta e^{i\chi} \\ -\cosh\theta \sinh\theta^* e^{-i\chi^*} - \cosh\theta^* \sinh\theta e^{-i\chi} & -|\cosh\theta|^2 - |\sinh\theta|^2 e^{2\mathrm{Im}\chi} \end{bmatrix} \end{aligned} \tag{B.25}$$

Analogously to the expressions for the first term, define

$$C_L = \mathrm{Tr}(\tau_3 - G^R \tau_3 G^A) = -2|\sinh\theta|^2 \sinh 2\mathrm{Im}\chi = -C_T, \tag{B.26}$$

and

$$D_T = \mathrm{Tr}(1 - \tau_3 G^R \tau_3 G^A) = 2 + 2|\cosh\theta|^2 + 2|\sinh\theta|^2 \cosh 2\mathrm{Im}\chi. \tag{B.27}$$

The third term reads $G^R \nabla G^R \tau_3 - \tau_3 G^A \nabla G^A$. Now,

$$\begin{aligned} G^R \nabla G^R &= \begin{bmatrix} \cosh\theta & \sinh\theta e^{i\chi} \\ -\sinh\theta e^{-i\chi} & -\cosh\theta \end{bmatrix} \begin{bmatrix} \sinh\theta & \cosh\theta e^{i\chi} \\ -\cosh\theta e^{-i\chi} & -\sinh\theta \end{bmatrix} \frac{\partial\theta}{\partial x} \\ &\quad + \begin{bmatrix} \cosh\theta & \sinh\theta e^{i\chi} \\ -\sinh\theta e^{-i\chi} & -\cosh\theta \end{bmatrix} \begin{bmatrix} 0 & i\sinh\theta e^{i\chi} \\ i\sinh\theta e^{-i\chi} & 0 \end{bmatrix} \\ &= \begin{bmatrix} 0 & e^{i\chi} \\ e^{-i\chi} & 0 \end{bmatrix} \frac{\partial\theta}{\partial x} + \begin{bmatrix} i\sinh^2\theta & i\cosh\theta\sinh\theta e^{i\chi} \\ -i\cosh\theta\sinh\theta e^{-i\chi} & -i\sinh^2\theta \end{bmatrix} \frac{\partial\chi}{\partial x}. \end{aligned} \tag{B.28}$$

From this it can be calculated that

$$\begin{aligned}&\mathrm{Tr}(G^R\nabla G^R) = 0,\\ &\mathrm{Tr}(\tau_3 G^R\nabla G^R) = 2i\sinh^2\theta\frac{\partial\chi}{\partial x}.\end{aligned} \tag{B.29}$$

Similarly, for $G^A\nabla G^A$

$$\begin{aligned}G^A\nabla G^A &= \begin{bmatrix}-\cosh\theta^* & -\sinh\theta^* e^{i\chi^*}\\ \sinh\theta^* e^{-i\chi^*} & \cosh\theta^*\end{bmatrix}\begin{bmatrix}-\sinh\theta^* & -\cosh\theta^* e^{i\chi^*}\\ \cosh\theta^* e^{-i\chi^*} & \sinh\theta^*\end{bmatrix}\frac{\partial\theta^*}{\partial x}\\ &+\begin{bmatrix}-\cosh\theta^* & -\sinh\theta^* e^{i\chi^*}\\ \sinh\theta^* e^{-i\chi^*} & \cosh\theta^*\end{bmatrix}\begin{bmatrix}0 & -i\sinh\theta^* e^{i\chi^*}\\ -i\sinh\theta^* e^{-i\chi^*} & 0\end{bmatrix}\frac{\partial\chi^*}{\partial x}\\ &=\begin{bmatrix}0 & e^{i\chi^*}\\ e^{-i\chi^*} & 0\end{bmatrix}\frac{\partial\theta^*}{\partial x}+\begin{bmatrix}i\sinh^2\theta^* & i\cosh\theta^*\sinh\theta^* e^{i\chi^*}\\ -i\cosh\theta^*\sinh\theta^* e^{-i\chi^*} & -i\sinh^2\theta^*\end{bmatrix}\frac{\partial\chi^*}{\partial x}.\end{aligned} \tag{B.30}$$

From this it can be calculated that

$$\begin{aligned}&\mathrm{Tr}(G^A\nabla G^A) = 0,\\ &\mathrm{Tr}(\tau_3 G^A\nabla G^A) = 2i\sinh^2\theta^*\frac{\partial\chi^*}{\partial x}.\end{aligned} \tag{B.31}$$

From equations (B.29) and (B.31) it now follows that

$$\begin{aligned}&\mathrm{Tr}(G^R\nabla G^R - G^A\nabla G^A) = 0.\\ &\mathrm{Tr}(\tau_3(G^R\nabla G^R - G^A\nabla G^A)) = 2i\sinh^2\theta\frac{\partial\chi}{\partial x} - 2i\sinh\theta^*\frac{\partial\chi^*}{\partial x} = -4\mathrm{Im}(\sinh^2\theta\frac{\partial\chi}{\partial x}).\end{aligned} \tag{B.32}$$

This latter quantity is defined as ImIs.

B.3.2 Parametrised Keldysh equation

With the expressions from the previous section, equations (B.23), (B.24), (B.26) and (B.27) the Keldysh differential equation (B.19) can be put in parametrised form. Taking the trace of equation (B.19) gives

$$\nabla(D_L\nabla f_L) + \nabla(C_L\nabla f_T) + \mathrm{ImIs}\nabla f_T + \mathrm{Tr}(S) = 0. \tag{B.33}$$

The second equation is found by taking the trace of equation (B.19) after multiplying by τ_3. This gives

$$\nabla(D_T\nabla f_T) + \nabla(C_T\nabla f_L) + \mathrm{ImIs}\nabla f_L + \mathrm{Tr}(\tau_3 S) = 0. \tag{B.34}$$

Compared with expressions in literature [2], [101], there is one extra term in each equation, $\nabla(C_L\nabla f_T)$ and $\nabla(C_T\nabla f_L)$. Now, these terms are proportional to $\sinh 2\mathrm{Im}\chi$, which means that they vanish if χ is real. Thus, in case χ is real the equations presented in [2], [101] are recovered.

B.4 Boundary condition

In this section the Tanaka Nazarov boundary conditions will be calculated for the VT junction. I will start from equation 9 of [85]. The boundary condition can be expressed as

$$G\frac{\partial}{\partial y}G = \sum_n I_n, \tag{B.35}$$

where

$$\begin{aligned} I_n &= 2[G, B_n] \\ B_n &= \left(-T_{1n}[G_1, H_-^{-1}] + H_-^{-1}H_+ - T_{1n}^2 G_1 H_-^{-1} H_+ G_1\right)^{-1} \left(T_{1n}(1 - H_-^{-1}) + T_{1n} G_1 H_-^{-1} H_+\right). \end{aligned} \tag{B.36}$$

In this equation G_1 is the Green's function in the normal metal. On the superconducting side, $H_\pm = \frac{1}{2}(G_{2+} \pm G_{2-})$, where $G_{2\pm}$ are Green's functions in the superconductor with $\pm$ indicating direction of motion towards or away from the interface. A problem with expression 1 is that it contains H_-^{-1}. In conventional superconductors the superconducting potential is isotropic, so $G_{2+} = G_{2-}$, that is $H_- = 0$. Moreover, in unconventional superconductors we can have $H_- \approx 0$ for some of the channels as well. Note that for H_+ this will not be the case. For that reason, it is useful to rewrite B_n by inserting $\left(H_+^{-1}H_-\right)^{-1}\left(H_+^{-1}H_-\right)$ as follows

$$\begin{aligned} B_n =& \left(-T_{1n}[G_1, H_-^{-1}] + H_-^{-1}H_+ - T_{1n}^2 G_1 H_-^{-1} H_+ G_1\right)^{-1} (H_+^{-1}H_-)^{-1} \\ & (H_+^{-1}H_-)\left(T_{1n}(1 - H_-^{-1}) + T_{1n} G_1 H_-^{-1} H_+\right) \\ =& \left(-T_{1n}H_+^{-1}H_- G_1 H_-^{-1} H_+ H_+^{-1} + T_{1n}H_+^{-1}G_1 + 1 - T_{1n}^2 H_+^{-1}H_- G_1 H_-^{-1} H_+ G_1\right)^{-1} \\ & \left(T_{1n}(H_+^{-1}H_- - H_+^{-1}) + T_{1n}H_+^{-1}H_- G_1 H_-^{-1} H_+\right) \end{aligned} \tag{B.37}$$

In this last expression H_-^{-1} is still present, but only in the combination $H_+^{-1}H_- G_1 H_-^{-1} H_+ = H_+^{-1}H_- G_1 (H_+^{-1}H_-)^{-1}$. It is this latter expression that can be used for both the retarded and Keldysh component. In the following sections both components will be discussed.

B.4.1 Retarded component

This derivation holds in case the superconducting order parameter in the superconducting electrodes is $\Delta = \Delta_0$ or $\Delta = \Delta_0 \cos\phi - \alpha$, where ϕ is the angle made with the surface and α is the angular mismatch between electrodes and normal metal. For the case $\Delta = \Delta_0 e^{i\phi}$ a different strategy is used, which will be elaborated upon in the end.
The retarded component of B_n is

$$\begin{aligned} B_R =& \left(-T_{1n}R_p^{-1}R_m G_1 (R_p^{-1}R_m)^{-1} + T_{1n}R_p^{-1}G_1 + 1 - T_{1n}^2 R_p^{-1}R_m G_1 (R_p^{-1}R_m)^{-1} G_1\right)^{-1} \\ & \left(T_{1n}R_p^{-1}R_m - T_{1n}R_p^{-1} + T_{1n}^2 R_p^{-1}R_m G_1 (R_p^{-1}R_m)^{-1}\right). \end{aligned} \tag{B.38}$$

We can write

$$G_{2\pm} = \begin{bmatrix} g_\pm & f_\pm e^{i\psi} \\ -f_\pm e^{-i\psi} & -g_\pm \end{bmatrix}, \tag{B.39}$$

where ψ is the superconducting phase of the electrode. Therefore

$$\begin{aligned} R_p &= \frac{1}{2}\begin{bmatrix} g_+ + g_- & (f_+ + f_-)e^{i\psi} \\ -(f_+ + f_-)e^{-i\psi} & -(g_+ + g_-) \end{bmatrix} \\ R_p^{-1} &= \frac{1}{1 + g_+g_- - f_+f_-}\begin{bmatrix} g_+ + g_- & (f_+ + f_-)e^{i\psi} \\ -(f_+ + f_-)e^{-i\psi} & -(g_+ + g_-). \end{bmatrix} \\ R_m &= \frac{1}{2}\begin{bmatrix} g_+ - g_- & (f_+ - f_-)e^{i\psi} \\ -(f_+ - f_-)e^{-i\psi} & -(g_+ - g_-) \end{bmatrix} \end{aligned} \tag{B.40}$$

With this, $R_p^{-1}R_m$ can be calculated. Using that $g_+^2 - f_+^2 = g_-^2 - f_-^2 = 1$ and $(g_+ + g_-)(f_+ - f_-) - (g_+ - g_-)(f_+ + f_-) = g_+f_+ - g_+f_- + g_-f_+ - g_-f_- - g_+f_+ - g_+f_- + g_-f_+ + g_-f_- = 2(g_-f_+ - g_+f_-)$, it follows that

$$R_p^{-1}R_m = \frac{g_-f_+ - g_+f_-}{1 + g_+g_- - f_+f_-}\begin{bmatrix} 0 & e^{i\psi} \\ e^{-i\psi} & 0 \end{bmatrix} = A\begin{bmatrix} 0 & e^{i\psi} \\ e^{-i\psi} & 0 \end{bmatrix} = A\Psi, \tag{B.41}$$

where $A = \frac{g_-f_+ - g_+f_-}{1+g_+g_- - f_+f_-}$ and $\Psi = \begin{bmatrix} 0 & e^{i\psi} \\ e^{-i\psi} & 0 \end{bmatrix}$. But then

$$\begin{aligned} &R_p^{-1}R_m G_1 (R_p^{-1}R_m)^{-1} \\ &= A\begin{bmatrix} 0 & e^{i\psi} \\ e^{-i\psi} & 0 \end{bmatrix} G_1 \frac{1}{A}\begin{bmatrix} 0 & e^{i\psi} \\ e^{-i\psi} & 0 \end{bmatrix} = \begin{bmatrix} 0 & e^{i\psi} \\ e^{-i\psi} & 0 \end{bmatrix} G_1 \begin{bmatrix} 0 & e^{i\psi} \\ e^{-i\psi} & 0 \end{bmatrix} = \Psi G_1 \Psi. \end{aligned} \tag{B.42}$$

With this B_R can be expressed as

$$B_R = \left(-T_{1n}\Psi G_1 \Psi R_p^{-1} + T_{1n}R_p^{-1}G_1 + 1 - T_{1n}^2 \Psi G_1 \Psi G_1\right)^{-1}\left(T_{1n}R_p^{-1}R_m - T_{1n}R_p^{-1} + T_{1n}\Psi G_1 \Psi\right). \tag{B.43}$$

This expression does not contain R_m^{-1} and can thus be computed using a computer program.
A connection can be made to the expression found in [85]. Parametrising G_1 using the θ-parametrisation as in [2], $\Psi G_1 \Psi$ can be calculated as follows:

$$\begin{aligned} \Psi G_1 \Psi &= \begin{bmatrix} 0 & e^{i\psi} \\ e^{-i\psi} & 0 \end{bmatrix}\begin{bmatrix} \cosh\theta & \sinh\theta e^{i\chi} \\ -\sinh\theta e^{-i\chi} & -\cosh\theta \end{bmatrix}\begin{bmatrix} 0 & e^{i\psi} \\ e^{-i\psi} & 0 \end{bmatrix} \\ &= \begin{bmatrix} 0 & e^{i\psi} \\ e^{-i\psi} & 0 \end{bmatrix}\begin{bmatrix} \sinh\theta e^{i(\chi-\psi)} & \cosh\theta e^{i\psi} \\ -\cosh\theta e^{-i\psi} & -\sinh\theta e^{-i(\chi-\psi)} \end{bmatrix} \\ &= \begin{bmatrix} -\cosh\theta & -\sinh\theta e^{-i(\chi-2\psi)} \\ \sinh\theta e^{i(\chi-\psi)} & \cosh\theta \end{bmatrix} \\ &= -G_1 + 2i\sinh\theta\sin\chi - \psi\begin{bmatrix} 0 & e^{i\psi} \\ e^{-i\psi} & 0 \end{bmatrix}. \end{aligned} \tag{B.44}$$

If the superconducting phases in the electrodes and the normal metal are the same, this reduces to $\Psi G_1 \Psi = -G_1$, and in that case equation (B.43) reduces to the expression found in [85].

B.4.2 Chiral p-wave

Lastly, the case $\Delta = \Delta_0 e^{i\phi}$ is discussed. In that case

$$\begin{aligned} R_p &= \frac{1}{2}\begin{bmatrix} g_+ + g_- & f_+e^{i\psi_+} + f_-e^{i\psi_-} \\ -(f_+e^{-i\psi_+} + f_-e^{-i\psi_-}) & -(g_+ + g_-) \end{bmatrix} \\ R_m &= \frac{1}{2}\begin{bmatrix} g_+ - g_- & f_+e^{i\psi_+} - f_-e^{i\psi_-} \\ -(f_+e^{-i\psi_+} - f_-e^{-i\psi_-}) & -(g_+ - g_-) \end{bmatrix} \\ &, \end{aligned} \tag{B.45}$$

and in this case the diagonal elements of $R_p^{-1}R_m$ do not vanish. However, since $g_\pm = \frac{E}{\sqrt{E - |\Delta_{pm}|^2}}$ and $|\Delta_\pm| = |\Delta e^{i\psi_\pm}| = \Delta_0$, the diagonal elements of R_m do vanish, and the procedure that was applied to $R_p^{-1}R_m G_1 (R_p^{-1}R_m)^{-1}$ previously, may now be applied to $R_m G_1 R_m^{-1}$.

B.5 Keldysh component

The Keldysh component of the boundary condition can be expressed as follows:

$$I_K = 2([G, B_n])_K = 2(G^R B_K + G^K B_A - B_R G^K - B_K G^A). \tag{B.46}$$

Now, B_R has been calculated in section B.4.1, and B_A can be calculated from $B_A = -\tau_3 B_R^\dagger \tau_3$, where τ_3 is the third Pauli matrix. Thus, only B_K needs to be calculated. From equation (B.37) it can be read that $B = D^{-1}N$, where

$$\begin{aligned} D &= \left(-T_{1n}H_+^{-1}H_-G_1H_-^{-1}H_+H_+^{-1} + T_{1n}H_+^{-1}G_1 + 1 - T_{1n}^2H_+^{-1}H_-G_1H_-^{-1}H_+G_1\right)^{-1} \\ N &= \left(T_{1n}(H_+^{-1}H_- - H_+^{-1}) + T_{1n}H_+^{-1}H_-G_1H_-^{-1}H_+\right). \end{aligned} \tag{B.47}$$

With this expression B_K can be expressed as

$$\begin{aligned} B_K &= D_R^{-1}N_K - (D^{-1})_K N_A \\ &= D_R^{-1}N_K - D_R^{-1}D_K D_A^{-1}N_A. \end{aligned} \tag{B.48}$$

Following [85] $D_A^{-1}N_A = B_A$, which leaves only N_K and D_K to be calculated. In order to find these expressions, the Keldysh part of each of the terms of N and D will be calculated:

$$\begin{aligned} (1)_K &= 0. \\ (H_+^{-1})_K &= -R_p^{-1}K_pA_p^{-1} \\ &= R_p^{-1}h_s - h_sA_p^{-1}. \\ (H_+^{-1}G_1)_K &= R_p^1G^K + (H_+^{-1})_KG^A \\ &= R_p^1(R_1h - hA_1) + (R_p^{-1}h_s - h_sA_p^{-1})A_1. \\ (H_+^{-1}H_-)_K &= R_p^{-1}(H_-)_K + (H_+^{-1})_KA_m \\ &= R_p^{-1}R_mh_s - R_p^{-1}h_sA_m + R_p^{-1}h_sA_m - h_sA_p^{-1}A_m \\ &= R_p^{-1}R_mh_s - h_sA_p^{-1}A_m. \\ (H_+^{-1}H_-G_1H_-^{-1}H_+H_+^{-1})_K &= (H_+^{-1}H_-G_1H_-^{-1}H_+)_R(H_+^{-1})_K + (H_+^{-1}H_-G_1H_-^{-1}H_+)_KA_p^{-1} \\ &= \Psi R_1\Psi(R_p^{-1}h_s - h_sA_p^{-1}) + (H_+^{-1}H_-G_1H_-^{-1}H_+)_KA_p^{-1}. \\ (H_+^{-1}H_-G_1H_-^{-1}H_+G_1)_K &= (H_+^{-1}H_-G_1H_-^{-1}H_+)_RG^K + (H_+^{-1}H_-G_1H_-^{-1}H_+)_KA_1 \\ &= \Psi R_1\Psi(R_1h_s - h_sA_1) + (H_+^{-1}H_-G_1H_-^{-1}H_+)_KA_1. \end{aligned} \tag{B.49}$$

Substituting these expressions

$$\begin{aligned} D_K = &- T_{1n}\Psi R_1\Psi(R_p^{-1}h_s - h_sA_p^{-1}) - T_{1n}(H_+^{-1}H_-G_1H_-^{-1}H_+)_KA_p^{-1} + T_{1n}R_p^{-1}(R_1h - hA_1) \\ &+ T_{1n}(R_p^{-1}h - hA_p^{-1})A_1 - T_{1n}^2\Psi R_1\Psi(R_1h - hA_1) - T_{1n}^2(H_+^{-1}H_-G_1H_-^{-1}H_+)_KA_1. \end{aligned} \tag{B.50}$$

and

$$N_K = T_{1n}R_p^{-1}R_mh_s - T_{1n}h_sA_p^{-1}A_m - T_{1n}R_p^{-1}h_s + T_{1n}h_sA_p^{-1} + T_{1n}^2(H_+H_-G_1H_-^{-1}H_+)_K. \tag{B.51}$$

This leaves only $(H_+H_-G_1H_-^{-1}H_+)_K$ to calculate. To this end, first observe that

$$A_m^{-1}A_p = (-\tau_3(R_m^{-1})^\dagger\tau_3)(-\tau_3R_p\tau_3) = \tau_3(R_m^{-1})^\dagger R_p^\dagger\tau_3 = \tau_3(R_pR_m^{-1})^\dagger\tau_3. \tag{B.52}$$

Using that H_+ and H_-^{-1} anticommute it follows that

$$A_m^{-1}A_p = -\tau_3(R_m^{-1}R_p)^\dagger\tau_3 = -\frac{1}{A}\tau_3\Psi\tau_3 = \frac{1}{A}\Psi, \tag{B.53}$$

where it was used that Ψ is a Hermitian matrix and that its diagonal elements vanish.
Thus,

$$R_p^{-1}R_mG_1A_m^{-1}A_p = \frac{A}{A^*}\Psi G_1\Psi. \tag{B.54}$$

Now the remaining term can be calculated:

$$\begin{aligned}(H_+H_-G_1H_-^{-1}H_+)_K = \\ &(H_+H_-)_K A_1 (H_-^{-1}H_+)_A \\ +&(H_+H_-)_R (R_1h - hA_1)(H_-^{-1}H_+)_A \\ +&(H_+H_-)_R R_1 (H_-^{-1}H_+)_K.\end{aligned} \tag{B.55}$$

As calculated before, $(H_+^{-1}H_-)_K = R_p^{-1}R_m h_s - h_s A_p^{-1}A_m$. Thus,

$$\begin{aligned}(H_+H_-)_K A_1 (H_-^{-1}H_+)_A &= R_p^{-1}R_m h_s A_1 A_m^{-1}A_p - h_s A_p^{-1}A_m A_1 A_m^{-1}A_p \\ &= \frac{A}{A^*}\Psi h_s A_1 \Psi - h_s \Psi A_1 \Psi. \\ (H_+H_-)_R K_1 (H_-^{-1}H_+)_A &= R_p^{-1}R_m (R_1h - hA_1)A_m^{-1}A_p \\ &= \frac{A}{A^*}\Psi (R_1h - hA_1)\Psi \\ (H_+H_-)_R R_1 (H_-^{-1}H_+)_K &= R_p^{-1}R_m R_1 (R_m^{-1}R_p h_s - h_s A_m^{-1}A_p) \\ &= \Psi R_1 \Psi h_s - \frac{A}{A^*}\Psi R_1 h_s \Psi.\end{aligned} \tag{B.56}$$

With this the expression for $(H_+H_-G_1H_-^{-1}H_+)_K$ finally becomes

$$(H_+H_-G_1H_-^{-1}H_+)_K = \Psi R_1 \Psi h_s - h_s \Psi A_1 \Psi + \frac{A}{A^*}\left(\Psi R_1 (h - h_s)\Psi - \Psi (h - h_s) A_1 \Psi\right). \tag{B.57}$$

With this an expression for all terms of B_K has been found and I_K can be calculated.